www.uhasselt.be
Hasselt University
Martelarenlaan 42 | BE-3500 Hasselt
T + 32(0)11 26 81 11

2016 | Faculty of Sciences

DOCTORAL DISSERTATION

Continuous Photoflow Synthesis of Precision Polyacrylates - Complex Structures and Kinetic Insights

Doctoral dissertation submitted to obtain the degree of
Doctor of Science: Chemistry, to be defended by

Benjamin Wenn

Promoter: Prof. Dr Thomas Junkers

2016 | Faculty of Sciences

DOCTORAL DISSERTATION

Continuous Photoflow Synthesis of Precision Polyacrylates - Complex Structures and Kinetic Insights

Doctoral dissertation submitted to obtain the degree of
Doctor of Science: Chemistry, to be defended by

Benjamin Wenn

Promoter: Prof. Dr Thomas Junkers

D/2016/2451/53

Chairman:	Prof. Dr. Karin Coninx, UHasselt
Promoter:	Prof. Dr. Thomas Junkers, UHasselt
Members of the Jury:	Prof. Dr. Peter Adriaensens, UHasselt
	Prof. Dr. Christophe Detrembleur, ULg
	Prof. Dr. Filip Du Prez, UGent
	Prof. Dr. Wouter Maes, UHasselt
	Prof. Dr. Felix Schacher, Universität Jena

PRD
POLYMER REACTION DESIGN

Vielen Dank

Dank Je Wel

Thank You Very Much

Merci Beaucoup

Mange Tak

Muito Obrigado

Çok Teşekkür Ederim

Велике Спасибі

Liels Paldies

非常感谢你

どうもありがとうございました

정말 감사합니다

ขอบคุณ

Quality means doing it right
when no one is looking.

Henry Ford

Table of Contents

Chapter 1

Chapter 2

Chapter 3

Chapter 4

Chapter 5

Chapter 6

Chapter 7

Chapter 8

Chapter 9

List of Conference Presentations

List of Abbreviations

^{1}H NMR	proton nuclear magnetic resonance
1-Oct	1-octene
4Br^{i}Bu	pentaerythritol tetrakis (2-bromoisobutyrate)
6Br^{i}Bu	dipentaerythritol hexakis (2-bromoisobutyrate)
^{13}C NMR	carbon nuclear magnetic resonance
21BrCD	heptakis[2,3,6-tri-O-(2-bromo-2- methylpropionyl]-*ß*-cyclodextrin
AA	acrylic acid
Ag	silver
API	active pharmaceutical ingredient
ATRP	atom transfer radical polymerization
Au	gold
b	block
C	carbon
conv.	conversion
CMP	copper-mediated polymerization
CMRP	cobalt-mediated radical polymerization
Cl	chlorine
Co	cobalt
co	copolymer

$Co(acac)_2$	Bis(acetylacetonato)cobalt (II)
CRP	controlled radical polymerization
Cu	copper
$CuBr_2$	copper(II) bromide
$Đ$	dispersity
DB	degree of branching
DCM	dichloromethane
DEGA	di(ethylene glycol) ethyl ether acrylate
DLS	dynamic light scattering
DMF	dimethyl formamide
DMSO	dimethyl sulfoxide
DP	degree of polymerization
E_A	activation energy
EA	ethyl acrylate
ECTFE	ethylene chlorotrifluoroethylene
eq	equivalents
Eq	equation
ESI/MS	electro-spray ionization/mass spectrometry
EtOAc	ethyl acetate
EtOH	ethanol
f	monomer feed ratio
F	copolymer composition

FRP	free radical polymerization
FTIR	Fourier transformation – infrared spectroscopy
GPC	gel permeation chromatography
H	hydrogen
HEA	2-hydroxyethyl acrylate
HMB	2-hydroxyethyl 2`-methyl-2`-bromopropionate
HMP	2-hydroxy-4’-(2-hydroxyethoxy)-2-methylpropiophenone
$h\nu$	photon
I	initiator
Ir	iridium
J	Joule
K	Kelvin
k_{bb}	backbiting rate coefficient
k_{deact}/ k_{act}	rate constant for de-/activation reaction
k_{p}	rate constant for chain propagation
$k_{\mathrm{p}}^{\mathrm{app}}$	apparent propagation rate coefficient
$k_{\mathrm{p}}^{\mathrm{eff}}$	effective propagation rate coefficient
$k_{\mathrm{p}}^{\mathrm{SPR}}$	secondary propagating radical propagation rate coefficient
$k_{\mathrm{p}}^{\mathrm{tert}}$	mid-chain radical propagation rate
k_{t}	rate constant for termination reaction

M	monomer
MA	methyl acrylate
MeOH	methanol
Me_6TREN	tris[2-(dimethylamino)ethyl]amine
MMA	methyl methacrylate
M_n	number-average molecular weight
MS	mass spectrometry
$[M]$	monomer concentration
M_w	weight-average molecular weight
MCR	mid-chain radical
MWD	molecular weight distribution
*n*BA	*n*-butyl acrylate
NMR	nuclear magnetic resonance
NMP	nitroxide-mediated polymerization
NP	nanoparticle
Pd	palladium
PEG	polyethylene glycol
PFA	perfluoroalkoxy alkane
photoCMP	photo-induced copper-mediated polymerization
photoRDRP	photo-induced reversible-deactivation radical polymerization
PLP	pulsed laser polymerization

PMDETA	*N,N,N′,N′′,N′′*-pentamethyldiethylenetriamine
p	polymer
PS	polystyrene
Pt	platinum
PTFE	polytetrafluoroethylene
r_{act}	reaction rate activation
RAFT	reversible addition-fragmentation chain transfer polymerization
RDRP	reversible-deactivation radical polymerization
Rh	rhodium
RTD	residence time distribution
SEC	size exclusion chromatography
SET-LRP	single electron transfer – living radical polymerization
SPR	secondary propagating radical
t	time
tert	tertiary
tBA	*tert*-butyl acrylate
TFA	trifluoroacetic acid
THF	tetrahydrofuran
UV	ultraviolet
v	frequency in hertz
VAc	vinyl acetate

Chapter 1

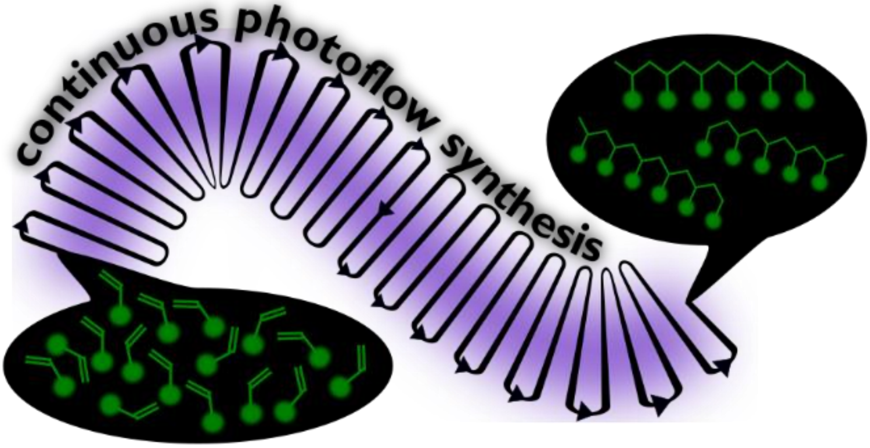

1. Introduction[*]

1.1. General Introduction

Polymers are among the most important materials of the 21st century. Nowadays, our modern lifestyle depends largely on the unique properties of polymers. They are present in almost every daily used product, ranging from plastic bottles, over car and bike tires, coatings and glue to nanomedicine. Polymers were first described as macromolecules by Hermann Staudinger in 1920.[1] He and researchers after him discovered that a lot of known materials consist of long chains of similar or identical repetition units. The IUPAC defines a polymer as "A molecule of high relative molecular mass, the structure of which essentially comprises the multiple repetition of units derived, actually or conceptually, from molecules of low relative molecular mass".[2]

The development of several polymerization techniques in the past decades has allowed to synthesize different advanced polymeric architectures. Synthesized polymers can be categorized in three main groups (Figure 1.1). First, the composition of the polymer can be influenced and determined. Well known compositions are homopolymers as well as block, statistical, periodic or gradient copolymers. A second differentiation between synthesized polymers is the topology. Nowadays, structures like stars, cyclic, or branched polymers can be designed and made. The third criteria to group polymers is how the structures are functionalized. Functionalities are mainly introduced by using specific initiators or monomers which contain a functional group. These groups are mainly at the chain end of the polymers, but can also be in the center or on the grafted side chain. Almost all possible combinations of the three main groups can be created.

---

[*] First published partly as: "Continuous Photoflow Synthesis of Precision Polymers", T. Junkers, B. Wenn, *React. Chem. Eng.* **2016**, 1, 60-64 and "Photoflow Material Synthesis" in Photochemical processes in continuous-flow reactors: From engineering principles to chemical applications, B. Wenn, T. Junkers, T. Noël Ed., Imperial College Press. 2016, submitted.

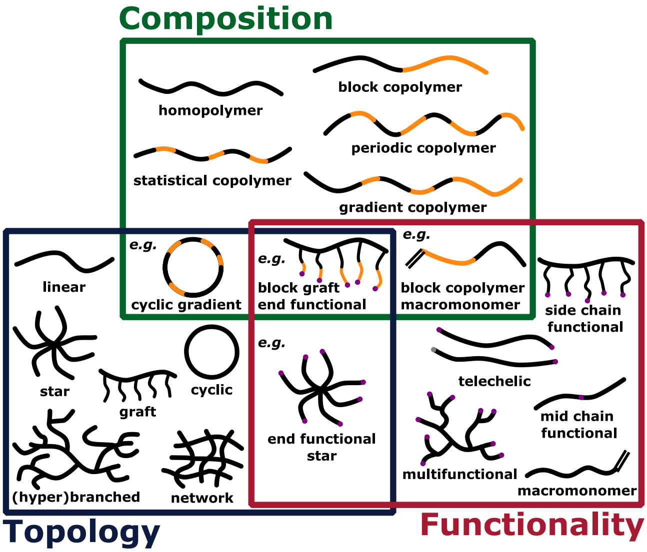

Figure 1.1 Overview of the three main groups to characterize complex polymer architectures.

1.2. Radical Polymerization Techniques

Polymerization mechanisms can be differentiated in the way the polymerization occurs. Three different ways have been discovered, (1) the step-growth, (2) the chain-growth and (3) the living chain-growth mechanism. In the step-growth polymerization, first small molecules like oligomers, trimers, etc. are formed. At higher monomer conversion these small molecules react and form high molecular weight polymer chains. Examples for step-growth polymerizations are polycondensation or polyaddition reactions.

In comparison, during the chain-growth mechanism relatively high molecular weights are reached already at low monomer conversion. During a chain-growth pathway, unsaturated monomer units are continuously and one by one added to the active polymer chain. The polymerization is started via an initiator and continues very fast till the chain is terminated. If the active polymer chain does not terminate and stays "alive", the polymerization follows the living chain-growth mechanism. Ideally, in that case, a linear increase of molecular weight with

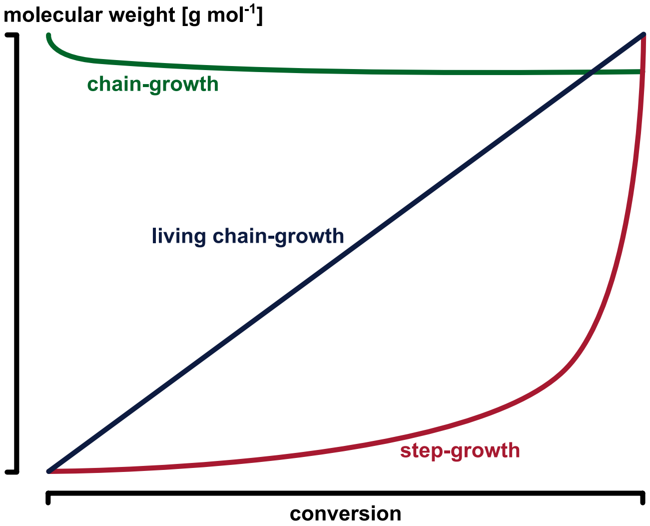

Figure 1.2 Development of molecular weight with increasing monomer conversion for step-, chain-, and living chain-growth polymerizations.

monomer conversion is observed. The development of molecular weight with increasing monomer conversion for all three polymerization methods is shown in Figure 1.2.

An important method to synthesize the above mentioned complex polymeric architectures is via radical polymerizations. In these polymerizations the active center carries a radical which is transferred to another monomer after chain extension.[3] Radical polymerizations are divided into two groups, (i) free radical polymerizations (FRP) and (ii) reversible-deactivation radical polymerizations (RDRP). The second group is also commonly known as controlled radical polymerization (CRP). Besides radical polymerization techniques, other methods such as cationic and anionic polymerization methods exist.[4, 5] Free radical polymerizations are following the chain-growths mechanism, reaching high molecular weights almost instantaneous. On the other hand reversible-deactivation radical polymerizations follow the living chain-growth path showing a linear increase in molecular weight.

1.2.1. Free Radical Polymerization

The probably most important polymerization method in industry is the free radical polymerization. It is mainly used for bulk-produced polymers, the production of which amounts to several million tons per year. Some commonly known materials made via FRP are polystyrene (PS), polypropylene (PP), polymethyl methacrylate (PMMA) or low-density polyethylene (LD-PE).

Free radical polymerization was defined as a chain-growth polymerization where the molecular weight increases with decreasing monomer concentration.[6] The polymerization can be divided into three mechanistic steps (see Scheme 1.1). First, an initiator generates two radicals. This cleavage can be triggered by different stimuli, e.g. temperature, light or electricity. The generated radicals attack the carbon-carbon double bond of the monomers and form an initiator-monomer radical. After the propagation step is reached, more monomer molecules are added to the growing chain. Due to fast termination reactions, a growing polymer chain usually has a lifetime of about one second. There are two main termination pathways in FRP: disproportionation and combination. Disproportionation yields one saturated and one unsaturated polymer chain.

Decomposition:

$$\text{initiator} \longrightarrow 2\,I^{\bullet}$$

Initiation:

$$I^{\bullet} \xrightarrow{+\,M} P_n^{\bullet}$$

Propagation:

$$P_n^{\bullet} \xrightarrow{+\,M} P_{n+1}^{\bullet}$$

Termination:

by disproportionation $P_n^{\bullet} + P_m^{\bullet} \longrightarrow P_n\text{-H} + P_m^{=}$

by combination $P_n^{\bullet} + P_m^{\bullet} \longrightarrow P_{n+m}$

Scheme 1.1 The three main steps occurring during free radical polymerization.

Combination produces one polymer with a molecular weight that equals the sum of both radical polymer chains.[7]

1.2.2. Reversible-Deactivation Radical Polymerization

Reversible-deactivation radical polymerization techniques generally give access to polymer materials with defined length, end group functionality and narrow dispersity. Polymers are 'reactivatable', and hence allow for block copolymer formation. Combined with an advanced initiator and a control agent design, macromolecular architectures ranging from rather simple linear structures to brush or star-shaped complex dendritic materials can be produced. By adjusting the solubility of the various blocks incorporated in the macromolecules, so-called 'smart materials' can be obtained. These are able to react to outer stimuli such as pH, temperature, light or electrical current. Photo-induced reaction modes exist for practically all reversible deactivation radical polymerization mechanisms, but are nowadays not yet exploited to their full potential. These RDRP protocols are often very robust and can be carried out under less stringent reaction conditions compared to other living polymerizations, e.g. anionic polymerization.

As the name already tells, during RDRP, the propagation radicals can be reversibly deactivated and brought into a dormant state. This leads to a reduced active radical concentration which can cause termination reactions. Termination plays a minor role during RDRP ($r_{deact}>r_{act}>>r_t$). When all monomer molecules are consumed, the polymer chains stay in the dormant state and can be reinitiated later.

Generally, two different types of reversible-deactivation radical polymerization exist, (1) degenerative chain transfer equilibria and (2) reversible termination reactions. For the first, control over the polymerization reactions can be exerted via complex degenerative chain transfer equilibria in which the chain propagation probability is evenly distributed over all present polymer chains. Reversible termination reactions work via a reduction of free-radical concentrations during polymerization.

1.2.2.1. Reversible Addition–Fragmentation Chain-Transfer Polymerization

The best known degenerative transfer RDRP is the reversible addition-fragmentation chain-transfer polymerization (RAFT). RAFT is very versatile and features the advantage of being driven by conventional radical initiators, and as such is inherently photoactivatable under any condition (unlike reversible termination, which requires specific reaction conditions). RAFT is often controlled by di- or trithiocarbonyl end groups.

The iniferter (*ini*tiator-trans*fer* agent-*ter*minator) polymerization can be seen as a precursor of RAFT polymerization.[8, 9] In 1982, Otsu *et al.* were the first to report on iniferter polymerizations. An iniferter was defined as a molecule which can decompose into radicals to initiate chain growth. These generated radicals are also expected to reversibly end-cap the growing chains (Scheme 1.2).

Photo-initiated iniferter polymerizations established for the first time a reversible termination equilibrium. In the photoiniferter polymerization, an UV-labile bond is cleaved, the radicals start the polymerization and the chains are end-capped. Mostly molecules containing a disulfide are used as a photoiniferter agent. If the end-capping functionality is a specific thioether or thioester, the bond can also be cleaved by UV-light.[10] For photoiniferter reactions, classical RAFT-agents, like dithiobenzoates or trithiocarbonates can be used.

Compared to the iniferter polymerization, an initiator is used to start a reversible addition-fragmentation chain-transfer polymerization. The RAFT mechanism consists of four main steps (Scheme 1.3). First a photo or thermo-labile initiator decomposes and forms radicals. These radicals react with monomer molecules

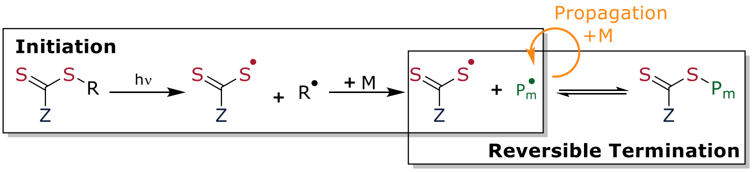

Scheme 1.2 Reaction scheme for (photo)iniferter polymerizations.

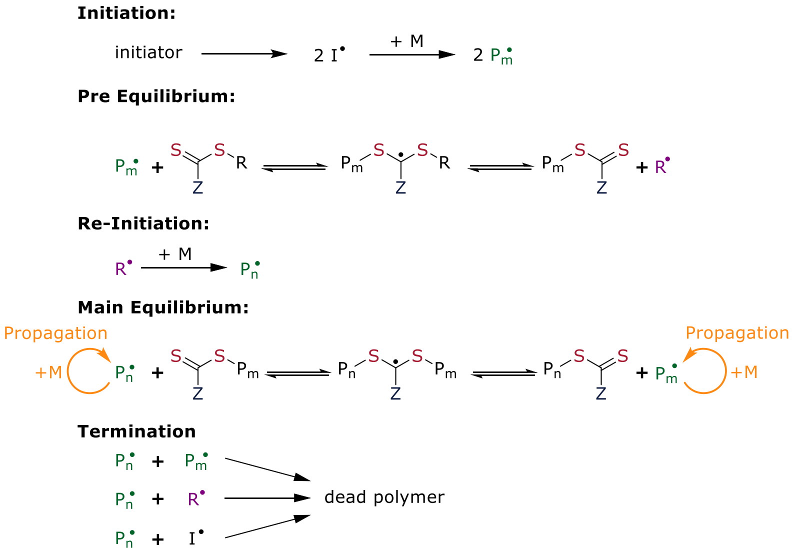

Scheme 1.3 General reaction scheme for reversible addition-fragmentation chain-transfer polymerization (RAFT).

and start the chain growth in the initiation step. With these growing polymer chains the RAFT polymerization reaches the pre equilibrium. The propagating chain covalently binds to the RAFT-agent to form an intermediate. This radical containing intermediate can proceed in two ways: (1) the leaving group R is released and reinitiates to create a macroradical by adding monomer units, (2) or the added macroradical is released again to continue the chain growth. If all initial initiator radicals and the RAFT-agent radicals have been consumed, the polymerization reaches the main equilibrium. From here, one macroradical continues to grow while another is covalently linked to the RAFT-agent and forms a macroRAFT-agent. In this stage, an equilibrium between the active and dormant species is established and the chains propagate evenly.

Until today, research on RAFT has mainly focused on thermally initiated reactions in batch[11] as well as in flow reactors.[12] However, photo-initiated RAFT is long known.[13-15]

1.2.2.2. Copper-Mediated Radical Polymerization

Copper-mediated radical polymerization (CMP) belongs to the group of reversible termination polymerization methods. Here, the propagating radicals are deactivated reversibly in an efficient control equilibrium. The majority of chains are at any instance in the dormant state and radical concentrations are largely reduced, hence avoiding radical termination and inducing living character. Several methods have been developed using copper to control polymerizations. The most known ones are atom-transfer radical polymerization (ATRP) and Cu(0)-mediated polymerizations, mainly known single-electron transfer living radical polymerization (SET-LRP). Besides those two, activator (re)generation by electron transfer (ARGET) ATRP,[16] initiators for continuous activator (re)generation (ICAR) ATRP,[17] electrochemically mediated *e*ATRP,[18] and supplemental activators and reducing agents (SARA) ATRP[19-22] have been reported. Recently, two groups reported on metal-free ATRP using organic catalysts.[23, 24]

In ATRP, a ligand complexes a transition metal and helps to dissolve it in the solvent. As metal catalyst, halogenated copper[25], iron[26], cobalt[27], ruthenium[28], thellurium[29] or osmium[30] salts are used. The most commonly used transition metal is copper. It can be used in a broad range of solvents as well as for different

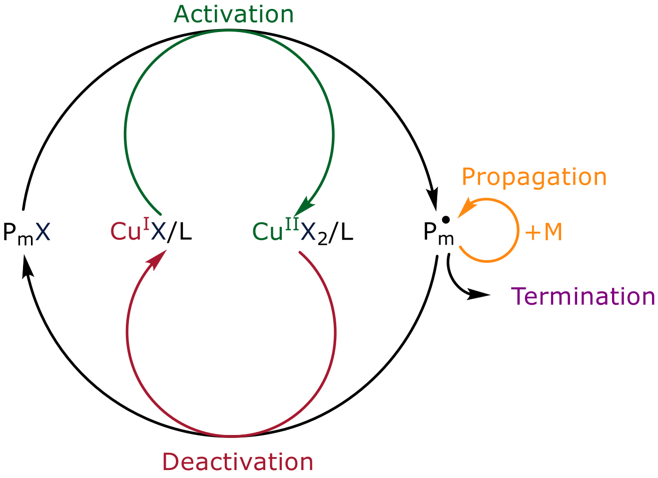

Scheme 1.4 General reaction scheme for an atom-transfer radical polymerization (ATRP).

monomers. Additionally, copper is cheap and commercially available. The polymerization is started via the oxidation of the transition metal complex (Scheme 1.4). When going back to the dormant state, the metal is reduced again. ATRP can only be used for activated monomers such as acrylates. A drawback of ATRP is the removal of the used copper catalyst from the final polymer.

To be able to polymerize non-activated monomers like vinyl acetate or α-olefines, the so called single-electron transfer living radical polymerization (SET-LRP) was discovered in 2006.[22] Recently new discoveries in the field of copper-mediated polymerizations led to call SET-LRP now Cu(0)-mediated polymerizations. Besides non-activated monomers, activated systems like for ATRP can be polymerized via Cu(0)-mediated systems.[31-33] Cu(0)-mediated polymerizations can be carried out under very mild reaction conditions. Room temperature or lower can be used as well as different polar organic solvents. The used Cu(0) catalyst is more reactive than the Cu(I) in conventional ATRP so that the used amounts can be significantly reduced.[22] Obtained polymers have a higher purity and end group fidelities.

In the Cu(0)-mediated polymerization mechanism, the used Cu(I) halogen disproportionates rapidly to Cu(0) and Cu(II) (Scheme 1.5). This happens in the presence of a ligand and in polar solvents. The halogen-terminated polymer chain

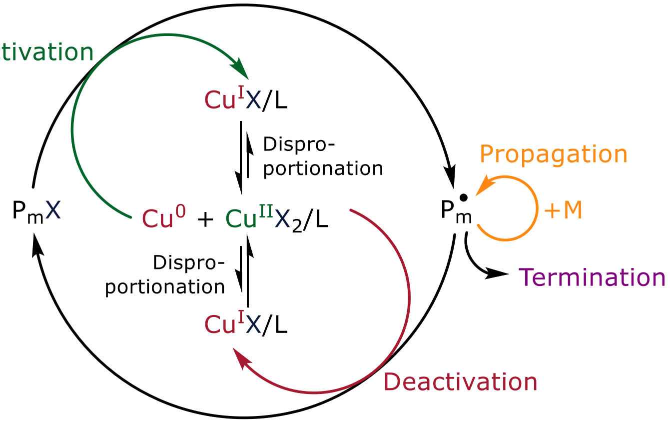

Scheme 1.5 Reaction scheme for Cu(0)-mediated polymerization or known as single-electron transfer – living radical polymerization (SET-LRP).

is now activated and starts to propagate. Cu(0)-mediated systems can also be used by starting with Cu(0) and Cu(II) where Cu(I) is formed in situ.

The activation of transition metal-mediated polymerizations via light has become focus of research. Reports on using cobalt,[34-36] copper,[37-40] iridium[41-43], ruthenium[44-46] or iron[47-49] for photo-induced polymerizations can be found in literature. In 2014 the Hawker group[24] and in 2015 the Matyjaszewski group[23] reported on metal-free photoATRP polymerizations.

1.2.2.3. Cobalt-Mediated Radical Polymerization

Besides copper, also cobalt can be used as a transition metal to control polymerizations. Wayland *et al.* developed in 1994 the so called cobalt-mediated radical polymerization (CMRP) technique.[50] Here, a cobalt complex presents the deactivating species and end-caps the polymer chains. Therefore, an in situ or preformed generated cobalt(III) complex generates a radical after a thermal or UV treatment (Scheme 1.6). The radical adds a first monomer molecule to initiate the chain growth. During propagation, more monomer molecules are added to the chain. The radical on the polymer chain can be reversely deactivated through the Co(II). Reactivation occurs with an additional thermal or UV treatment by cleavage of the weak Co-C bond.

After the discovery of CMRP, only acrylic monomers could be polymerized. In 2004, Jérôme *et al.* found a cobalt complex that also expands the reaction to vinyl acetate.[51] Major drawbacks of CMRP are the limitation in monomer variations and the high quantities of the expensive and hard-to-handle cobalt complexes.

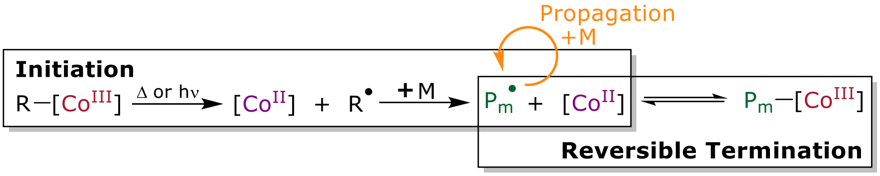

Scheme 1.6 General mechanism for cobalt-mediated radical polymerization (CMRP).

1.3. Continuous (Photo)Flow Material Synthesis

Continuous flow processing is the method of choice in the large-scale production of everyday materials. Many bulk (co)polymers are produced at ton scale in large flow reactors. Until recently no significant interest was found for continuous production in the field of precision materials engineering.

In the last years, also academic researchers discovered that continuous flow processing is an interesting tool. Especially since flow reactors at different scales became more and more commercially available. Micro-scale reactors with only a few microliter of internal volume mostly exist out of a glass reactor chip, a heating/cooling unit and syringe pumps in order to deliver the reaction mixtures. Compared to this, reactors with several milliliters of volume are often made out of copper or steel tubing wrapped around a heat source. For photoflow reactions, often self-made reactors are employed. These reactors consist of a transparent polymer tubing wrapped around the UV-light source. This polymer-based tubings offer an excellent light transmission, high chemical stability, are commercially available and easy to handle. Most literature uses fluorinated polymers for tubing, such as PTFE, PFA, or ECTFE, which are relatively cheap and available in different length and diameters. Examples of different flow reactor setups are shown in Figure 1.3.

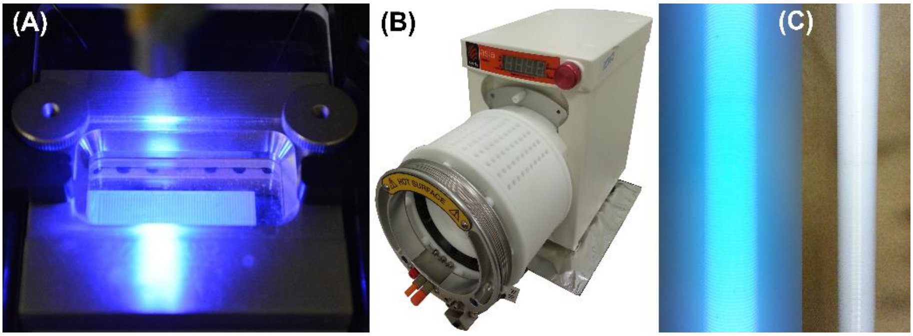

Figure 1.3 Commercially available and home-made (photo)flow reactors. (A) Chemtrix microflow reactor with an internal volume of 19.5 µL equipped with a UV-light source. (B) Syrris Asia system for thermally-initiated reactions in a 16 mL stainless steel tubing. (C) Home-made photoflow reactor consisting of PFA-tubing wrapped around a UV-light tube.

Continuous (photo)flow reactors offer some advantages compared to the commonly used batch reactors (see Figure 1.4). One major advantage of continuous flow reactors is the fast heat exchange, and thus stable reaction conditions. Due to the high surface to volume ratio, the heat created during exothermic reactions (like polymerizations) is directly removed so no hot spots are created. This leads to less side reactions and to an improved yield quality.[52-56] To obtain these stable reaction conditions, flow reactors enable fast and efficient mixing through added or built-in mixing units.[57-59] With flow reactors, it is easier to increase the reaction pressure in the system (up to 20 bar). Due to the higher pressure, boiling points of the used solvents are increased, which allows to use a broad range of solvents to carry out reactions under optimized reaction conditions.[60, 61] Since flow reactors are mostly used for smaller volumes than batch reactors, it increases the safety during operation. Smaller amounts of chemicals need to be handled and prepared by the operator. Especially for the synthesis of highly precise materials and molecules, it is very important to have reproducible and reliable processes and procedures.[62, 63] If inline purification and

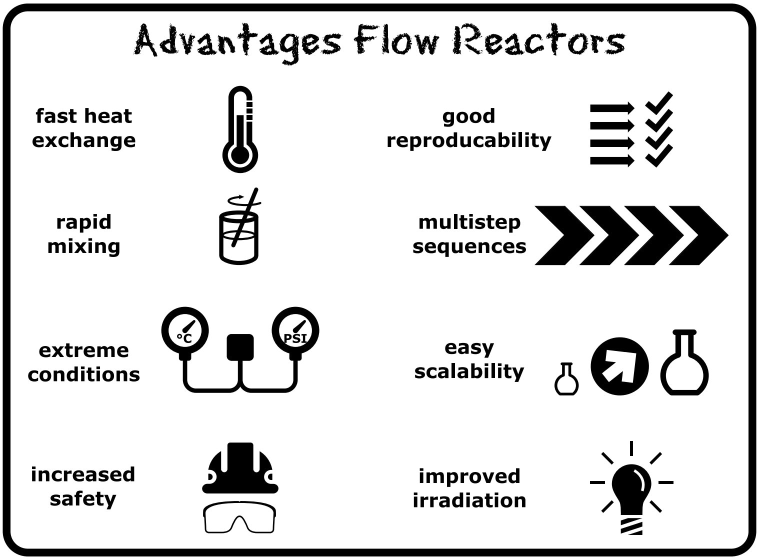

Figure 1.4 Overview of the advantages which flow reactors can offer for organic synthesis and polymerizations.

monitoring are added to the flow setup complex, multistep reaction sequences can be addressed, yielding high quantities.[62, 64] Another important advantage of continuous flow processing is the easy scalability. To increase the outcome of the system, the reactor volume can be increased by using longer reactors or tubing with larger diameters. It is also possible to parallelize several reactors and multiply the output.[65] The scalability in combination with the improved irradiation makes flow reactors an optimal tool for photo-induced reactions. Batch reactors struggle during reaction upscaling with the long optical pathlengths. When optical pathlengths are short, full illumination of the reaction mixture in its full volume can be reached. In batch reactors, light intensity gradients are unavoidable (see Figure 1.5). Following Lambert-Beer's law, light is absorbed by the UV-active ingredients in the mixture, quickly lowering the intensity of the following volume increment. Typically, UV-light does not penetrate much deeper than a few centimeters into a reaction mixture. Thus, while batch processing requires rigorous stirring in order to make sure that all reaction components reach the vessel surface (and hence the irradiated area) within a certain amount of time, practically full illumination and hence full excitation of the active ingredients is

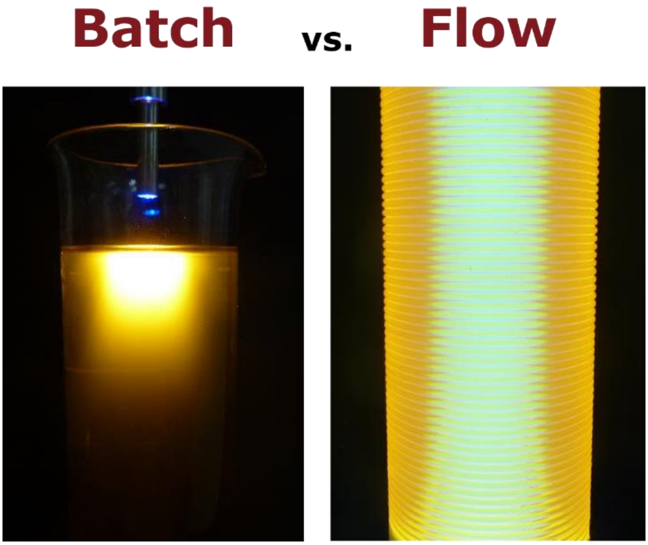

Figure 1.5 Light intensity profile in a batch reactor (left) and a tubular flow reactor (right).

reached in the flow process. The consequence is a largely reduced reaction time of photoreactions. At the same time, the overall light intensity can be reduced significantly, which avoids photo-degradation reactions that are otherwise often observed.[54, 59, 66-69]

1.3.1. Photoflow in Organic Synthesis

Photochemical reactions are mainly known and used in organic synthesis and modifications. The first reported light-induced experiment was done by Hermann Trommsdorf in 1834.[70] Since then, the field of photochemistry has developed and the range of applications was broadened. A lot of work was done on the synthesis of complex molecules such as natural products.[71-73] In industry, a photochemical process was first used to synthesize vitamin D_3.[74] Later, in 1963, a first photochemical production unit was installed to synthesize ε-caprolactam as precursor for the Nylon-6 production.[74, 75] Reactions in photochemical tubular reactors were already reported in the 1960s.[76] In the beginning of the 21st century, the first combinations of photochemical reactions and microflow reactors were reported.[77, 78] The first reported light-driven reactions in microflow reactors were photoadditons.[69, 78] Isopropanol for example was synthesized via a photopinacolization of benzophenone.[78]

The advantages of photoflow reactors are used extensively for photocycloaddition reactions.[79] Besides the short reaction times as well as the easy accessibility of complex organic molecules and the equimolarity of the reaction partners benefit the usage of photoflow reactors. A comparison of photoflow and photobatch reactions was done by Loubière *et al.* They demonstrate that [2 + 2] cycloadditions show higher conversions and better energy efficiencies in photoflow reactors.[75, 80] In 2005, Booker-Milburn and coworkers performed a photocycloaddition in a simple meso-scale photoflow reactor.[59] They synthesized up to 500 g / day of different organic molecules in this reactors.

Photoflow reactors are also used to bring molecules into excited states so as to cause isomerizations. This allows to make complex organic molecules like cyclobutenone rings from simple starting substrates.[66, 75, 81] If the photoisomerization is reversible, chemical switches or molecular motors can be made.[82-84] At industrial scale, photoisomerizations are used to make precursor molecules for anti-cancer drugs. With parallelization of several photomicroflow reactors, 2 kg of product per day can be synthesized.[54, 85]

1.3.2. Continuous Photo-initiated Polymerizations

The precise synthesis of (polymeric) materials allows for the detailed study of structure-property relationships and in consequence for a rational design of novel materials based on *ab-initio* considerations. Although highly powerful from a synthetic point of view, upscaling remains a significant problem for RDRP techniques. Scaling-up polymerizations (or polymer modifications) often leads to a loss of structural integrity, a broadening of macromolecular weight distributions and an increased number of defects. In many aspects flow chemistry can offer suitable solutions to this upscaling problem. Especially the increasing use of micro- and mesoscale reactors allows not only for simple upscale, but also for improved reaction conditions and outcomes compared to classical batch processes.

Polymerizations are inherently not simple to carry out in continuous processes. With polymerization, a viscosity increase (see Figure 1.6) is unavoidably occuring, which leads to potential blockages, increased reactor fouling, changed flow profiles and significant pressure drops. Yet, with a careful design of reactors – using dilute conditions or by working in droplet phases – these problems can be overcome. Due to the excellent heat transfer often associated with micro- and mesoflow reactors, stable temperature conditions can easily be achieved in flow. The exothermicity of polymerizations is often a crucial aspect. For example, the Cu(0)-mediated polymerization method,[33, 86] a technique commonly referred to as a "room temperature polymerization", usually heats up to 50-60 °C even in the absence of any external heat source when being carried out on a few mL scale. Recently, Derboven *et al.*[87] showed how the quality of the obtained polymer

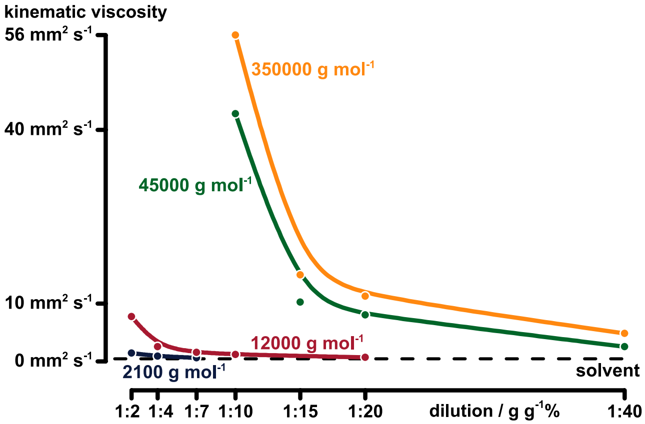

Figure 1.6 Evolution of the kinematic viscosity with increasing number average weight and dilution. The measured poly methyl acrylate was polymerized via free radical polymerization. For the viscosity determination the polymers were dissolved in acetonitrile.

product is significantly increased in microstructured flow reactors, simply due to the fact that side reactions are under better control due to isothermal processing.

The distinct advantage of increased product quality has been exploited for a number of (homogenous) polymerization reactions and polymer modifications. RAFT, ATRP, NMP and Cu(0)-mediated polymerizations[12, 56, 60, 61, 66, 86-102] have all been performed in continuous flow numerous times, each time showing that the product quality regarding dispersity, end group fidelity and overall yield in time was improved. Increasing reactor diameters can lower the beneficial effect. However, products never fall behind the associated batch process. Also classical living polymerizations have been studied, where flow reactors were identified to be ideal tools to carry out anionic and cationic polymerizations.[94, 103, 104] Similar advantages of the controlled radical polymerization techniques were observed. For polymer modifications, advantages were also identified when processing those in flow (even though this can be largely attributed to the inherently easier optimization of flow reactors[64] and not to an isothermicity effect). For instance, thiol-ene modifications of RAFT polymers were optimized to reaction times of several minutes (compared to hours in batch).[60] Additionally block copolymer formation via copper-catalyzed azide-alkyne click reactions could be carried out in less than one hour, while usually being done in batch as overnight reactions.[105] The fact that flow polymerizations are superior to their batch counterparts is not only evident when comparing dispersity data, but it is also directly observed that flow reactions aid significantly in the sequential design of multiblock copolymers. To this end, pentablock copolymers were obtained by consecutive RAFT flow polymerizations, even though the according batch process did not allow for any block extension after formation of a triblock copolymer due to the larger loss of active end groups.[102] By coupling of flow reactors, multiblock copolymers can also be obtained in one-step processes – again in a way that is not achievable in batch.[94, 106]

What occurred at the same time with polymer design is a renaissance of photo-induced reactions. Within only a few years, photo-induced reaction routes for all above mentioned synthesis techniques have been developed and optimized (Figure 1.7). Research activities in the field are rising fast and new variations of photoactivated RDRP methods are published constantly. Especially the ability to choose between different activator/sensitizer systems gives room for broad and efficient protocol optimizations.[38, 39, 107-110] Photopolymerizations feature less side product formation and give access to fast, yet simple reaction protocols. As advantageous as these reactions are, they also feature a significant disadvantage; inherently, photo-induced reactions are difficult to scale up since increasing reactor volumes lead to intensity gradients in the reactors and hence to loss of reaction efficiency. Only few options exist to overcome this problem.

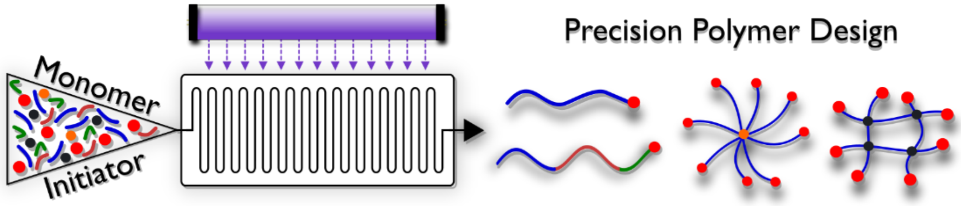

Figure 1.7 General scheme displaying precision polymer synthesis in photoflow reactors.

As discussed above, the Lambert-Beer penalty can be overcome by using a photoflow reactor. Due to the much better light efficiency of photoflow reactors, reactions are also significantly speeded up, in some cases from days of reaction time to a few minutes.[67] The formation of degradation products can be avoided as total illumination times are shorter, and lower light intensities can be used. A good example for such a scaling up from the polymer world is the [2+2] cycloaddition reaction between polymers bearing maleimide end groups and functionalized alkenes. Such reaction proceeds on a timescale of tens of hours in conventional batch reactors, but is efficiently carried out within 1 min under photoflow processing.[96, 97]

Light-induced transition metal-mediated polymerizations are known since several years for batch processes. Reports on the use of cobalt,[34-36] copper,[37-40] iridium[41] or iron[47] can be found in literature. So far, continuous photoflow polymerization using these methods has only been reported for iridium. Poelma and coworkers used an iridium complex to control the polymerization of methyl methacrylate. In their study, they also report on the influence of different fluorinated polymer tubings on the reaction. When comparing the four materials, there is no significant influence on the reaction rate or the yield quality.

1.3.3. Polymer Modifications

A further application of photoflow reactors is the modification of polymeric materials. Conradi and Junkers demonstrated a significant increase in reaction rate by employing a photoflow reactor compared to batch for an end group photomodification.[97, 111] As photoflow reactor, a PFA tubing with 0.75 mm inner diameter was wrapped around the quartz-glass cooling mantle of a 400 W medium-pressure UV lamp.

The reaction that was tested for end group modification was a [2+2] ene-enone cycloaddition. Therefore, a polymer containing an enone end group (maleimide) was reacted with a series of alkenes. The polymer bearing the maleimide end group (poly(butyl acrylate)) was synthesized stepwise via atom transfer radical polymerization. A *N*-hydroxysuccinimide-functionalized initiator was employed in the ATRP, which could then be exchanged by a maleimide after polymerization. The success of the polymerization and of the maleimide introduction was proven via electrospray ionization mass spectrometry (ESI-MS).

The first step for a successful [2+2] cycloaddition is the excitation of the UV absorbing "ene" in order to create the reactive intermediate which can react with an alkene. Efficiency in this step is dramatically increased by switching from conventional batch reactors to a photoflow system. With this change in reactors, the reaction time was reduced from days to minutes. Additionally to the significant reduction in reaction time, a reduction of the ene : enone ratio was achieved. In batch, a 20:1 ene : enone ratio is needed to reach a quantitative conversion of the starting material. In flow, it was reduced to an equimolar ratio for the reaction between two low-molecular weight compounds. When switching to the polymer maleimide, the addition of 10 mol% of a photosensitizer was required, which is, however, accompanied by a further rate increase (quantitative conversion within 1 minute).

Via this [2+2] polymer modification, various functional alkenes were introduced into the polymer chain, such as alcohols, ethers and multifunctional allyl components. Good yields were achieved in all cases (Scheme 1.7). In summary, the efficient and fast [2+2] cycloaddition can be a useful tool for polymer

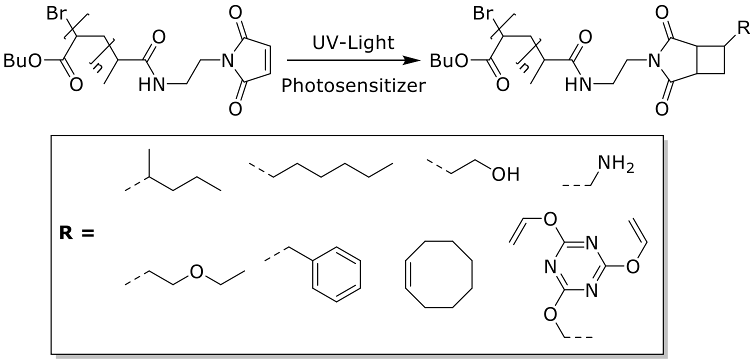

Scheme 1.7 Polymer end group modification in photoflow via [2+2] alkene-enone cycloaddition in the presence of a photosensitizer.

modification and the introduction of functionalities when being performed in flow, which is remarkable when keeping the low efficiency of the associated batch processes in mind.

1.3.4. Microparticles from UV-Photoflow Polymerization

As viscosity is a severe obstacle in solution polymerization, polymer synthesis is largely limited to low to intermediate molecular weights when carried out in a homogeneous solution. Only in very high dilution, high molecular weights are achievable in continuous flow. By changing the reaction mode to droplet-based or emulsified systems, high-molecular weight materials become available, as viscosity is in such cases no longer directly correlated with molecular weight. For such flow systems, also photo-induced polymerizations are of high interest, as they allow to separate the droplet formation and/or the nucleation process from the polymerization itself. In this section, the synthesis of polymer particles will be outlined, followed by approaches on inorganic nanoparticles, where the same advantage is utilized.

Different research groups have reported the synthesis of microparticles in microfluidic chip reactors via photo-initiated polymerization. Yeh and Lin described how to make very uniform microparticles via a water-in-oil emulsion flow technique.[112] With their developed microfluidic chip in combination with a 365 nm UV-light source, they produced microparticles at low cost and high throughput. By varying the mineral oil flow rate, they are able to control the particle size between 75 and 300 µm diameter with narrow size distribution. Lee and coworkers present in their work a way to introduce a biocatalyst into polymeric microparticles. For this they also use an emulsion microfluidic system in combination with a UV-light source.[113] Hwang *et al.* encapsulated magnetic nanoparticles in hydrogel microparticles.[114] To reach this aim, they used a water-in-oil emulsion in a T-junction microfluidic device. By building microfluidic devices with different microchannels, the geometry of the particles can be influenced. After the monodisperse magnetic emulsion droplets were created in the T-junction, the morphology of the particles was locked-in via photo-initiated polymerization of the droplets. As geometries, spheres, disks and plugs were achieved. The obtained microparticles showed a superparamagnetic behavior. An earlier work of the same group described how the microparticle geometry can be influenced by the microchannel geometry at the light source.[115] They used a similar setup to make multifunctional superparamagnetic janus particles.[116] For this, they mixed a magnetic and non-magnetic pre-polymer solution as water phase in mineral oil and polymerized in flow via photo-initiation. Under an external magnetic field, the resulting janus spheres can self-assemble in stable chain like microstructures. Other janus particles via photo-initiated polymerization in emulsion-flow process were made by Chen *et al.*[117] and Nie *et al.*[118] Microfluidic emulsion technology was also used in combination with photo-initiated polymerization to create microcapsules.[119] To achieve this, a double emulsion system was employed which allowed to influence the mechanical properties of the microcapsules. The thickness of the shell could be influenced by varying the flow rates of the inner and intermediate phase.

Du Prez and coworkers showed the production of different polymer beads in continuous photoflow reactors.[120-123] They generated droplets in a water-in-oil high internal phase emulsion. After the photopolymerization of the monomer droplets, particles with large macropores were obtained. Besides small spherical polymer beads of less than 400 µm diameter, rods[120] and capsules[122] could be made. In later reports, they used thiol-ene and thiol-yne chemistry in similar reaction setups in order to produce monodisperse macroporous and non-porous functional beads. After the fast radical-mediated polymerization, no further functionalization steps were required to achieve the targeted functional polymer beads.[121]

1.3.5. Photoflow Inorganic Material Synthesis

Not only organic or polymer materials can be synthesized in photoflow reactors, but also inorganic nanoparticles. The synthesis of silver, gold, platinum, palladium, rhodium and iridium nanoparticles has been reported as well as the synthesis of hybrid polyacrylamide/silver composite particles. The high interest in academic research and industry for noble metal nanoparticles is driven by their catalytic activities [124-126] and plasmonic properties.[127-129] These properties depend on the materials as well as on the size and shape of the nanoparticles. In the past, different pathways were developed to synthesize small particles with high surface-to-volume ratios. Besides nanocrystals, nonspherical particles like nanorods, nanodisks and nanoprisms were made.[130] To create these specific particles, synthesis procedures with high reproducibility and yield quality, such as narrow particle dispersities, are required.[131] Batch processes often exhibit concentration and temperature gradients which lead to inhomogeneous reaction conditions and result in quite large dispersities.[130] Different research groups have proven that the employment of microflow approaches leads to a major improvement of noble metal nanoparticle homogeneity.[132-138] The short and good mixing conditions in microflow reactors allow for the homogeneous initiation of nucleation, and thus for narrow size distributions.

1.3.5.1. Platinum Group Nanoparticles

Hafermann and Köhler decouple the synthesis of noble metal nanoparticles into 4 partial processes:[130, 131]

(1) mixing of reactant solution

(2) initiation of nucleation

(3) termination of nucleation

(4) completion of particle growth

The process separation in microflow synthesis allows to work under optimal reaction conditions to obtain high quality yields. In batch reactions, all steps are performed simultaneously as they are hard to separate. Process separation itself is achieved by employing a photochemical micro-continuous flow process.

Noble metal nanoparticles, in particular gold[131], iridium[130], palladium[130], platinum[130] and rhodium[130] were synthesized. Through a change of the total flow rate the nanoparticle size can be influenced. There is no general trend visible if slow or fast flow rates are needed to obtain the smallest nanoparticles.

A comparison between batch and flow synthesis of gold nanoparticles shows similar particle diameters but a significant lower size distribution. For the other used noble metals, a clear reduction in particle size in the flow process is observed (

Table **1.1**).

The obtained gold nanoparticles can be used as seed particles for the preparation of enlarged gold nanoparticles with defined sizes between 4 and 15 nm depending on the seed particle concentration. In contrast to other particle growing methods, no surfactants or shape-controlling additives are required when employing seeds from the photochemical microflow process.

Table 1.1 Comparison of the size of noble metal nanoparticles synthesized via photochemical and thermal flow processes and conventional batch synthesis.

Metal	Precursor	Method/Reagent	Particle Sizes
Au	$HAuCl_4$	Batch	2.9 nm[131]
		Photoflow / HMP	2 – 3 nm[131]
Ir	H_2IrCl_6	Batch / Ethanol	5.8 nm[139]
	$IrCl_3$	Photoflow / HMP	2.5 nm[130]
Pd	$Pd(acac)_2$	Batch / Ligand Exchange	8.7 nm[140]
	$Pd(NO_3)_2$	Photoflow / HMP	2.5 nm[130]
Pt	H_2PtCl_6	Batch / Ethanol	5.0 nm[141]
		Flow	3.0 nm[142]
		Photoflow / HMP	2.5 nm[130]
Rh	$RhCl_3$	Batch / Ethylene Glycol	3-7 nm[140]
		Photoflow / HMP	2.5 nm[130]

1.3.5.2. Silver Nanoparticles

Maggini and coworkers demonstrated how to grow silver nanoparticles (AgNP) under continuous photoflow conditions.[143] In a first step, they generated via a photochemical process small (<10 nm) citrate-stabilized silver nanoparticles (seeds). With increasing irradiation time, the lamp induces extensive aggregation of the nanoparticles. In a second step, the growth of silver nanoparticles from these seeds with different shapes is possible[144, 145] through the so-called *photovoltage mechanism*.[146] This process requires citrate, which is adsorbed on the seed nanoparticles, oxygen and light. The adsorbed citrate is photooxidized, yielding acetone-1,3-dicarboxylate and CO_2. Electrons are injected into the particle with the decarboxylation. This induces the deposition and reduction of Ag^+ ions to silver.[143] The morphology of the nanoparticles is mainly influenced by the amounts of citrate and oxygen in the solution.[147, 148] Till today, this process is conventionally mainly performed in cuvettes with a limited volume. Due to these volume restrictions, the process is time-consuming and larger amounts of AgNPs are difficult to access conventionally. Also reproducibility poses a problem in the batch-based production. In this case continuous flow reactors can be used to increase the productivity and the reproducibility of this process.

1.3.5.3. Polyacrylamide/Silver Composite Particles

Other possible applications of metal nanoparticles lay in polymer/metal composite materials. These materials feature special mechanical, electronic, optical, and chemical properties, which trigger interest in diverse fields.[149-153] Composite materials are mainly made by mixing the components or through in situ formation by chemical synthesis.[154] One way to handle these composite materials is the synthesis of microparticles, which are synthesized by the application of a droplet-based microfluidic technique with high homogeneity in size and chemical composition.[155, 156] Therefore, preformed monomer droplets are polymerized via photo-initiated radical polymerization.[157] Polymer particles containing metal particles are of high interest due to the complementary nature of the chemical and physical properties of both materials.[158]

1.4. Aim and Outline of Research

Highly precise and defined polymers with complex architectures will be increasingly used for specific applications in the future. Several pathways to synthesize these polymeric materials are known. Most of the pathways employ a heat driven reaction mechanism in a batch process. This combination leads to yield quality issues and is not very energy efficient. A solution to this problem can be to switch to (UV) light initiated and driven processes. To increase the efficiencies and especially the reaction rates of photoreactions, continuous flow reactors can be used.

The research aim during the various PhD projects was to develop and translate photo-induced controlled radical polymerization protocols for the use in continuous flow reactors. Till today, most polymerizations conducted in academic research are initiated by heat and performed in batch reactors, like small vials or bigger round bottom flasks. In this work, commercially available as well as self-build photoflow reactors are used to carry out controlled radical polymerizations.

As a starting point, transition metal-mediated polymerizations, namely copper and cobalt, are performed for the first time in continuous photo flow reactors. (**Chapter 2 and 4**). Block copolymers as well as statistical copolymers are synthesized and analyzed.

In **Chapter 3** the developed photo-induced copper-mediated polymerization system in continuous flow reactors is used to develop and synthesize complex star polymers. Multiblock copolymers with up to 7 chain extensions are realized. Thermal and pH responsive materials are synthesized and analyzed.

Photo-induced reversible addition−fragmentation chain-transfer polymerizations in microflow reactors are investigated in **Chapter 5**. The influence of reaction temperature, the choice of photo-initiator and the light intensity on the reaction rate and yield quality is investigated.

To better understand acrylate polymerization in general, occurring side reactions are also determined and measured in this work. In **Chapter 6** branching reactions occurring during acrylate polymerizations are analyzed. The degree of branching with increasing monomer conversion is monitored for a photo-initiated free radical polymerization. The influence of different UV-light sources and photo-initiators is also investigated.

Detailed kinetic parameters for *tert*-butyl acrylate are measured and determined in **Chapter 7**. The so called pulsed-laser-polymerization method is employed to measure and calculate backbiting and tertiary carbon propagation rates.

The following chapters of this thesis were published or submitted to various peer-reviewed journals and are written in manuscript style.

Chapter 2

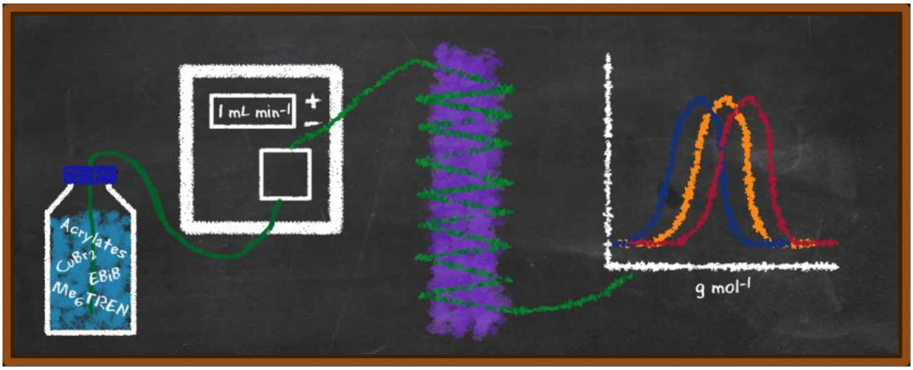

2. Photo-Induced Copper-Mediated Polymerization of (Meth)Acrylates in Continuous Flow Reactors[†]

2.1. Abstract

Photo-induced copper-mediated radical polymerization (photoCMP) was performed on a series of acrylate based monomers in continuous flow reactors. The monomers methyl (MA), ethyl (EA), *n*-butyl (*n*BA), 2-hydroxyethyl (HEA) and di(ethylene glycol) ethyl ether (DEGA) acrylate are investigated. All monomers show high livingness (dispersity in the range of 1.1 and linear first order kinetics) in the polymerizations. Conversions between 75 and 94 % are reached within 20 min reaction time. Apart from the commonly used solvent DMSO, a water/ethanol mixture was also used as a greener alternative without any loss in reaction control. Upscaling the reactor from 2 to 16 mL allows for the production of over 200 g of high-definition material (3000 g mol^{-1}, 1.1 dispersity) in overnight operation (18 h). Here it was demonstrated that the photoprocess can be run under very stable conditions even for extended reaction times. Besides homopolymers, block copolymers can also be successfully synthesized and poly(methyl acrylate)-*b*-poly(butyl acrylate) block copolymers with a similar low dispersity are obtained.

[†] First published partly as: “Photo-Induced Copper-Mediated Polymerization of Methyl Acrylate in Continuous Flow Reactors”, B. Wenn, M. Conradi, A. D. Carreiras, D. M. Haddleton, T. Junkers, *Polym. Chem.* 2014, 5, 3053-3060, “Ligand Switch in Photoinduced Copper-Mediated Polymerization: Synthesis of methacrylate-acrylate block copolymers”, Y.-M. Chuang, B. Wenn, S. Gielen, A. Ethirajan, T. Junkers, *Polym. Chem.* 2015, 6, 6488-6497 and “Photo-Induced Copper-Mediated Acrylate Polymerization in Continuous Flow Reactors” S. Railian, B. Wenn, T. Junkers, *J. Flow Chem.* 2016, DOI: 10.1556/1846.2016.00018. Parts of this chapter were done in cooperation with my colleagues Yami Chuang and Svitlana Railian.

2.2. Introduction

Photochemistry is an old branch of chemistry, which has, to date only played a minor role in materials synthesis outside of curing processes and in some highly specific applications in natural product synthesis. However, the enormous potential of photoreactions with regards to the economy and ecology reaction efficiencies is enormous. With the increasing popularity of continuous flow reactors, photochemistry has regained the interest of academic as well as industrial research.[54, 75, 159] Usage of photochemically triggered reactions allows for reaction pathways and mechanisms which are not or only indirectly accessible with thermally induced reactions. A main drawback of light induced reactions has always been the issues occurring with respect to scalability. Due to the Lambert-Beer´s law, light gradients developed in any photoreaction carried out in batch due to successive light absorption with increasing optical pathlength.[160] This problem might be negligible on small scale lab experiments but becomes rapidly significant in reaction upscaling, already at an intermediate laboratory scale. Continuous flow reactors, however, can give an obvious advantage and be a *game changer* for the application of photochemistry in (scalable) synthesis.

Within the realm of polymer chemistry, the large potential of using (photo)flow reactors for the synthesis of precision polymer materials has only recently emerged.[160] Precision polymer materials are commonly synthesized via living polymerization techniques, more specifically via reversible deactivation radical polymerization (RDRP) methods. RDRP gives access to polymers with high definition, narrow dispersity and sophisticated control over the macromolecular architecture. The advantage of using flow reactions for thermal RDRP has already been demonstrated.[87] The most applied RDRP methods are the so-called reversible addition-fragmentation chain transfer polymerization (RAFT)[11], nitroxide mediated polymerization (NMP)[161] and transition metal-mediated polymerization[162] such as atom transfer radical polymerization (ATRP)[163] and Cu(0)-mediated polymerizations.[164] In the past years, for all main RDRP methods also photo-induced processes have been discovered and investigated.[108, 110, 165] Successful photo-induced transition metal-mediated polymerizations are reported in literature using a broad range of catalysts, such as cobalt[166], iron[167], irridium[168] and copper.[38-40] Photo-induced copper-mediated polymerization (photoCMP) of acrylates in batch was introduced by the Haddleton group in 2014.[38] Shortly before, Mosnáček *et al.* reported on photo-induced ATRP polymerization of methyl methacrylate using ppm amounts of catalyst.[37] The detailed mechanism was investigated and proposed by Frick *et al.* via mass spectrometry measurements of the resulting species.[169] As mentioned above, photoflow polymerizations were also reported for cobalt[98] and iridium[93] mediated reactions. PhotoCMP was also successfully applied for grafting on silicon surfaces[170] or to make sequence defined oligomers with biological precision.[171] Additionally, two research groups reported lately on successful photo-induced RAFT polymerization in flow reactors.[99, 172] Baeten *et al.* used a photomicroflow reactor for inline UV-modification of phosphoesters via a thiol-ene reaction.[173]

While photoRDRP[10] has very interesting features, such as enhanced structural purity and ability for spatiotemporal control, its potential as a pure synthetic tool (where spatial control plays no major role) is to date largely unexplored, also owing to the scalability gap outlined above.

In this chapter, photoCMP is used in combination with continuous flow reactors, and the versatility of the technique is demonstrated. Continuous flow synthesis is demonstrated for a range of (acrylic) monomers, under variation of chain length and reaction solvent in order to reach greener reaction conditions (note that classical photoCMP required DMSO as solvent, which is certainly not sustainable with respect to commercial applications). In the final step, a two-stage reactor for a one step chain-extension is described, alongside an upscale to higher laboratory scale synthesis.

2.3. Results and Discussion

The application of photo-induced copper-mediated polymerization leads to a struggle with respect to these polymerization types to be directly solved when translating the reaction protocol to a flow system. Due to the rather low concentrations of copper that are required to mediate the polymerization (in the present case about 0.02 eq. compared to the initiator), strictly homogeneous reaction conditions are established and reaction blockage or fouling is eliminated. Thus the reactor channel widths play no important role and the polymerization can be applied to micro- and milliflow conditions. For the work described here, two different flow systems were compared: (i) a microflow glass-chip reactor (19.5 μL reactor volume, borosilicate) and (ii) tubular UV-flow systems with internal volumes of 2, 11 and 16 mL. Each system features distinct advantages. The microflow setup is best suited for kinetic studies under very economic conditions. Conversely, the tubular reactors are less sophisticated (the reactor itself consists of transparent PFA tubing wrapped around a UV-light source), but allow for synthesis of materials at significant scale due to the much higher internal volume. Light sources with peak wavelength at 365 nm were used; the irradiation spectrum is relatively broad. It should be noted that in the case of the microflow reactor, a conventional glass chip was used, thus optical transparency was limited at wavelengths below approximately 350 nm.

2.3.1. (Meth)Acrylate Polymerization in Continuous Tubular Photoflow Reactors

For the first steps, acrylate monomers and dimethyl sulfoxide as solvent were used. Good results were reported for this combination in batch processing.[38, 174] Thereby, the active copper species was generated from a Cu(II)Br_2 / tris[2-(dimethylamino)ethyl]amine (Me_6TREN) system (see Scheme 2.1). Literature has shown the good functionality of this metal/ligand pair.[38] Haddleton and coworkers also report on the usage of other ligands.[38] They show that the employment of tris(2-aminoethyl)amine (TREN) gives similar results in acrylate polymerizations looking at reaction rate and yield quality. As less promising ligand for acrylates *N,N,N′,N′′,N′′*-pentamethyldiethylenetriamine (PMDETA) was identified which led to higher dispersities and lower reaction rates. It was also

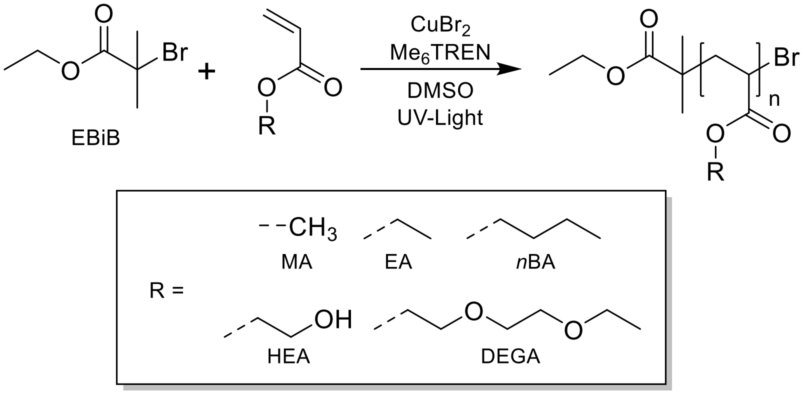

Scheme 2.1 Reaction scheme for photo-induced copper-mediated polymerization (photoCMP) and the used acrylate monomers.

stated that no polymer was formed using bipyridine (bpy) as ligand. As monomers, acrylate based systems with different polarities in the side chain were chosen and tested. Linear hydrophobic monomers such as methyl (MA), ethyl (EA) and *n*-butyl acrylate (*n*BA) were polymerized. Comparison of this short series of monomers helps to reveal the influence of the ester size on the polymerization performance. As more polar counterparts, 2-hydroxyethyl acrylate (HEA) and di(ethylene glycol) ethyl ether acrylate (DEGA) were tested, in order to cover synthetically more interesting materials (see Scheme 2.1 for structures of all monomers). All polymers were synthesized in a relatively simple, but efficient continuous tubular flow reactor consisting of PFA tubing wraped around a 15 W UV-light tube and a syringe pump to deliver the reaction solutions. All polymerizations were performed in DMSO between 50 and 55 °C (it must be noted that the temperature is a consequence of heat-up of the light source during reactor operation) with reaction times up to 20 minutes. In principle, longer reaction times could be used, but in order to allow for reasonable space-time yields, 20 min was chosen as an arbitrary maximum reaction time. Within 20 minutes, monomer conversion up to 95 % can be reached and longer reaction times did not lead to higher conversions. As initiator, EBiB was used in a ratio of 1:0.02:0.12 for [EBiB]:[$CuBr_2$]:[Me_6TREN]. All components were dissolved in the solvent, degassed and transfered into a plastic syringe. A second syringe was filled with degassed monomer with ratios of

25 or 45 to initiator and in a volumetric solvent ratio of 1:1. Both solutions were mixed right before entering the reactor in a static T-mixer.

Generally, conversion and thereby the degree of polymerization in a flow reaction are influenced by variation of the residence time. With increasing flow rates, lower residence times are achieved. The data shown in Figure 2.1 can simply be constructed from continuous polymerization under variation of the pump flow rate. At the same time, larger reactor volumes can be used at proportionally higher flow rates. Thus, increasing the reactor volume by a factor of two with concomitant increase of the flow rate by the same factor leaves the reaction product unaffected, but increases the overall yield of polymer twofold.

All polymerizations show high reaction rates with monomer conversions between 75 and 94 % within 20 minutes reaction time (see Table 2.1 for details). As important as high reaction rates for RDRP are, it is even more crucial to have a good control over the reaction and the length of the obtained polymer. Hence, linear growth of the polymer material alongside linear first-order kinetic plots with respect to monomer concentration must be observed. Obtaining a constant radical concentration means absence of radical termination. For all polymers, the measured number average molecular weights are in good agreement with the calculated theoretical values (Table 2.1). Dispersities (*Đ*) are around 1.1, indicating rather narrow molecular weight distributions (MWD) and a high control

Table 2.1 Overview over the obtained polymers from photoCMP in a continuous flow reactor for different acrylate monomers after 20 minutes reaction time.

	Monomer	**In:CuBr$_2$:Li:M**	**Conv. [%]**	**$M_{n,\,theo}$ [g mol^{-1}]**	**$M_{n,\,GPC}$ [g mol^{-1}]**	**Đ**
1	MA	1:0.02:0.12:45	77	3100	2600	1.12
2	EA	1:0.02:0.12:45	76	3600	2200	1.11
3	*n*BA	1:0.02:0.12:25	90	3000	3200	1.23
4	HEA	1:0.02:0.12:25	94	2900	1200	1.07
5	DEGA	1:0.02:0.12:25	83	4000	3000	1.10

over the polymerizations. The narrow distributions thereby do not only indicate good control, but also confirm that the residence time distribution (RTD) of the polymer is also narrow, since axial diffusion would increase the RTD and hence the overall dispersity of the resulting polymer. Only *n*BA is associated with a slightly increased dispersity of 1.2, which may still be regarded as in line with the other results. A similar deviating behaviour was reported previously for photoCMP polymerization of *n*BA in batch.[38] The reaction in flow is thus significantly faster compared to all previously reported batch photopolymerizations.

The kinetic first-order plots for all polymerizations show the required linear behavior (Figure 2.1), again underpinning the high level of control over the chain growth that is reached. Only few side reactions seemingly occur, and termination and radical transfer play no significant role in the reaction. Different slopes are observed in the plots, as well as a significant rate increase is observed for HEA, which can likely be correlated to a faster propagation of this monomer in highly polar media compared to the other monomers.

To test for chain length dependencies on the polymerization, the degree of polymerization (DP) was varied to 20, 45 and 110. No higher molecular weights

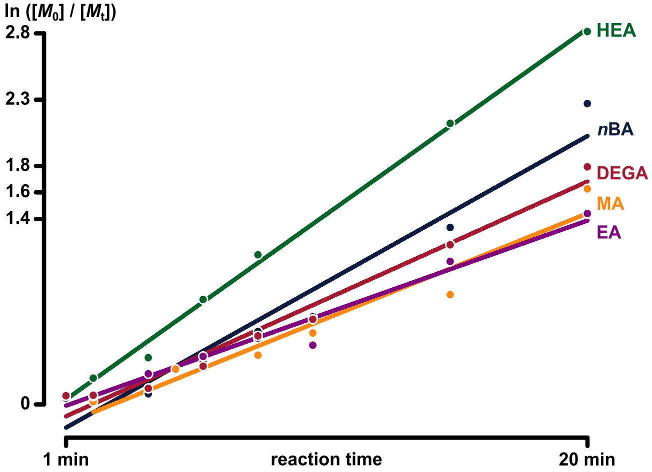

Figure 2.1 Kinetic first-order plots for photoCMP in DMSO of different acrylates in a continuous tubular photoflow reactor.

have been targeted at this point since DPs between 20 and 110 covers already a broad range of materials typically synthesized via controlled polymerizations. All three polymerizations show a linear increase in number average molecular weight (M_n) with respect to conversion, and very high conversions were reached in all cases within 20 minutes.

The molecular weight evolution of the three polymerizations can again be fitted linearly. In line with the observation of a well-controlled polymerization, a decrease in the dispersity of the polymers was observed (Figure 2.2). With a higher monomer conversion and a longer reaction time, the dispersity decreased for all the targeted molecular masses (from roughly 1.2-1.3 to about 1.1). Also in good agreement with the expected values, slightly higher initial dispersities were observed for increased monomer to initiator ratios.

As seen before for the different monomers, also for the three targeted DPs, the reaction proceeds under high control. All reactions showed good kinetic first-order linearity, indicating that the concentrations of the growing radicals remained approximately constant over the course of reactions. It can be assumed that radical concentrations in all three polymerizations were of a similar order.

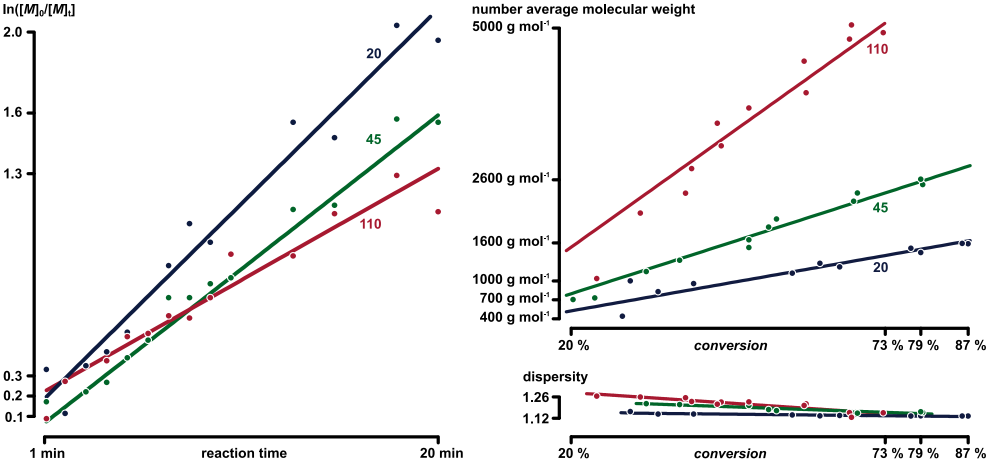

Figure 2.2 Development of the M_n of a photoCMP of MA, with targeted DPs of 20, 45 and 110, in a tubular milliflow reactor. The lines are best fits of the data.

Additionally, in combination with the linear increase in average molecular weight and low dispersity of the polymers obtained, it may be assumed that only very little transfer and termination events disturb the livingness of the reactions. Additionally, it was observed that no inhibition period occurs for the polymerization and that significant polymerization occurs already at very low residence times.

Besides the polymerization of acrylate, methyl methacrylate was polymerized via photoCMP in a continuous flow reactor. To achieve methyl methacrylate (MMA) polymerization via photoCMP, two parameters in the system were modified compared to the acrylate polymerization (Scheme 2.2). First, the solvent is switched from DMSO to a 80/20 vol% DMF/MeOH mixture. Secondly, Me_6TREN is changed to PMDETA, which showed in literature better results for the polymerization of MMA.[37, 169, 175] PMDETA as a ligand with lower activity, was reported to be more suitable for polymerizing MMA compared to a ligand with a higher activity (e.g. Me_6TREN). A recent report shows that in the presence of $CuBr_2$ and an initiator, MMA polymerization governed by Me_6TREN (i.e., a higher activity ligand) yields similar molar mass but broader dispersity compared to that governed by PMDETA (i.e. lower activity ligand).[175]

In a first attempt pMMA was synthesized in the presence of PMEDTA and $CuBr_2$ in DMSO. This reaction reached 80% monomer conversion in two hours. The broad distribution (Đ > 1.5) of pMMA after SEC measurement suggested a not-well defined control over polymerization and potential loss of end group fidelity. To gain a better control over pMMA polymerization, a different solvent, DMF/MeOH,

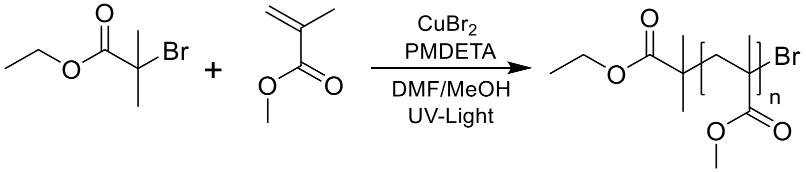

Scheme 2.2 PhotoCMP employing $CuBr_2$ and PMDETA in DMF/MeOH to synthesize pMMA.

was used to carry out the reaction. In this case, 76% monomer conversion was achieved. The so-obtained pMMA had an average molecular weight at 1500 g mol^{-1}, close to the theoretical value. The dispersity of the macroinitiator is 1.4, which is also in line with literature reports.[37, 176, 177]

Thus, MMA is mixed with $CuBr_2$, PMDETA and EBiB in DMF/Methanol (80/20 v/v%), degassed, and pumped into a tubular photoflow reactor for polymerization. Reactions were all well controlled. Figure 2.3 shows the increase in number average molecular weight with increasing reaction times. The reaction reaches a monomer conversion of close to 50 % with a residence time of 60 minutes in the photoflow reactor. In comparison to similar batch reactions the photoflow process is up to 3 times faster. Earlier, similar rate increases were also observed for the acrylate polymerizations. For small molecular masses (around 1000 g mol^{-1}), the dispersity of the photoflow pMMA is lower than a comparable batch product ($Đ$ = 1.15 instead of 1.37). What needs to be noted is that the dispersity slightly increases for longer targeted polymer chains (M_n = 2500 g mol^{-1}) made in the continuous tubular reactor setup ($Đ$ = 1.15 – 1.24). Still, definition of the

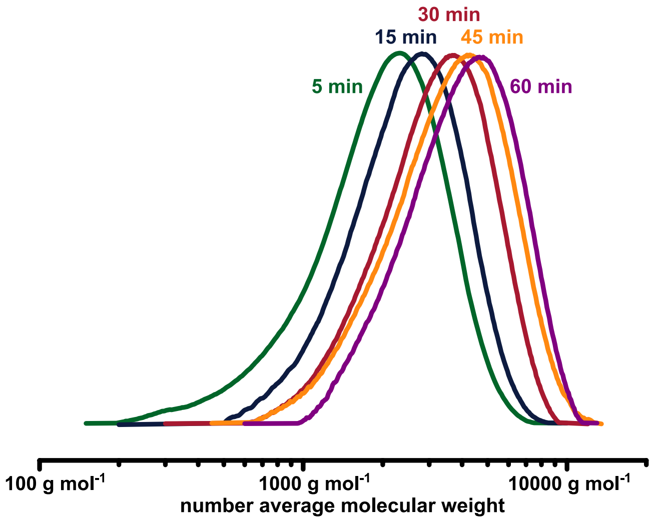

Figure 2.3 Development of molecular weight distributions of pMMA with increasing reaction times, synthesized via photoCMP in a continuous tubular photoflow reactor.

polymers is almost in all cases higher, underpinning the advantage that is gained by flow processing compared to batch reactions. The photoflow reactor clearly improves the reaction efficiency of the MMA photoCMP reaction.

2.3.2. Increasing Chain Length

After showing the wide applicability of photoCMP with methyl methacrylate and different acrylate monomers, the limits of the reaction concerning polymer chain length were tested. Increasing chain length is associated with several problems. Higher molecular weight material causes higher viscosities, and hence leads to increased pressure drops and eventually clogging of the reactor system. At the same time – characteristic for photoCMP – a lower polymerization rate must be expected when the initiator concentration is lowered (less bromine available for chain initiation). To my best knowledge, only degrees of polymerization up to 100 have been reported in literature for photoCMP flow processes. Here, the DP is increased stepwise, which corresponds to molecular weights in the range of 20000 g mol^{-1}. Target degrees of polymerizations were set to 500. However, due to limitations in the reaction rate (see above), maximum DPs reached in practice

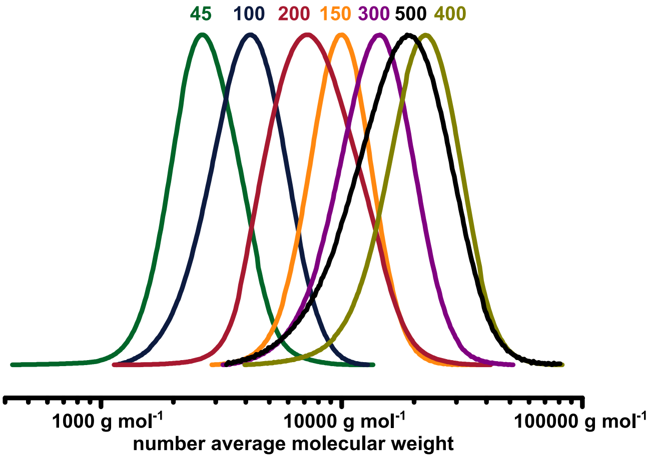

Figure 2.4 Molecular weight distributions for polymers made in continuous flow photoCMP of methyl acrylate under variation of the initiator concentration in order to produce materials with different target molecular weights.

Table 2.2 Target degree of polymerization (at hypothetical full monomer conversion), conversion after 20 min reaction time and theoretical and experimental number average molecular weight and dispersity for a series of methyl acrylate polymerizations.

	DP	**Conv. [%]**	**$M_{n,\ theo}$ [g mol^{-1}]**	**$M_{n,\ GPC}$ [g mol^{-1}]**	**Đ**
1	45	77	3100	2600	1.12
6	100	58	5100	3700	1.13
7	150	77	10000	9300	1.10
8	200	64	11000	8800	1.18
9	300	55	14300	12600	1.15
10	400	63	21800	19900	1.14
11	500	49	21200	16400	1.14

were about 250. Nevertheless, for most applications of high-precision polymer materials (i.e. biomedical use) as described herein, no longer polymer chains are required. The polymerizations were again performed in a continuous tubular reactor equipped with a 15 Watt UV-light tube. With higher targeted DP, an increase in number average molecular weight was observed, even if monomer conversions reached within 20 minutes decreased in accordance with the lowered initiation rate. In Figure 2.4 the MWDs of polymers obtained after polymerizations of 20 minutes are given, depicting a clear shift to higher molecular weights with increasing targeted DPs. Interestingly, while a rate reduction is observed, no quality loss in the product is seen, and all polymers are constant within error limits with respect to dispersity. All molecular weights obtained are in good agreement with calculated theoretical values, when monomer conversion is taken into account (Table 2.2).

2.3.3. Polymerization in a Chip Microflow Reactor

Besides the continuous tubular flow reactor, a microflow reactor was employed to carry out the photoCMP polymerization and to demonstrate that the reaction may also be performed in a true microfluidic device. In the microflow reactor, a reaction with a targeted DP of 45 was performed. A maximum conversion of 80 % was reached after a residence time of 20 minutes in this specific reactor and light source combination. Relatively comparable yields with the tubular flow reactor were observed. Overall, the polymerizations in the microflow reactor feature the same characteristics as in the continuous tubular flow reactor. Molecular weight evolution and dispersities are in the same range as in the polymerizations discussed above. Figure 2.5 displays the molecular weight distributions obtained from size exclusion chromatography (SEC), and scaled to monomer conversion of the respective samples. A clear shift of the distributions – also on the low-molecular weight side – is observed, which confirms that the reaction is easily applicable to a different reactor setup. The reaction is also interesting for larger

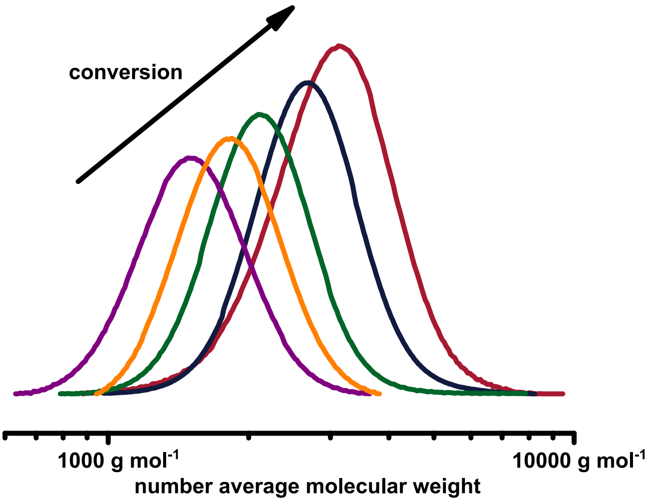

Figure 2.5 Molecular weight distributions of pMA with increasing residence time in the microflow reactor synthesized via UV-initiated copper-mediated polymerization and with a targeted DP of 45. All distributions are scaled to monomer conversion.

flow reactor systems in which kilogram (or higher) production of polymers can be achieved.

The first-order kinetic plot in micro- and milliflow reactions exhibit a good linearity, as seen in Figure 2.6. However, there is a somewhat lower slope, indicating that radical concentrations in both reactions are slightly different. Since the reactor volume and reactor type were changed and a light source of different intensity was used, this is not surprising. It must be noted that the linear fit of the microflow reactor data indicates that, at zero minutes residence time, some polymerization had already taken place (the reactor is fed by light-transparent syringes, thus polymerization could already occur in the feed). This demonstrates the sensitivity of the reaction. Therefore, it is important to keep the monomer separated from the initiator, ligand and $CuBr_2$, and mix them just before entering the reactor.

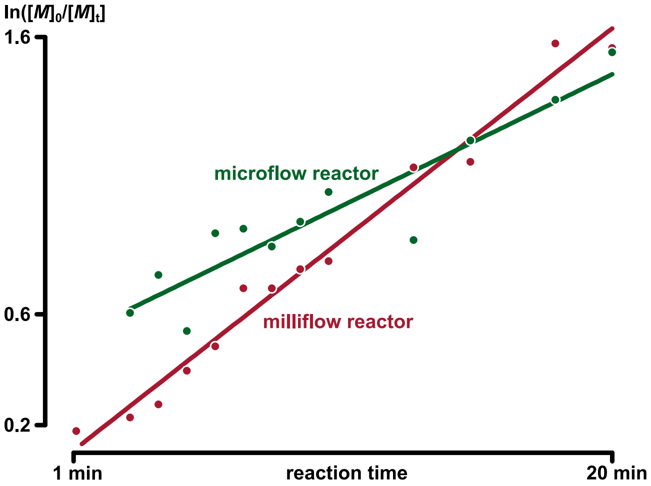

Figure 2.6 Comparison of the kinetic first-order plots of a UV-initiated copper-mediated polymerization of MA in a milli- and a microflow reactor.

2.3.4. Reaction Upscalling

As described, the main advantage of using continuous flow for photopolymerizations is the scalability of the reaction. In batch, photoCMP is usually not carried out above the lower gram scale, if not lower. Thus, the ability to go beyond this limitation was tested for the continuous tubular flow reactor design described above. While the above polymerizations were carried out in a 2 mL reactor with 0.75 mm inner diameter, a first scale-up was performed by employing PFA tubing with an inner diameter of 1 mm (outer diameter 1/16”) and a total internal volume of 16 mL was used (see right side of Figure 2.7). This reactor is relatively small and can easily be operated in a standard fume cupboard. Two Knauer Azura P2.1S HPLC pumps were used to deliver the two reaction solutions, which were chosen accordingly to the previous experiments (first solution containing initiator (EBiB, 1 eq.), $CuBr_2$ (0.02 eq.), Me_6TREN (0.12 eq.) and DMSO; second feed was bulk methyl acrylate). Also in this case, a relatively simple static T-mixer was used to efficiently mix both feed streams right before entering the reactor. At a reaction time of 40 min (as shown above, a slightly higher residence time does not harm the product and ensures better conversions), this reactor setup produces roughly 11 g of pMA per hour with a number average molecular weight of 3000 g mol^{-1} and a dispersity of 1.1. Important to note is that if the reaction conditions would change during operation of the reactor (due to fouling or inconsistent mass transport due to the viscous flow), a broadening of the molecular weight distribution of the collected material would inevitably occur, as variations in residence time lead to variations in absolute molecular weight. The reactor was operated continuously for 18 hours yielding over 200 g of high quality polymer (see Figure 2.7), still retaining very narrow molecular weight distributions. No further reaction optimization was required to achieve this upscale from the 2 mL to the 16 mL reactor. Further, 200 g of material may, for high precision photoCMP polymers, be regarded as a very significant production scale (due to the very high value of these materials), that are not easily reached on laboratory scale, even in conventional thermal batch polymerizations. Thus, scaling up the reaction is indeed simple, and reactor setups that produce 100 or

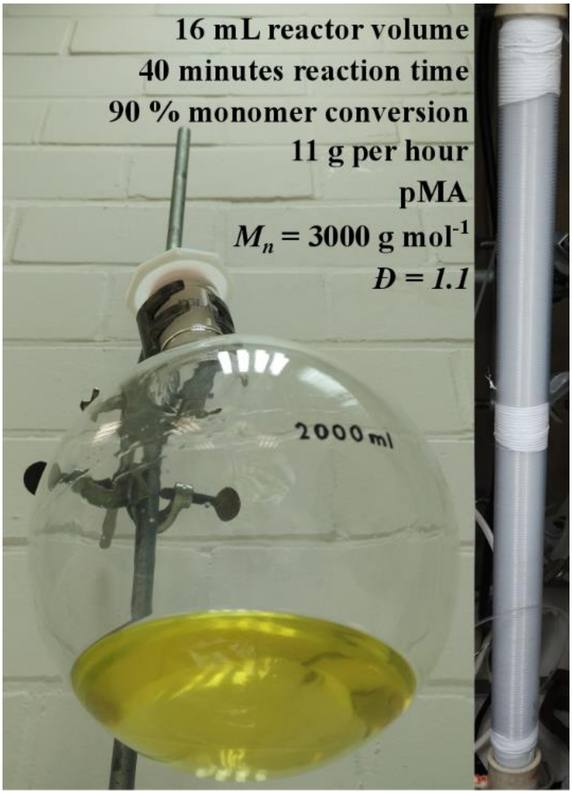

Figure 2.7 Photo of the tubular flow reactor with an internal volume of 16 mL (right) and the 200 g pMA obtained by collection of product over 18 hours in the same reactor (left).

more grams of highly precise polymers per hour should be no significant hurdle. Even larger amounts may only be limited by the available light choice. Further efficient upscaling can be achieved by increasing the tubing length/size or via reactor parallelization.[65]

2.3.5. PhotoCMP Using H_2O/EtOH as Solvent

PhotoCMP is routinely carried out in DMSO. Other polar solvents are equally suitable, with alcohol/water mixtures being a benign alternative. It should be noted that polymerizations should ideally be carried out in pure water. However,

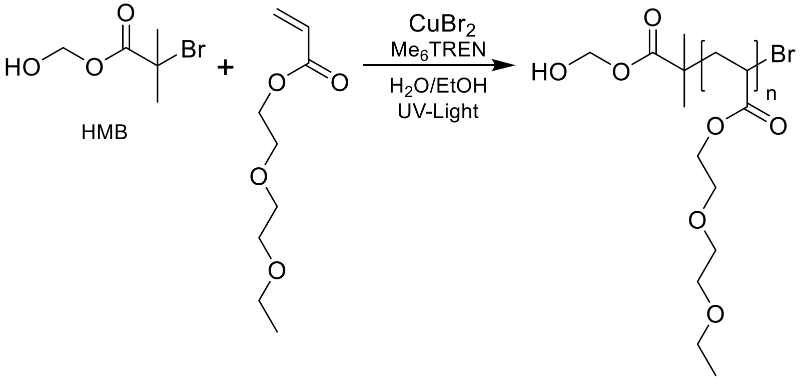

Scheme 2.3 Reaction scheme for the synthesis of pDEGA in H_2O/EtOH (50:50 vol%) via photoCMP

this has been shown to lead to a loss of control for batch reactions, which is a surprising result as Cu(0)-mediated reactions are in principle well compatible with water.[178] Here, it was tested whether the photoCMP reaction is suitable for flow processing when being carried out in a 50:50 vol% H_2O/Ethanol solvent mixture. For these tests, the water soluble monomer DEGA was used. The initiator was changed from EBiB to the more hydrophilic HMB (Scheme 2.3). For the polymerization, different chain lengths are targeted to show again the robustness of the system. Reactions with target DPs of 25, 50 and 100 were carried out, reaching almost quantitative conversion of monomer in all cases within 20 min reaction time (Table 2.3). In comparison to the polymerization of DEGA in DMSO (see Table 2.1, line 5), the conversion increased by 15 %, which may again be attributed to polar effects on the propagation rate of the monomer. However, the

Table 2.3 Number-average molecular weights, dispersities and conversion for the polymerization of DEGA via photoCMP in 50/50 vol% H_2O/EtOH in a photoflow reactor after a reaction time of 20 minutes.

	DP	**Conv. [%]**	**$M_{n,\ theo}$ [g mol^{-1}]**	**$M_{n,\ GPC}$ [g mol^{-1}]**	**Đ**
12	25	98	4800	5600	1.22
13	50	98	9400	6900	1.23
14	100	92	17500	12800	1.17

reaction in DMSO provided material with slightly better dispersity compared to reaction carried out in H_2O/EtOH.

Number-average molecular weights up to 13000 g mol^{-1} within 20 minutes reaction time were reached (Figure 2.8). Closer inspection of the kinetics reveal that 20 minutes are in these cases almost unnecessary as conversions above 90 % are observed after only 10 min. In many cases this might be regarded as sufficient for synthesis purposes. On the other hand, extending the reactor residence time also has no destructive influence on the reaction outcome. Dispersities remain widely constant, indicating that the polymerization comes to a mere halt rather than entering side reactions when monomer concentration diminishes (like it is often observed for other RDRP techniques).

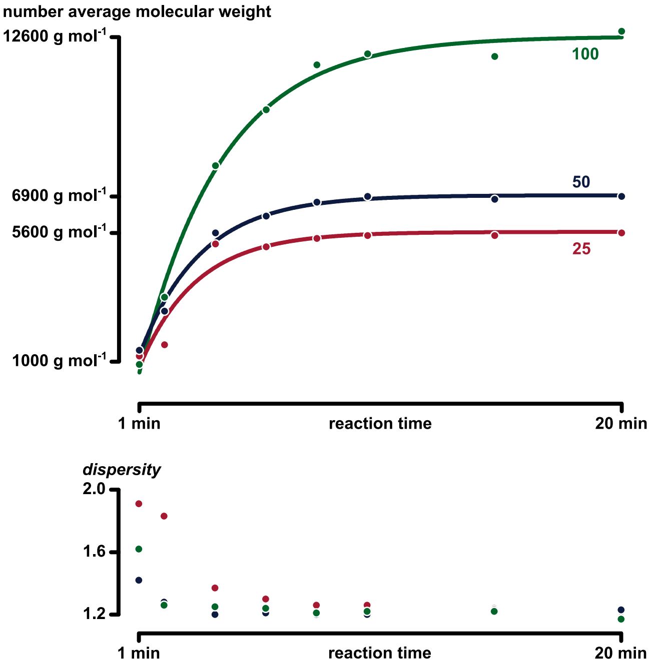

Figure 2.8 Evolution of number average molecular weights and dispersities of pDEGA in photoCMP using a 50/50 vol% H_2O/EtOH mixture as solvent for various target DP.

2.3.6. End Group Fidelity

Usage of sequential polymerization approaches unfolds the full potential of RDRP reactions. Through isolation of the polymer, followed by mixing it with fresh monomer and the catalyst, block copolymers become available after reinitiation. Especially when polymers with different solubility and miscibility are used, interesting materials can be quickly synthesized. To achieve this, an active end group on the polymer chain is necessary. The quality of the polymers was analyzed by mapping the end group fidelity via electrospray ionization mass spectrometry (ESI-MS). Samples of polymers from the polymerization with a target DP of 20 (M_n = 2000 g mol^{-1}) after a reaction time of 20 minutes were taken to check for the presence of termination products, which may decrease the livingness of the process. The polymer sample had a monomer conversion of 87 % and showed a very high degree of end group fidelity (see Figure 2.9 and Table 2.4). The ESI-MS spectra display only one single-charged product species, this being the sodium adduct of the expected structure with the initiator group in α position and a bromine atom at the ω site (Figure 2.9). With increasing reaction time, more double-charged polymers can be observed, which is associated with the increase in overall chain length of the samples. Even though traces of side products may be seen in the baseline of the spectra, there is no sign of termination products (as given in the table for one of the disproportionation species). The mass spectrometric analysis confirms the previous observation of the excellent livingness of the process. Although this observation was expected at this stage, this is a very satisfying result. UV-irradiation may cause several side products, ranging from self-initiated chains over crosslinking to polymer degradation. The practical absence of such product species confirms that the flow conditions only favor the desired product, but do not trigger other processes like it is often the case for UV-initiated batch reactions at similarly high light intensities. It should thereby be noted that additional samples taken at even higher conversions were analyzed with virtually the same result.

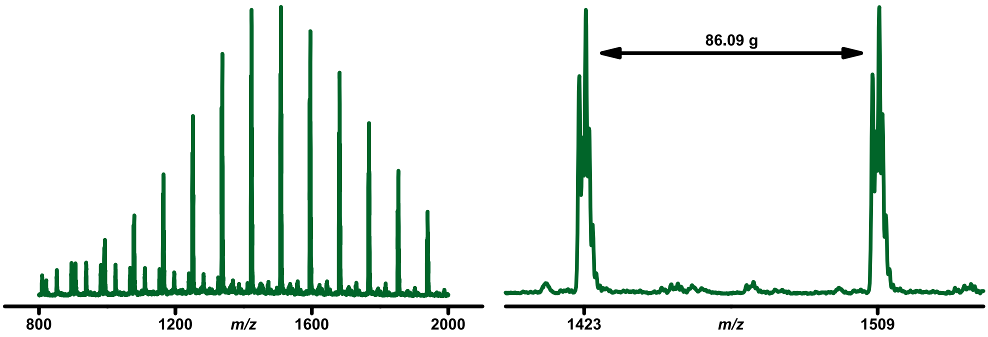

Figure 2.9 ESI-MS spectra and zoom in of poly(methyl acrylate) obtained by UV-copper-mediated polymerization in flow reactors after 20 minutes reaction time.

Table 2.4 Peak assignment of the ESI-MS spectra and the mass differences between experimental and theoretical m/z.

α end group	**ω end group**	**units MA**	**ion**	**m/z_{exp}**	**m/z_{theo}**	**δ / Da**
EBiB	Br	14	Na^+	1421.74	1421.54	0.22
EBiB	H	15	Na^+	-	1429.67	-

2.3.7. Block Copolymer Formation

Based on a pMA obtained from the continuous tubular flow reactor, block copolymers were synthesized in the microflow reactor. For chain extensions, *n*-butyl acrylate was polymerized with a maximum reaction time of 20 minutes. Reaction conditions analogous to the homopolymerizations were chosen. pMA with an M_n of 3100 g mol^{-1} and a dispersity of 1.10 was chosen as the starting material. The targeted M_n of the block copolymer was 7700 g mol^{-1} (at full *n*BA conversion, DP = 26) and a good control over the second block was achieved (Figure 2.10). Polymerizations proceed to high conversions and feature low dispersities. For example, at a *n*BA conversion of 51 %, a pMA-*b*-p*n*BA polymer with a M_n = 5000 g mol^{-1} and a dispersity index of 1.16 was obtained (theoretical M_n at this conversion is 5400 g mol^{-1}). Block copolymerizations can thus also easily be

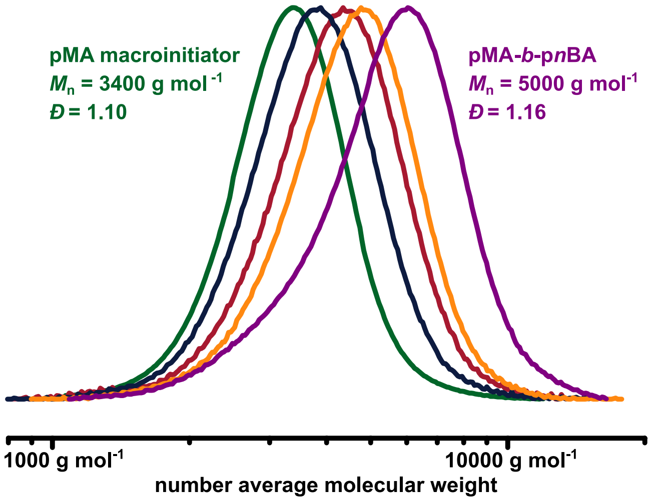

Figure 2.10 Evolution of molecular weight distributions for the pMA-*b*-p*n*BA block copolymers obtained in a microflow reactor and the distribution of the pMA macroinitiator.

addressed in flow reactions, again underpinning the versatility of the process, as well as the high livingness of the polymerizations.

In the next step, the synthesis of pMMA-*b*-pMA block copolymers was carried out in the continuous tubular flow reactor. First pMMA was synthesized as described above using PMDETA as ligand and DMF/MeOH as solvent. Before chain extenson the pMMA was purified and isolated. All residues of solvents, monomer, ligand and copper were removed. For the second flow stage, the pure pMMA macroinitiator (2600 g mol^{-1}, $Đ$ = 1.30) was dissolved with $CuBr_2$, Me_6TREN and MA in a DMSO/DMF (80/20 v/v%) solution and pumped through the tubular photoflow reactor channel. The choice of solvent was based on literature data[37, 100, 179], as well as on the experience gained throughout the linear homopolymers synthesis. The analysis of the pMMA-*b*-pMA block copolymer via SEC shows a clear shift in molecular weight to a higher mass for the chain extended polymer (Figure 2.11), even if some tailing to the low molecular weight side seems to occur. The addition of the pMA block to the pMMA macroinitiator occurs also faster in photoflow compared to the corresponding batch reaction. For the same conversion, however, similar molecular weight and dispersity was obtained.[100]

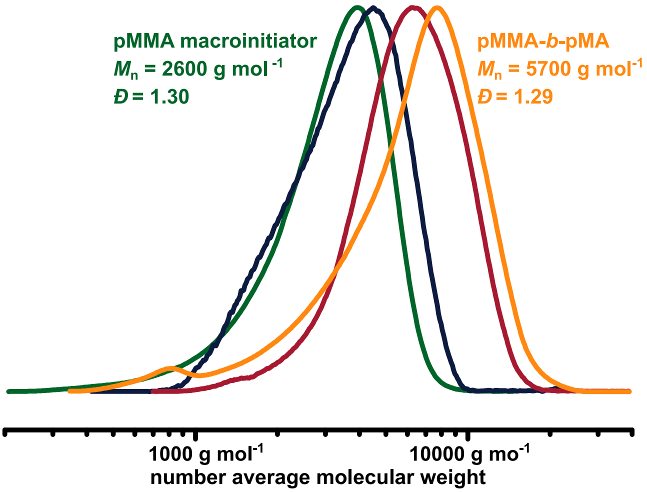

Figure 2.11 Increase in molecular weight after chain extension of pMMA to pMMA-*b*-pMA in the continuous flow photoreactor.

So far, the polymers were purified before their usage as macroinitiator for chain extention reactions. The purification between the two reactions makes the full process labor intensive and thus expensive. Using a reactor cascade can solve this problem. In case almost all monomer is used up in the first reaction stage, no purification is required before the addition of fresh monomers. Two serial flow reactors hence give direct access to (multi)block copolymers.[94, 106, 180] Consequently, the reactor setup was extended with a second stage. In principle, no additional light source is required as the tubing for both stages can conveniently be wrapped around the same light bulb. Two reaction solutions were prepared, degassed and filled in individual plastic syringes. One reaction solution contained the initiator, $CuBr_2$, Me_6TREN and the solvent (H_2O/EtOH). The second syringe was used to deliver the first monomer batch (DEGA). Both solutions were mixed in a static mixer before entering the reactor tube, which was wrapped around the UV-light tube. The exit of this reactor was connected with a second static mixer where the second monomer solution was added. Dilution is required in the second stage to avoid increasing viscosities with increasing polymer chain length. Polymer samples are collected after the first reactor stage and after passing through both stages. The experimental setup is schematically given in

Figure 2.12. It should be noted that in the present case, DEGA was used for both polymer blocks. No true block copolymer was hence obtained. DEGA is a very interesting monomer for amphiphilic block copolymer synthesis, and it is more convenient to chain extend with the same monomer for the sake of simpler polymer analysis (no change in Mark-Houwink parameters). In principle, the second monomer could be replaced by any alkyl acrylate; only molecular weight determination would be hampered in such case.

Two examples of successful one step chain extension reactions in batch reactors via photoCMP are reported.[181, 182] In both approaches, DMSO was employed. Here, the above tested H_2O/EtOH system was adopted to demonstrate the working principle of the coupled reactor setup, to not only accelerate block copolymer synthesis, but also to provide greener processing conditions at the same time. The reactor residence times were in both reactor stages set to 10 minutes, which allowed for a monomer conversion of 83 % and a number average molecular weight of 4500 g mol^{-1} ($Đ$ = 1.19, theoretical molecular weight of 4100 g mol^{-1}, see Figure 2.13) in the first stage. The reactor outlet was then directly mixed with a DEGA/H_2O/EtOH solution (50/25/25 vol%) and injected in the second reactor. After 10 more minutes reaction time, a polymer with a total molecular weight of 6500 g mol^{-1} (theoretical molecular weight of 6100 g mol^{-1}) and a dispersity of 1.2 was collected (Figure 2.13).

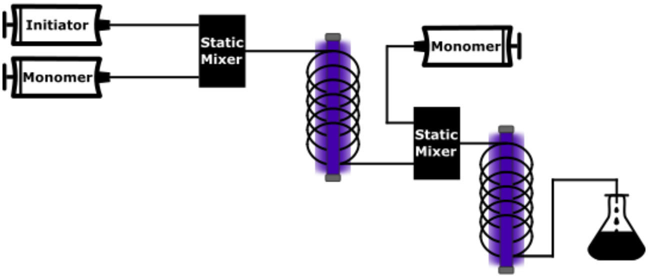

Figure 2.12 Schematic photoflow reactor setup for the one step synthesis of diblock copolymers.

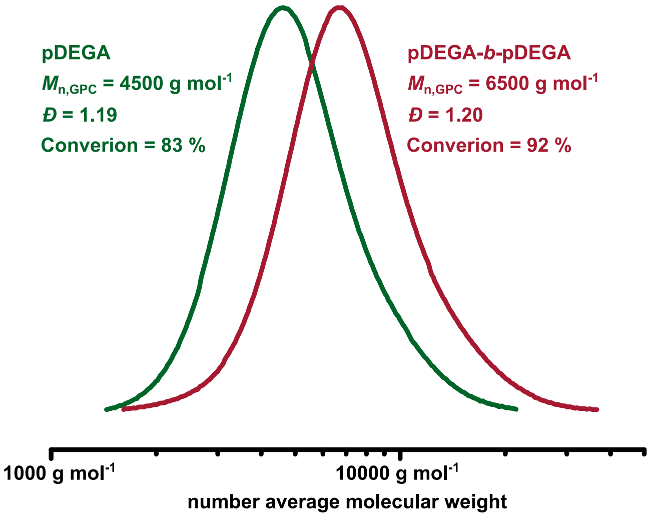

Figure 2.13 Molecular weight distributions of polymer obtained after the first and after the second reactor stage (both residence times set to 10 min per reactor coil).

2.4. Conclusions

Photo-initiated copper-mediated radical polymerization offers intriguing features for the design and synthesis of complex materials. The translation of the batch process to flow chemistry offers to scale this reaction up to the production of significant amounts. In batch, such scales are not directly possible due to light absorption profiles and insufficient penetration of light at increased optical pathlengths. The good applicability of photo-initiated copper-mediated polymerization for various acrylate monomers as well as for methyl methacrylate was demonstrated. Reactions could be performed in a commercial glass-chip microflow reactor (volume 19.5 μL) as well as simple tubular milliflow reactors (2, 11 and 16 mL). Excellent control over polymerizations is observed in both cases. Reactions follow first order kinetics, number average molecular weight increases linearly with monomer conversion and low dispersities are reached for all polymers obtained. Reactions are particularly fast and conversions in the range of 90 % are reached within 20 minutes reactor residence time. Polymers feature excellent end group fidelity and allow for efficient block copolymerizations. Further, the regularly used solvent DMSO can be exchanged with an ethanol/water mixture when polar monomers are used, making the process inherently greener. A first scale-up of the polymerizations is successful, hinting also at the commercial viability of the photopolymerization, with over 200 g of high-definition polymer materials being available without large efforts in a relatively small-size photoreactor (16 mL internal volume). Lastly, reactor couplings were determined, which allows in principle to obtain block copolymers in a single step procedure without requiring of intermediate polymer isolation.

Overall, the reactions described in this chapter provide an additional example for the increasing number of polymer reactions that benefit from microflow reactor applications and flow chemistry in general. The methods described herein make use of comparatively simple and versatile flow reactors and thus do not require sophisticated instrumentation. Both the microflow and the tubular reactor are comparatively cheap, easy to set up, and are thus of interest for the whole polymer community as a novel way to produce materials for a broad range of research projects. At the same time, the photo-induced copper-mediated polymerization process solves the general problem of inhomogeneity, which is commonly observed in thermal copper-mediated polymerizations in flow devices. Again, the photo-initiated process represent an attractive choice for the flow synthesis of materials from controlled polymerization.

Chapter 3

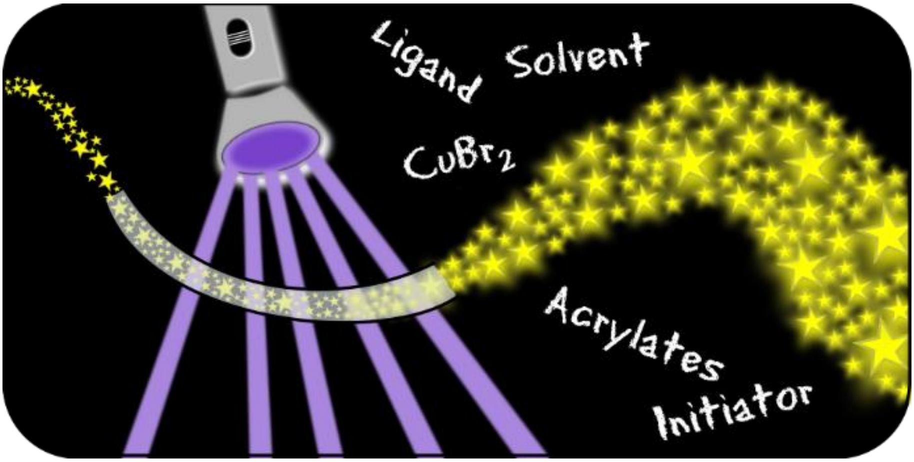

3. Efficient Multiblock Star Polymer Synthesis from Photo-Induced Copper-Mediated Polymerization with up to 21 Arms [‡]

3.1. Abstract

Photo-induced copper-mediated polymerization (photoCMP) is employed for the synthesis of multiarm-multiblock star copolymers. Based on a core-first approach, star polymers with four, six and twenty-one arms were synthesized. Due to the high efficiency of the photoCMP process with respect to reaction rate and end group functionality, each arm could be chain extended multiple times, allowing for up to 8 sequential polymerizations on the 4-arm star and up to 4 blocks on the 21-arm star. Relatively high dilutions of the reaction mixtures and premature stopping of the polymerizations between 50-70 % monomer conversion must be maintained in order to avoid occurrence of star-star coupling reactions. For the optimization of the reactions, microflow reactor polymerizations were used to achieve an economic and fast screening of the reaction. Flow reactors show improved control over the polymerizations, and are beneficial in the handling of large amounts of solvents, which are required to synthesize the multiblock star polymers in significant quantities. By switching between a n-alkyl acrylate and *tert*-butyl acrylate (that can be hydrolized to acrylic acid segments after polymerization) in the chain extensions, hierarchically structured star polymers are obtained, in which hydrophilic and hydrophobic blocks are alternated. These materials show pH responsiveness and complex self-assembly in aqueous phase depending on the number of arms and length of the individual blocks.

[‡] First published as: “Efficient multiblock star polymer synthesis from photo-induced copper-mediated polymerization with up to 21 arms”, B. Wenn, A. C. Martens, Y.-M. Chuang, J. Gruber, T. Junkers, *Polym. Chem.* 2016, 7, 2720-2727.

3.2. Introduction

The importance of UV-light to trigger reactions in industrial and academic polymer synthesis has been increasing for several years.[183] Significant advances were made in the field of photo-induced reversible-deactivation radical polymerization (photoRDRP) techniques.[39, 165, 183] For all main RDRP mechanisms, reversible addition-fragmentation chain transfer (RAFT),[15, 108] nitroxide-mediated polymerization (NMP)[161] and transition metal-mediated polymerisations like atom-transfer radical polymerization (ATRP)[28, 164, 184, 185] or Cu(0)-mediated polymerizations,[22, 31-33, 186] very efficient light initiated reaction pathways were identified.[15, 41, 99, 107, 108, 165, 187, 188] Since the first discovery of photoCMP for a linear system, the scope of the reaction has been continuously widened and various photo-initiators, ligands and solvents have been applied. The reaction rate of photoCMP can be increased by using a flow process instead of conventional batch reactors.[91] Additionally, flow reactors enable to easily upscale the photoreaction without increasing the reaction time or losing yield quality, which is difficult to reach in batch operation.[91] The very high reaction efficiency with respect to end group fidelity at high monomer conversions was unambiguously demonstrated by the synthesis of sequence controlled multiblock copolymers with up to 11 blocks in a one pot process without significant purification.[181, 189] However, most of the reported synthesis procedures focus on linear polymer architectures. To my best knowledge, only one example of photoCMP with a bi-functional initiator is to date reported (which strictly speaking still results in linear polymers). With such initiator, multiblock copolymers with up to 23 blocks (11 block extensions in both growth directions) and a degree of polymerization per block of up to 100 was obtained.[182]

In this chapter the focus is on the concept of multifunctional initiators in photoCMP reactions. Star polymers from 4 to 21 arms are synthesized and chain extended towards multiblock copolymer structures, thereby making use of the excellent performance of photoCMP with respect to reaction rate and end group fidelity (Figure 3.1). In order to tune the reactions towards maximum efficiency, the advantages of continuous (micro)flow reactors are employed (that is fast

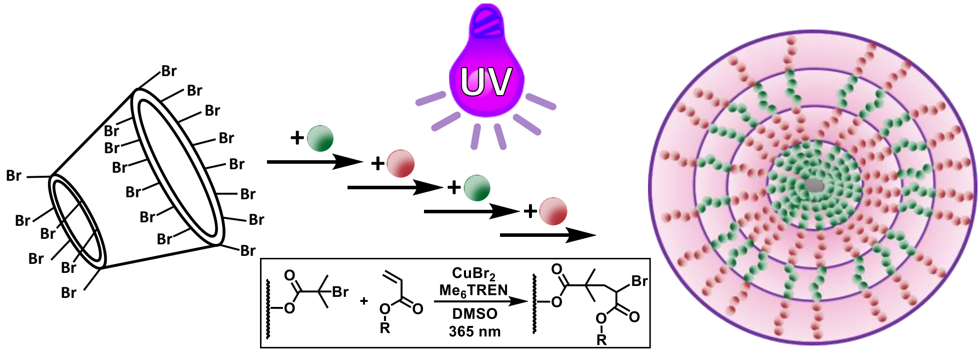

Figure 3.1 Reaction scheme for the polymerization of a multilayer 21 arm tetra block copolymer via photo-induced copper-mediated polymerization.

optimization of reactions, increased reaction stability). It allows to increase end group fidelities and to rapidly screen reaction conditions.

Two general synthesis approaches are available and used in the preparation of star polymers: the arm-first[190] and the core-first method.[191] In the arm-first approach, a mono-functional linear polymer chain is synthesized and coupled in a second step with a multifunctional core molecule. A drawback in this approach are the steric effects which come into play for arms with high molecular weights and/or high number of arms. This leads to less quantitative yields and a distribution of number of arms.[192] For the core-first approach a multifunctional initiator, that defines the number of arms to be grown, is required.[192, 193] Ionic polymerization methods were first used to demonstrate the core-first approach.[194] This approach has been successfully applied to RDRP techniques.[192, 193, 195-197] For these techniques, an in-depth optimization of the reaction conditions is necessary to supress and minimize side reactions, such as star-star coupling or chain transfer.[196, 197] Thus, highly efficient polymerization methods are required to allow for very high end group fidelities. Whittaker and coworkers demonstrated for Cu(0)-mediated polymerization the synthesis of a penta-block 5 arm star polymer without star-star coupling.[192] Becer and coworkers recently optimized this star polymerization by switching to water-based polymerization and achieved the synthesis of pentablock three-arm star polymers within 1.5 hour reaction time.[198]

In this study, photo-induced copper-mediated polymerizations are hence employed to target star shaped multiblock copolymers, whereby the scope of star polymer synthesis is largely extended by addressing systems with 4, 6 and 21 arms, starting from a core-first approach. As it will be shown, up to 8 blocks can be created per arm, thus extending the sequential multiblock copolymer concept.[199] For reaction optimization, a photoflow reactor was employed. Further, the obtained stars were investigated towards their self-assembly behaviour and responsiveness to pH changes.

3.3. Results and Discussion

3.3.1. Initial Tests on Star Polymer Synthesis via PhotoCMP

In this study, three different multifunctional initiators with 4, 6 and 21 initiating groups were employed (Figure 3.2). Multiblock star copolymers with up to 8 blocks per arm were obtained and analyzed. To best of my knowledge, this was the first time a 21-arm tetra-block copolymer with the core-first approach was synthesized. All polymerizations were carried out in DMSO as solvent, in batch and flow reactors.

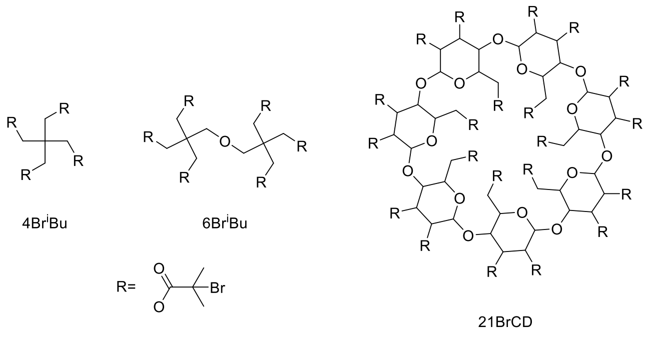

Figure 3.2 Structures of the synthesized multiarm initiators for photo-induced copper-mediated polymerization. Pentaerythritol tetrakis(2-bromoisobutyrate) (4Br^{i}Bu), dipentaerythritol hexakis(2-bromoisobutyrate) (6Br^{i}Bu) and, heptakis[2,3,6-tri-O-(2-bromo-2-methylpropionyl]-*ß*-cyclodextrin (21BrCD).

In a first step, a diblock 4-arm star polymer, starting from $4Br^{i}Bu$, was synthesized in a batch reactor at around 30 °C. The reactor was equipped with an online FTIR-probe for online monitoring the conversion. First, a methyl acrylate block with a corrected number average molecular weight of 2300 g mol^{-1} per arm (total corrected M_n = 9800 g mol^{-1}, $Đ$ = 1.10) was obtained with [CH-Br] : [Cu(II)] : [Me_6TREN] : [MA] equal to 1 : 0.01 : 0.075 : 23, where [CH-Br] stands for one initiating group. It should be noted that in conventional SEC calibration, an error occurs due to the star shaped structure of the polymers. This effect can, however, be largely corrected by applying a correction factor for star polymers.[200] While M_n is in this way determined with reasonable accuracy, the influence of calibration uncertainties on the dispersity is not assessed. This influence is, however, assumed to be negligible. The reaction mixture was diluted with DMSO (10:1 solvent to monomer volume). After degassing the solution by purging with argon, the reaction was started by switching on the UV-light. When the reaction reached a monomer conversion of 95 %, light was switched off and a sample for molecular weight distribution (MWD) analysis was taken. After adding *tert*-butyl acrylate (*t*BA) for the second block, the solution was purged again. The reaction for the second block was stopped after 4 hours with a monomer conversion of 75 %. The size exclusion chromatography data show a clear increase in molecular weight (Figure 3.3). A significant high molecular weight shoulder was identified for both curves, indicating the formation of undesired star-star coupling products during the reaction.

Previous studies demonstrated different ways to avoid star-star coupling at high monomer conversion, such as varying the copper concentration or employing two-phase systems.[192, 197] For the purpose of synthesizing star polymers, the copper(II) bromide concentration and the overall dilution of the reaction mixture was modified as a preventive measure. For the investigation of the effect of these parameters on star-star coupling, a 19.5 µL microflow reactor was used for fast

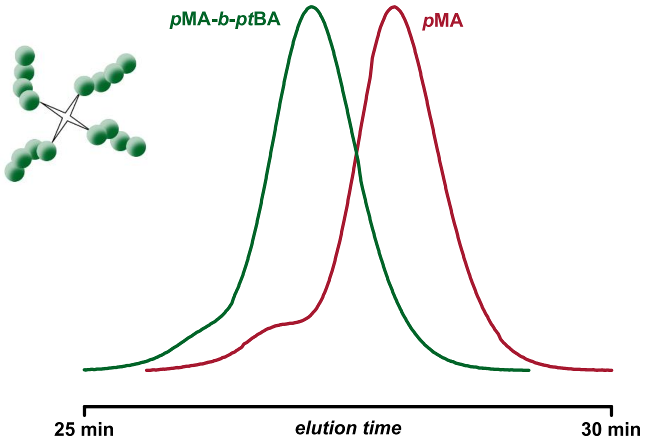

Figure 3.3 SEC traces from the synthesis of a pMA-*b*-p*t*BA blockcopolymer in a one-pot process with the 4-arm initiator (4Br^{i}Bu). The reaction mixture had a [CH-Br] : [Cu(II)] : [Me$_6$TREN] : [MA] ratio of 1 : 0.01 : 0.075 : 23 and was diluted with DSMO (10 : 1 DMSO to monomer volume).

and economic screening of the reaction parameters. Microflow, compared to batch reactions, offers the additional advantage that reaction progress over time can be screened systematically in a short period by simply changing the flow rate of the pumps (the flow rate determines the residence time in the reactor, and thus defines the total reaction time).

3.3.2. Reaction Optimization for Star-Star Coupling Reduction in Microflow Reactors

Flow reactors feature increased reaction stability, and can produce easily reproducible results in a short amount of time with minute amounts of reactants. Reaction outcomes between a flow and batch operation are comparable, even if better dispersities can sometimes be observed for a flow operation. In the present case, however, no significant difference was seen. For all further reaction optimization investigations, the 4Br^{i}Bu initiator system was chosen. First, the influence of the Cu(II) concentration on the star-star coupling was investigated. For this purpose, [CH-Br] to [Cu(II)] ratios of 1 : 0.01, 0.02 and 0.05 were

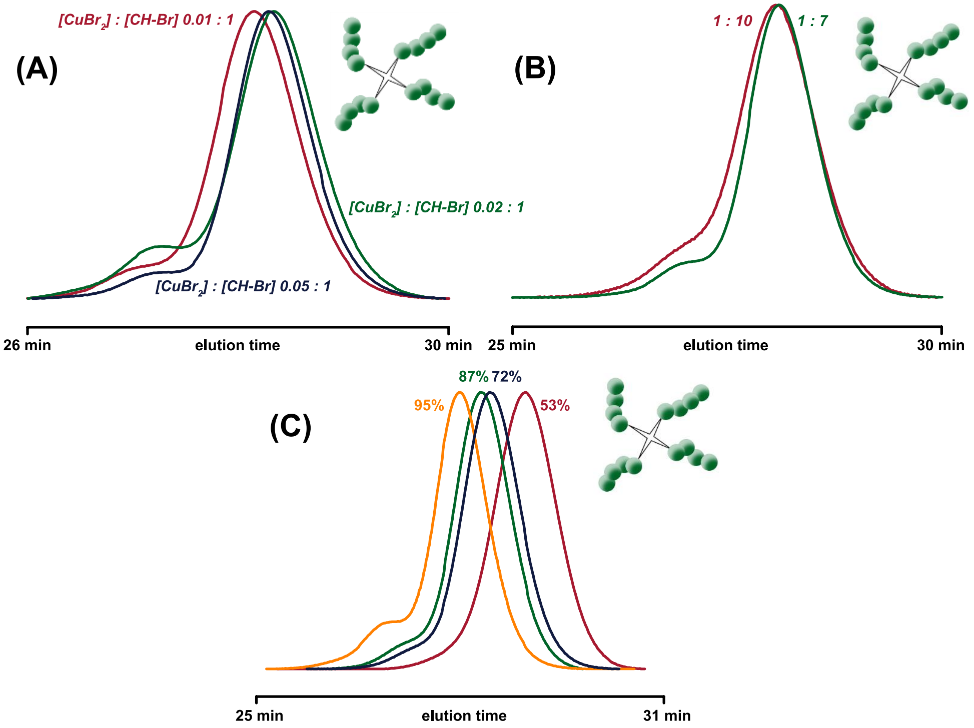

Figure 3.4 Influence of CuBr$_2$ concentration (A), dilution (B) and monomer conversion (C) on the occurrence of star-star coupling in photo-induced copper-mediated polymerization of methyl acrylate in DMSO using 4Br^{i}Bu as initiator.

employed. Me$_6$TREN as ligand and MA as monomer were added in a ratio of 0.075 : 23 : 1 with respect to CH-Br. DMSO was used as solvent with a dilution factor of 7:1 (solvent to monomer volume). After reaction times of 20 minutes, monomer conversions of up to 90 % were reached. Samples close to 90 % monomer conversion were analyzed via SEC (Figure 3.4 (A)). It was directly observed that the Cu(II) concentration has an influence on the star-star coupling reaction. Note that the nature of the star-star coupling reaction was not the focus of the present study. The sample taken from the polymerization with a CuBr$_2$ to CH-Br concentration of 0.02 : 1 exhibits the strongest shoulder in the MWD. Higher copper concentrations can potentially reduce the level of coupling during star polymer synthesis by suppressing termination events.[192] Indeed, for the highest tested concentration of 0.05 CuBr$_2$ per CH-Br unit the lowest high molecular weight shoulder was observed. However, for lower Cu(II) concentrations a reduction in coupling was also seen, which might be due to reaching an optimum concentration with respect to light activation in the system. For a $CuBr_2$ to CH-Br ratio of 0.01 : 1 a similar star-star formation rate was observed as for the highest concentration. Based on these results, experiments were continued with a copper concentration of 0.01 eq. per CH-Br group. Lower Cu(II) concentrations are desirable for biomedical application. A lower $CuBr_2$ concentration reduces the risk of reactor clogging in (micro)flow reactors due to salt precipitation.

After identifying optimal Cu(II) concentrations concerning star-star coupling, the influence of dilution on the system was tested. MWD analysis of a series of samples, made under increasing dilution, unsurprisingly demonstrate a beneficial influence of high dilution on star-star coupling (Figure 3.4 (B)), as an encounter between two star polymers in the active state is made less likely.

To obtain a full view over the appearing of star-star coupling in the synthesis of 4-arm star polymers, the development of coupling with increasing monomer conversion needs to be mentioned as well. The SEC elugrams of a 4-arm pMA star polymer, synthesized via photoCMP with ratios of 1 : 0.01 : 0.075 : 23 for [CH-Br] : [$CuBr_2$] : [Me_6TREN] : [MA] (1 : 7 dilution), are shown in Figure 3.4 (C) at different levels of monomer conversion. It can be clearly seen that until a monomer conversion of roughly 50% is reached, no significant coupling occurs. With increasing conversion up to 95%, the high-molecular weight shoulder becomes more and more pronounced. Accordingly, the dispersity increases from 1.11 at 53% monomer conversion to 1.22 for the polymer with 95% conversion. This dispersity increase might seem modest, however, very significant star coupling products are already formed (see Figure 3.4 (C)). It must also be taken into account that the dispersity of the individual arms is always larger than the dispersity of the full star molecule.

As a conclusion from these tests, star-star coupling is reduced by choosing an optimal $CuBr_2$ concentration in relation to the initiator concentration. Secondly, a higher dilution is favored and, finally, reactions must be stopped prematurely in the range between 50 and 70% monomer conversion. In this conversion range, coupling does not occur even at higher concentrated reaction mixtures. Higher dilutions may in principle allow to go towards even higher monomer conversions. Wether a higher dilution or an earlier stop of the reaction is favored is, however, an economic question. Sacrificing significant amounts of monomer – which are in principle easily removed from the system – may be seen as the 'lesser evil', and for the upcoming experiments, intermediate dilutions in conjunction with stopping polymerizations at lower conversions were used. As a side note, here the photo-induced character of the reaction is very advantageous, as reactions can be stopped without addition or subtraction of any reagent.

3.3.3. Synthesis of Star Shaped Block Copolymers

After optimization of the reaction protocol, various star shaped block copolymers were targeted to evaluate if the photoCMP process is equally effective for multifunctional initiators as for linear chain propagation. Methyl acrylate (MA), *n*-butyl acrylate (*n*BA), *tert*-butyl acrylate and di(ethylene glycol) ethyl ether acrylate (DEGA) were chosen to cover a variety of acrylate monomers with different properties. As a first proof of principle, a star shaped pentablock copolymer starting from $4\mathrm{Br}^{i}\mathrm{Bu}$ was synthesized. MA, DEGA and *n*BA were used as monomers for the different blocks. For the synthesis, the above described optimal reaction conditions were used in a dilution of 1 : 10. The reaction was carried out as a batch process for the sake of simplicity. Figure 3.5 shows the MWDs of the 4-arm star shaped block copolymer after each block extension. The molecular mass increased with the addition of each block and showed a clear and clean shift in the distributions. Note that since Mark-Houwink parameters are unknown for the specific block copolymers the number average molecular weight cannot be determined precisely and that the given values (see Table 3.1) are based on methyl acrylate homopolymers. Each reaction was stopped at a monomer conversion between 25 and 40 % to avoid star-star coupling. For each of the four arms, a degree of polymerization of 23 with a molecular weight of 2000 g mol^{-1} was targeted. SEC analysis gives a $M_{\mathrm{n,\ star}}$ value of 2700 g mol^{-1} for the first block after application of a correction factor of 1.42 for a 4-arm star.[200] The core has a mass of around 700 g mol^{-1}, which leads to an average weight of 500 g mol^{-1} per arm. This value is in agreement with the expected chain length for a monomer conversion of 33 %. For the other values and conversion numbers, the reader is referred to Table 3.1, line 1. With increasing length per arm, the risk of star-star coupling increased. Thus, for each extension the dilution successively increases. Starting from a monomer to solvent ratio of 1 : 10 it is increased to 1 : 20, 1 : 25, 1 : 30 and 1 : 35 in the fifth block. While this dilution of monomer seems large, the polymer content decreases less in the sequence as molecular weight increases significantly in each step.

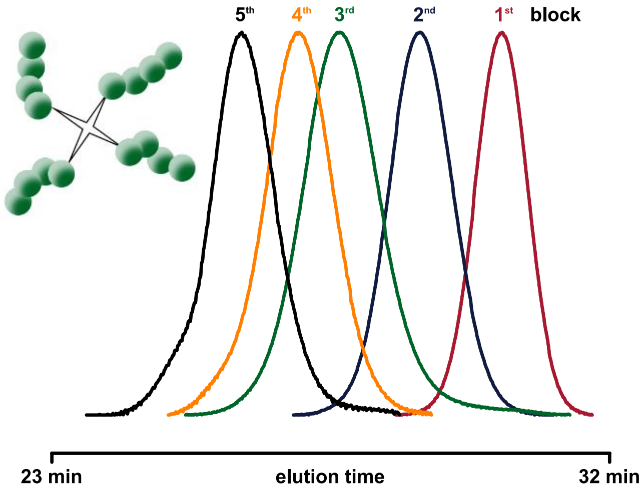

Figure 3.5 SEC diagram of a pentablock copolymer synthesized via photo-induced copper-mediated radical polymerization with a tetrafunctional initiator in the core-first approach. The reaction was done in a batch process with reactant ratios of 1 : 0.01 : 0.075 : 23 for [CH-Br] : [$CuBr_2$] : [Me_6TREN] : [Monomer]. For the block synthesis the following monomers were used MA (1st + 5th block), DEGA (2nd + 4th block) and *n*BA (3rd block). An increase of molecular weight for each block can be seen.

Table 3.1 Overview over the synthesized star polymers with number average molecular weights corrected with literature known correction factors[200] for the whole molecule ($M_{\mathrm{n,\,star}}$) and for each arm. [a] pMA-*b*-pDEGA-*b*-p*n*BA-*b*-pDEGA-*b*-pMA, [b] pMA-*b*-p*t*BA-*b*-pMA-*b*-p*t*BA-*b*-pMA-*b*-p*t*BA-*b*-pMA-*b*-p*t*BA, [c] pMA-*b*-p*t*BA, [d] pMA-*b*-p*t*BA-*b*-pMA-*b*-p*t*BA, [e] pMA-*b*-p*t*BA, [f] pMA-*b*-p*t*BA-*b*-pMA-*b*-p*t*BA, [g] pMA-*b*-pDEGA. Dispersity: $Đ = M_{\mathrm{w}}/M_{\mathrm{n}}$.

	Initiator		**1st**	**2nd**	**3rd**	**4th**	**5th**	**6th**	**7th**	**8th**
1[a]	4Br^{i}Bu	$M_{\mathrm{n,\,star}}$ [g mol^{-1}] ($Đ$)	2700 (1.07)	5400 (1.10)	10900 (1.18)	17300 (1.13)	29700 (1.15)			
		$M_{\mathrm{n,\,star\ theory}}$ [g mol^{-1}]	3400	7500	11200	15500	26300			
		$M_{\mathrm{n,\,per\ arm}}$ [g mol^{-1}]	500	1200	2600	4200	7300			
		conversion [%]	33	34	31	36	75			
2[b]	4Br^{i}Bu	$M_{\mathrm{n,\,star}}$ [g mol^{-1}] ($Đ$)	2800 (1.08)	4400 (1.08)	8900 (1.09)	11800 (1.10)	14500 (1.10)	16000 (1.11)	17200 (1.11)	17900 (1.12)
		$M_{\mathrm{n,\,star\ theory}}$ [g mol^{-1}]	4100	8800	9800	15100	16700	17800	21300	22300
		$M_{\mathrm{n,\,per\ arm}}$ [g mol^{-1}]	500	900	2100	2800	3500	3800	4100	4300
		conversion [%]	42	76	45	52	41	41	67	64
3[c]	4Br^{i}Bu	$M_{\mathrm{n,\,star}}$ [g mol^{-1}] ($Đ$)	21000 (1.16)	33700 (1.13)						
		$M_{\mathrm{n,\,star\ theory}}$ [g mol^{-1}]	22300	42000						
		$M_{\mathrm{n,\,per\ arm}}$ [g mol^{-1}]	5100	8300						
		conversion [%]	30	40						
4[d]	6Br^{i}Bu	$M_{\mathrm{n,\,star}}$ [g mol^{-1}] ($Đ$)	8400 (1.08)	16400 (1.08)	22500 (1.09)	29400 (1.11)				
		$M_{\mathrm{n,\,star\ theory}}$ [g mol^{-1}]	10900	17000	27900	31000				
		$M_{\mathrm{n,\,per\ arm}}$ [g mol^{-1}]	1200	2500	3600	4700				
		conversion [%]	41	36	48	53				
5[e]	6Br^{i}Bu	$M_{\mathrm{n,\,star}}$ [g mol^{-1}] ($Đ$)	25300 (1.15)	41200 (1.34)						
		$M_{\mathrm{n,\,star\ theory}}$ [g mol^{-1}]	22800	48300						
		$M_{\mathrm{n,\,per\ arm}}$ [g mol^{-1}]	4000	6700						
		conversion [%]	30	32						
6[f]	21BrCD	$M_{\mathrm{n,\,star}}$ [g mol^{-1}] ($Đ$)	30000 (1.12)	50000 (1.21)	51600 (1.22)	55700 (1.14)				
		$M_{\mathrm{n,\,star\ theory}}$ [g mol^{-1}]	21100	39700	68500	61300				
		$M_{\mathrm{n,\,per\ arm}}$ [g mol^{-1}]	1200	2200	2300	2500				
		conversion [%]	40	23	44	23				
7[g]	21BrCD	$M_{\mathrm{n,\,star}}$ [g mol^{-1}] ($Đ$)	98000 (1.19)	135100 (1.15)						
		$M_{\mathrm{n,\,star\ theory}}$ [g mol^{-1}]	145400	213900						
		$M_{\mathrm{n,\,per\ arm}}$ [g mol^{-1}]	4500	6200						
		conversion [%]	56	46						

3.3.4. Increasing Number of Blocks and Arms per Molecule

In this section, more complex architectures were approached. The number of attached blocks per arm was increased to eight, with a total corrected molecular mass of 17900 g mol^{-1} (Figure 3.6). Each arm had a molecular weight of 4300 g mol^{-1} consisting of MA and *t*BA blocks in an alternating order. Assuming that two arms together form in principle one linear element in the polymer structure, a total length of 15 blocks was obtained.

Larger star shaped polymer architectures were created by employing multifunctional initiator molecules containing more initiating groups. First an initiator carrying six initiating groups (6Br^{i}Bu) was used to attach up to 4 blocks to each arm. Here, a corrected total molecular mass of 29400 g mol^{-1} or 4700 g mol^{-1} per arm was realized. With both initiators, diblock MA and *t*BA copolymers were also synthesized with an increased block length. The 4Br^{i}Bu based polymer reached a total corrected molar mass of 33700 g mol^{-1} or 8300 g mol^{-1} for each arm. 41200 g mol^{-1} as corrected total molecular mass was achieved for the initiator core with six initiating units. The largest star shaped

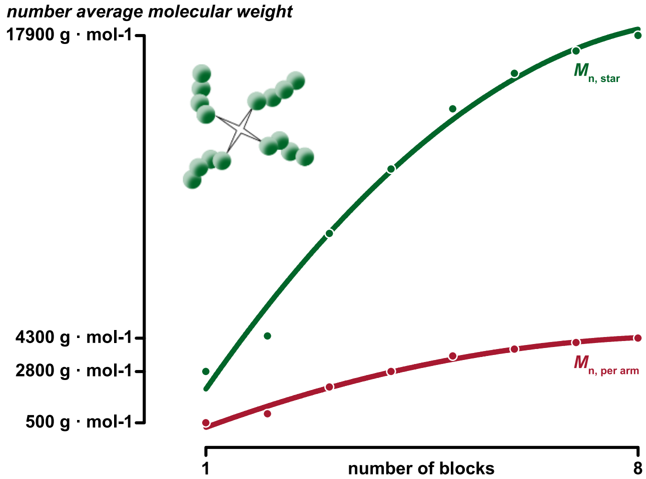

Figure 3.6 Number average molecular weights for the synthesized octablock copolymer based on a 4-arm core molecule (4Br^{i}Bu). The measured molecular weights were corrected with a literature known factor[200] to obtain more accurate values.

polymer in this work is based on a *ß*-cyclodextrin core carrying 21 initiating groups. With this core, up to four chain additions were realized, reaching molecular weights of a total of 135000 g mol^{-1}. It was demonstrated that not only a very significant number of arms can be achieved, but also relatively high overall molecular weights. As a word of caution, it should be mentioned that with every progressive chain extension an increasing number of arms will have lost their bromine end group due to termination, as is the case for any multiblock copolymerization. Additionally, if the inserted block length is too short, a statistical probability exists where certain arms may not add a single monomer unit – again an effect that is common to all multiblock copolymerizations.[201] Hence, numbers given for arm length and number of blocks must always be considered with certain care, as sequence defects exist.

3.3.5. Self-Assembly Behavior

One promising application for multiarm amphiphilic star polymers is its use as a unimolecular drug delivery system. As many active pharmaceutical ingredients (APIs) are hydrophobic, drug carriers are required that are able to carry such payload, while being hydrophilic on the outside.[202] The development of such carriers is an ongoing task. The herein synthesized multiblock-star polymers can give access to such property, if the alternating blocks switch from hydrophilic to hydrophobic. In such case, the inner hydrophobic segments can load molecules and serve as a transporter protected by the hydrophilic shell segments, a concept that is very well studied for a large body of micelles formed from linear amphiphilic polymers. By connecting the different arms in a star polymer, a more stable system can be designed, which then constitutes a single molecule drug delivery system.[203] As a further advantage, the materials obtained from multiblock copolymers with significant number of arms feature a hierarchical structure in that hydrophobic and hydrophilic segments alternate, ideally in an onion-like structure, which might aid binding of materials inside the polymer.

Table 3.2 Measured micelle diameter for different star block copolymers containing alternating pMA-*b*-pAA blocks measured via DLS. 0.01 g mL^{-1} polymer dissolved in a 90/10 v/v% H_2O/EtOH mixture and ultra-sonicated for 15 s before measurement. Remains of TFA in the polymer created an acidic solution (pH 2). [a] Measured before hydrolysis, [b] basic environment (pH 13), [c] neutral environment (pH 7), pMA-*b*-pDEGA block copolymer, [d] measured at 10 °C, [e] measured at 25 °C, [f] measured at 35 °C.

Initiator	**Blocks**	**$M_{n,\ per\ arm}$[a] [g mol^{-1}]**	**Particle diameter – D_{50} [nm]**	**Đ**
4Br^{i}Bu	2	900	56	0.24
	4	2800	25	0.32
4Br^{i}Bu	2	8300	143	0.31
			13[b]	0.44
21BrCD[c]	2	6200	79[d]	0.18
			103[e]	0.22
			135[f]	0.15

To create amphiphilic systems, the *tert*-butyl functionalities in the multiblock copolymers were hydrolysed to acrylic acid (AA) under acidic conditions. ^{1}H NMR was used to confirm the successful hydrolysis by the disappearance of the characteristic *t*BA peak. As the core molecule is connected via ester moieties, its stability was tested prior to *t*BA hydrolyzation, and trifluoroacetic acid (TFA) treatment of the core alone shows that it is stable under the given conditions.

In the following, the particle size of the amphiphilic star shaped block copolymer systems was determined via dynamic light scattering (DLS) in an aqueous solution. Overall, self-assembly of the star polymers was observed, and unless very dilute conditions were chosen, the polymers were not in a single-molecule state. Changes in the size of the aggregates were observed depending on the block length, number of arms and pH (Table 3.2). Micelles of 4-arm pMA-*b*-pAA block copolymers with short block length decreased in size with the addition of additional blocks (Table 3.2 line 1). This can be explained by a decreasing number of star polymers forming the resulting micelle, thus getting closer to a single-

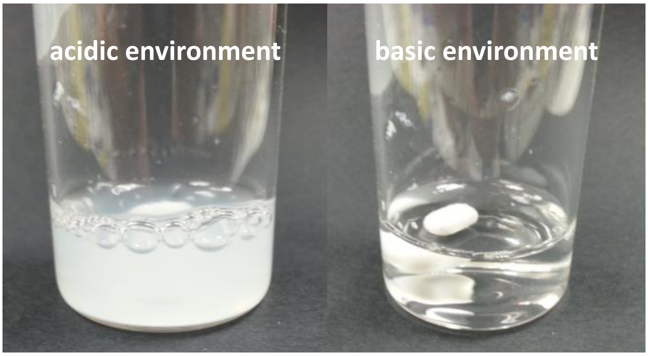

Figure 3.7 Turbidity of a 4-arm pMA-*b*-pAA star copolymer (Table 3.2, line 2) in acidic and basic solutions.

molecule nanoparticle. For a $4Br^iBu$ based pMA-*b*-pAA polymer with an average mass of 8300 g mol^{-1} per arm, a particle diameter of 143 nm in an acidic environment was measured. When changing to a basic system the size drops to 13 nm. This change in particle size was also be observed with the naked eye, with a change in the turbidity of the solution. This indicates a clear and expectable pH-response of the pAA segments (Figure 3.7).

Besides pH sensitive star block copolymers, a thermal responsive material was synthesized. To achieve this, the pAA(p*t*BA)-block was replaced by a thermal responsive poly(ethylene glycol) acrylate block. For a thermal responsive 21-arm star block-copolymer an increase in particle size with increasing temperature was observed (Table 3.2, line 3), which offers the possibility for a wide range of applications for the synthesised multi-arm block copolymers.

3.4. Conclusions

PhotoCMP was applied for the synthesis of multiarm-multiblock star copolymers. Reaction conditions were optimized for the multiblock copolymerization of a 4-arm star, following the core-first technique. Cu(II) concentration, the factor for dilution, and monomer conversion were optimized for best performance of the reaction with respect to reaction rate and occurrence of star-star coupling products. Various multiblock copolymers were obtained with 4-arm star materials with up to 7 consecutive chain extensions (resulting in linear elements of 15 blocks). Further, six-arm and finally 21-arm star polymers were successfully obtained, with a four-block 21-arm star polymer reaching a molecular weight of up to 135 000 g mol^{-1}. By copolymerization of a linear alkyl acrylate and *tert*-butyl acrylate, and after post-polymerization hydrolysis of the *tert*-butyl ester, amphiphilic materials were created. These materials featured a hierarchical structure in the sense that hydrophilic and hydrophobic segments are alternated. The resulting materials show pH-responsiveness and a complex self-assembly behavior in aqueous solution. Investigations of the properties and potential applications of these multiarm-multiblock star copolymers are currently underway in the Junkers research group.

Chapter 4

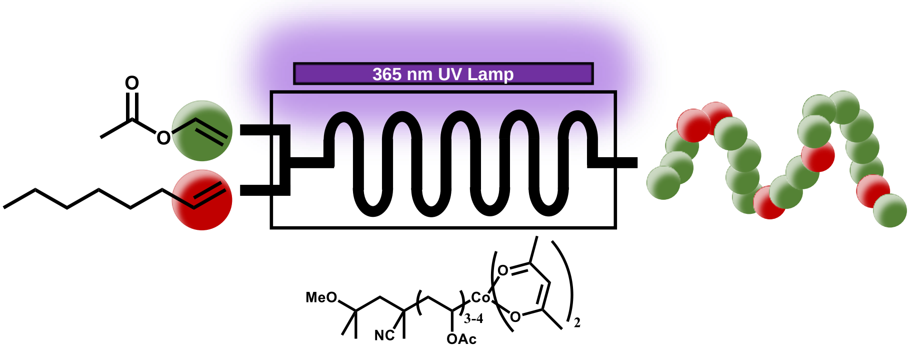

4. Improved Photo-Induced Cobalt-Mediated Radical Polymerization in Continuous Photoflow Reactors[§]

4.1. Abstract

The implementation of cobalt-mediated radical polymerization (CMRP) into continuous microflow reactor synthesis is described. It is demonstrated how the utilization of photoflow reactors allows to speed up the polymerization of vinyl acetate (VAc) under UV irradiation without losing the polymerization control. Microfluidics under UV irradiation is also successfully implemented for the copolymerization of VAc with the less reactive olefin 1-octene (1-Oct). Reactivity ratios are deduced for this copolymerization system and poly(VAc-*co*-1-Oct) copolymers containing up to 50 mol% of 1-Oct were synthesized. To the best of my knowledge, this is the first report on a photopolymerization where continuous flow techniques did not only lead to an improvement of reaction rates and dispersity, but also to the avoidance of significant side products that were previously observed in batch processing.

4.2. Introduction

Over the last decade, a great interest for developing chemical processes in microflow reactors has emerged.[204-208] Continuous flow reactors on laboratory scale allow for high control over reaction parameters including better thermal heat transfer, precise dosing of reactants, very efficient light irradiation (due to small pathlength, absorption intensity profiles may be neglected), small scale reactions

---

[§] Fist published as: "Improved Photo-Induced Cobalt-Mediated Radical Polymerization in Continuous Flow Photoreactors", A. Kermagoret, B. Wenn, A. Debuigne, C. Jerome, T. Junkers, C. Detrembleur, *Polym. Chem. 2015*, 6, 3847-3857. The research in this chapter was done in collaboration with the University of Liege.

and the ability to perform reactions outside the usual operation window. This often leads to accelerated reactions with concomitantly improved yields and less formation of side products.[55, 159, 209-212] Recently, flow reactor technology was implemented for macromolecular design by exploiting continuous flow controlled radical polymerization (CRP) techniques.[56, 206, 213-217] Flow reactors give access to very stable reaction conditions, and thus reduce batch-to-batch variations. At the same time, better defined polymers are often obtained. The ideal heat transfer properties of the reactors lead to fast exothermic heat dissipation, which prevents overheating of the reaction mixture. In this way, polymerizations proceed more steadily, resulting in lowered dispersities and higher end group fidelities of the obtained polymers.[105, 218, 219] Especially photo-induced polymerizations can benefit from microreactors.[91, 97, 159, 220] Flow channel widths are generally small, and thus no intensity gradients exist, giving access to homogenous irradiation profiles. Not only an acceleration of photoreactions is generally observed but also simple scalability is reached since the feature of short pathlength is easily retained when increasing reactor volumes or when carrying out reactions in parallel. This strongly contrasts with batch reactions, where photoreactions usually lose significant efficiency with increasing reactor volumes.

Cobalt-Mediated Radical Polymerization (CMRP) is an important class of CRP techniques that is based on the reversible deactivation of the growing radical chains by a cobalt complex.[50, 221-225] Bis-(acetylacetonato)cobalt(II) ($Co(acac)_2$) is a very efficient controlling agent for the polymerization of conjugated vinyl monomers including acrylonitrile[226] and *n*-butyl acrylate (*n*BA),[227] as well as non-conjugated vinyl monomers such as vinyl esters,[228] vinyl chloride,[229] N-vinyl amides[230, 231] and N-vinylimidazolium salts.[232] More important, this technique enables the copolymerization of VAc with ethylene,[233] and with 1-octene,[234] giving access to new well-defined functional poly(α-olefin)s that are otherwise difficult to synthesize.[235] However, these VAc/α-olefins copolymerizations are slow, probably as the result of a more stable C-Co bond at the polymer chain-end when the α-olefin is the last incorporated monomer unit. As a consequence, the synthesis of well-defined copolymers containing a high α-olefin content remains limited.[236]

Photo-induced radical controlled polymerization processes are raising more and more interest.[237-241] As highlighted in recent articles,[242-246] the C-Co bond at the chain end of polymers formed by CMRP is photolabile and the use of UV-light can therefore significantly increase the rate of polymerization. However, in the case of monomers that form very reactive growing radicals (such as VAc), the system is too reactive in the bulk under UV irradiation, leading to the contamination of controlled pVAc with a non-negligible amount of undefined high molar mass polymer resulting from branching and other side reactions, even when the polymerizations were conducted at low temperature (0 °C).[247]

In this study, it will be demonstrated that CMRP can be carried out efficiently in microflow reactors. Further it is demonstrated, how the utilization of photoflow reactors allows to speed up the polymerization of VAc under UV irradiation without losing the polymerization control, thus avoiding the above described side reactions. Finally, microfluidics under UV irradiation is successfully implemented for the copolymerization of VAc with a less reactive olefin (1-octene). Reactivity ratios are deduced for this copolymerization system and poly(VAc-*co*-1-Oct) copolymers containing up to 50 mol% 1-Oct were synthesized. To the best of my knowledge, this is the first report on a photopolymerization where continuous flow techniques did not only lead to an improvement of reaction rates and dispersity, but also to the avoidance of significant side products that always occur in batch processing.

4.3. Results and Discussion

4.3.1. VAc Homopolymerization

To begin with, the conventional CMRP of VAc in flow is discussed. Polymerizations were initiated by an alkyl cobalt(III) adduct ([$Co(acac)_2$-($(CHOCOCH_3)CH_2)_{<4}R_0$; R-$Co(acac)_2$] that generates the radical initiator and the controlling agent upon thermolysis[248] or photolysis (Scheme 4.1).[247]

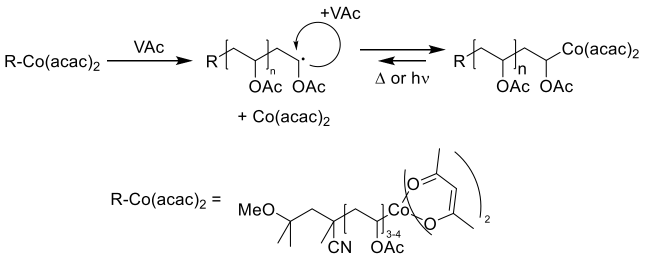

Scheme 4.1 VAc radical polymerization conducted by alkyl cobalt(III) adduct R-Co(acac)$_2$.

CMRP of VAc is carried out in ethyl acetate (EtOAc) solution (20 vol%) using a [VAc]/[R-Co(acac)$_2$] ratio of 529 (targeting a pVAc molar mass of 45500 g/mol at full conversion). Two different flow systems were used: *(i)* a 2 mL continuous flow reactor and *(ii)* a 19.5 µL microflow reactor. The first flow system requires comparatively large solution volumes (3 mL of solution were consumed before sampling) but allows reaction times (residence times) of up to 8 h. The 19.5 µL microflow reactor is more suitable for kinetic studies of fast polymerizations because reaction times are limited to 20 min.

In both cases, VAc polymerization is studied under thermal activation with and without photo-activation using UV irradiation. Both flow reactors are glass-chips made out of conventional borosilicate. Only light with wavelengths above 350 nm may start or support and accelerate the polymerization reaction.

The first CMRP experiments were conducted in the 2 mL continuous flow reactor at 40 °C with and without UV irradiation. Monomer conversions and molecular parameters of pVAc are determined by ^{1}H NMR and SEC-THF. Samples were collected from the reactor outlet after different reactor residence times. To highlight the benefit of using continuous flow reactors combined with UV irradiation, the polymerization of VAc is also carried out in the bulk or in ethyl acetate solution (20 vol%) in conventional Schlenk tubes.

Under thermal activation at 40 °C, similar polymerization rates are observed for CMRP of VAc performed in a flow reactor (at a concentration of 20 vol% solution in EtOAc) and in bulk using conventional Schlenk tubes (Figure 4.1).

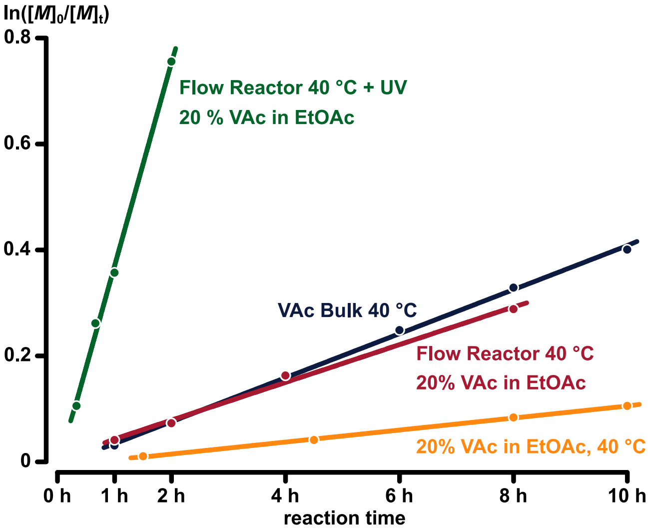

Figure 4.1 Plots of $\ln([M]_0/[M]_t)$ with time for the VAc polymerization initiated by R-Co(acac)$_2$ in a 2 mL flow reactor at 40 °C under UV irradiation, in bulk at 40 °C, in a 2 mL flow reactor at 40 °C or in 20 vol% VAc solution in EtOAc.

As expected, dilution of the polymerization medium in the Schlenk tube by EtOAc decreases the rate of polymerization compared to bulk, while the control over the molar mass is maintained (Figure 4.2). With the same reactant concentrations (20 vol% in EtOAc) and the same temperature (40 °C), the polymerization of VAc is almost 4 times faster when carried out in the microflow reactor compared to polymerization in Schlenk tubes. Importantly, under these microflow conditions, the control of VAc polymerization is preserved as demonstrated by the linear increase of the semilogarithmic plot of VAc conversion as a function of time ($\ln([M]_0/[M])$ *vs* time, Figure 4.1) and the linear increase of number average molar mass (M_n) with conversion (Figure 4.2).

In addition, the dispersities of pVAc are low ($Đ$ = 1.06-1.21). The rate increase in the continuous flow reactor is at first glance somewhat surprising as the reaction mode has no direct influence on the reaction rate when conditions are identical. Yet, the micromixer unit on the flow chip allows for rapid mixing of components, which may allow a more homogenous and faster initiation of the reaction.

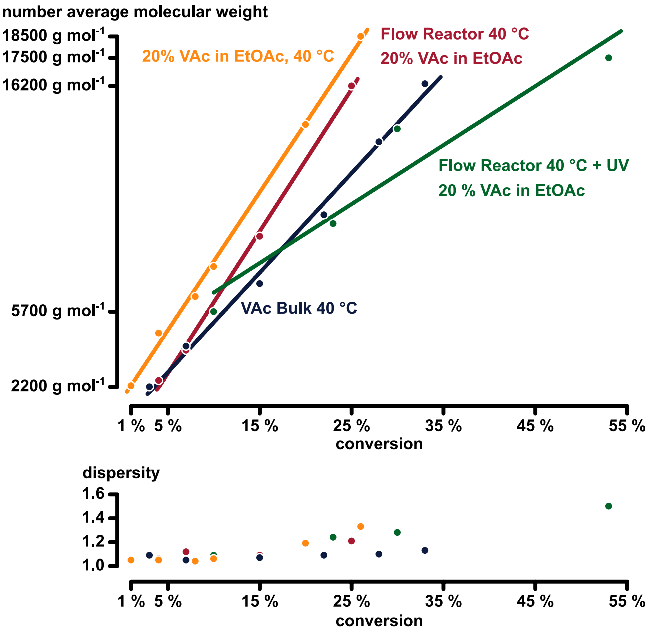

Figure 4.2 Dependence of pVAc number average molar weight with conversion and dependence of dispersity with conversion for the VAc polymerization initiated by R-Co(acac)$_2$ in a 2 mL flow reactor at 40 °C under UV irradiation, in bulk at 40 °C, in a 2 mL flow reactor at 40 °C or in 20 vol% VAc solution in EtOAc.

A further remarkable boost of the flow polymerization rate is observed when the flow reactor is irradiated by UV-light, with 53 % conversion reached after a reaction time of 2 hours. In comparison, only 7 % is reached under identical conditions without UV.

Although the dispersities are slowly increasing with increasing time (indicating that termination reactions are operational, see Figure 4.2), the SEC chromatograms remain mainly monomodal and shift towards higher molar masses with increasing monomer conversion (Figure 4.3). This is in sharp contrast to pVAc produced by CMRP in bulk under UV irradiation at 0 °C. As mentioned above, two different pVAc populations are collected under these experimental conditions. A well-defined pVAc with a low dispersity and high molar mass fraction with a very high dispersity resulting from branching and coupling reactions.[247]

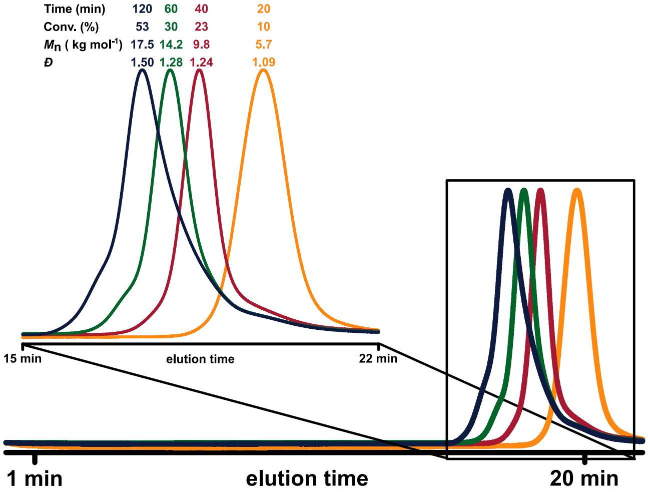

Figure 4.3 SEC traces of pVAc synthesized in a 2 mL flow reactor at 40 °C under UV irradiation.

Even more important, when the VAc polymerization is carried out in the bulk under UV-irradiation at 30 °C instead of at 0 °C, the reaction becomes highly exothermic, resulting in the production of a crosslinked, insoluble polymer. It becomes immediately apparent that the flow reaction mode allows for much more stable reactions when combining the advantage of high UV-penetration with the ideal heat transfer of such reactors, effectively preventing overheating by slow heat dissipation. In this way, side reactions (mainly branching and coupling reactions) are prevented when the VAc polymerization is carried out in a microflow reactor under UV.

These promising results obtained in a 2 mL flow reactor led us to further investigate CMRP in microflow reactors. These reactors are not suitable for gram-scale polymer production, but they allow for short residence times, even more efficient thermal heat transfer and homogeneous light irradiation. At the same time, they allow to screen a large variety of reaction conditions with minute amounts of reactants. Microflow reactors are therefore the tool of choice for investigating the influence of various reaction parameters on the CMRP of VAc in a broader range. The radical polymerization of VAc initiated by R-Co(acac)$_2$ is therefore evaluated using a 19.5 µL reactor at various temperatures (40 - 100 °C) with and without UV irradiation for residence times between 0.25 and 20 min.

Under thermal activation at 40 °C, no VAc conversion is measured after a residence time of 20 min. At 60 °C, a VAc conversion of 23 % is obtained after a period of 20 min. As expected, increasing the polymerization temperature increases the rate of polymerization with a conversion of 68 % after only 20 min at 80 °C and 53 % after 10 min at 100 °C (Figure 4.4). At 60 and 80 °C, $\ln([M]_0/[M]_t)$ plots are almost linear with time while a deviation from linearity is observed at 100 °C, due to some loss of control. The molar mass of the polymer increases with the monomer conversion for the three experiments, however, some deviation from linearity is observed with an increase of the dispersity after about 25 % conversion. In contrast to batch reactions, thermally activated CMRP of VAc can be conducted in microflow reactors under relative high temperatures, allowing the synthesis of well-defined pVAcs in short reaction times. Nevertheless, some loss of polymerization control is observed at moderate conversions. Dispersities

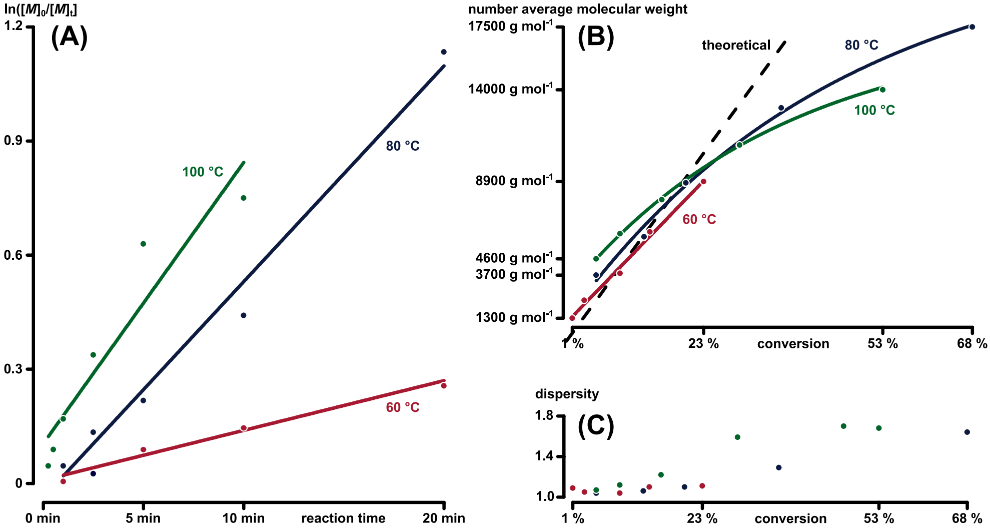

Figure 4.4 Plots of $\ln([M]_0/[M]_t)$ with time (A) and dependence of pVAc number average molecular weight (B) with conversion and dispersities with conversion (C) for the VAc polymerization initiated by R-Co(acac)$_2$ in a 19.5 µL flow reactor at 60 °C, 80 °C, and 100 °C.

of polymers obtained at conversions above 25 % are above 1.5, and thus slightly above expectations for a well-controlled radical polymerization process.

Nevertheless, a steady increase in M_n is observed, and a high-temperature flow process may be useful for certain applications. Especially since similar deviations from ideal polymerization behavior are also frequently observed for various CRP techniques in batch processing as well. Although some irreversible termination reactions might occur, the main reason for the observed deviation of M_n at higher conversion is assumed to be the result of the occurrence of transfer reactions that are temperature dependent.

Under UV irradiation (Figure 4.5), the VAc polymerization is also accelerated in the microflow reactor with conversions of 12 and 31 % for reaction times of 20 min at 40 and 60 °C, respectively. In both cases, a controlled radical polymerization is observed with the linear increase of M_n with monomer conversion and low dispersity (Figure 4.5). Moreover, no high molar mass polymer resulting from branching or other side reactions was detected on the SEC chromatograms. These experiments clearly show that – in agreement with the observations made in the

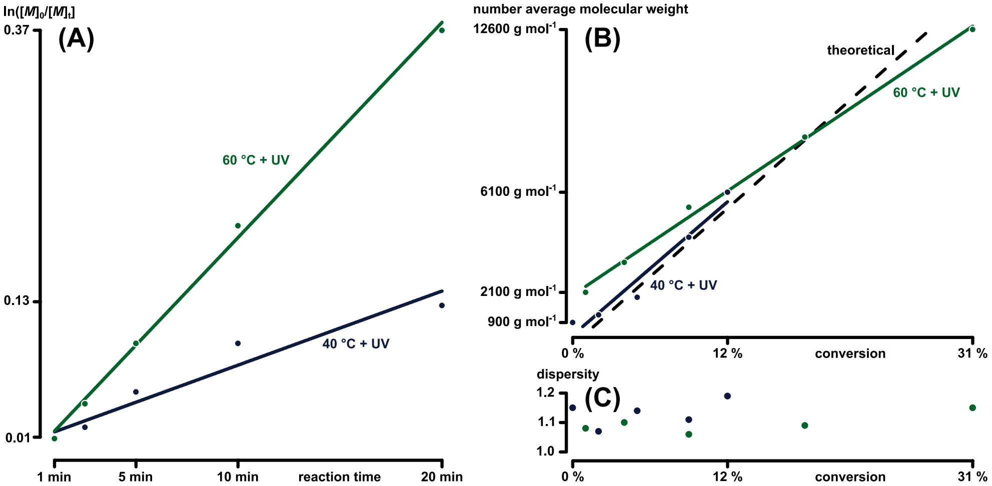

Figure 4.5 Plots of $\ln([M]_0/[M]_t)$ with time (A) and dependence of PVAc number average molecular weight with conversion (B) and dispersity with conversion (C) for the VAc polymerization initiated by R-Co(acac)$_2$ in a 19.5 µL flow reactor under UV irradiation at 40 °C and 60 °C.

2 mL reactor – the combination of UV-light with 19.5 µL flow reactor did not favor such side reactions in contrast to VAc polymerization performed in bulk under UV.[247]

The combination of increased temperature and UV-light has in both reactor systems strong advantages over the classical batch synthesis. Reactions can be performed at ease at significant scale, and in case of the milliscale reactor allow to reach high monomer conversions in reaction times significantly below the times required for the batch process.

4.3.2. VAc/1-Oct Copolymerization

Copolymerization of α-olefins and polar monomers is a challenging research topic. Yielding materials are combining the excellent physical and chemical properties of poly(olefin)s and the functionalities of polar groups.[233, 235, 249-251] The copolymerization of VAc with 1-Oct was previously described by CMRP using a combination of $Co(acac)_2$ as controlling agent with an azo-radical initiator at 30 °C in bulk.[234] This method allowed for the synthesis of well-defined copolymers but also required very long reaction times while the incorporation of 1-Oct was limited to about 15 mol%.

As demonstrated above, the use of flow reactors significantly speeds up the CMRP of VAc, in particular under UV irradiation. The research hypothesis could thus be drawn that the VAc/1-Oct copolymerization might also be accelerated under these conditions.

In this section, for the first time the VAc/1-Oct copolymerization initiated by R-$Co(acac)_2$ under microflow conditions and UV irradiation at different temperatures (40, 60 or 80 °C) was investigated. Results are compared with a conventional Schlenk tube batch reaction in bulk at 40 °C to obtain a reference for the continuous flow reactions.

The copolymerization is first carried out in bulk at 40 °C with R-Co(acac)$_2$ using a VAc/1-Oct/Co ratio of 383/127/1 (VAc/1-Oct of 75/25 mol%). Monomer conversions and molecular weight parameters of copolymers are determined by ^{1}H NMR and SEC-THF, from samples withdrawn during the reaction. Since the conversion of 1-Oct is low in the copolymerization (> 7 % after 72 h), its conversion is not determined precisely by ^{1}H NMR. Hence, VAc conversion is used to plot the kinetic graphs, i.e. the time dependence of $\ln([M]_0/[M]_t)$ and M_n with VAc conversion (Figure 4.6). The linear character of both graphs confirms the good control over the copolymerization during the first 12 hours of reaction. Deviation from linearity of the semi-logarithmic plot is observed after 29 hours reaction time. Translating a decreased reaction rate, which may be attributed to the occurrence of some termination reactions and the accumulation of excess Co(acac)$_2$. The dispersity is relatively low ($Đ$ < 1.20) during the first 12 h of reaction but then increases significantly to 1.83 for a VAc conversion of 38 % after 72 h (Figure 4.6). The incorporation of 1-Oct in the copolymer, determined by ^{1}H NMR after evaporation of the monomers, is around 10 mol% and remains constant during the reaction.

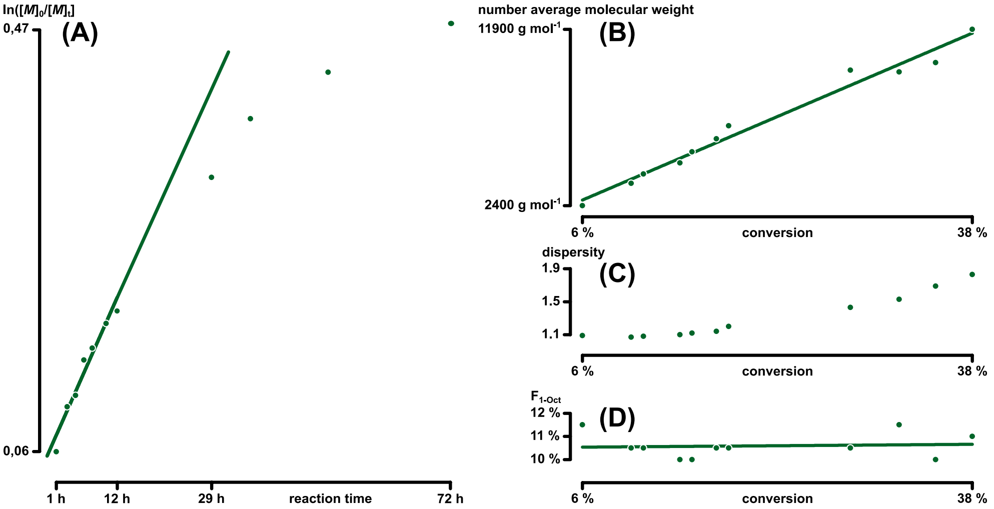

Figure 4.6 Plots of $\ln([M]_0/[M]_t)$ with reaction time (A) and dependence of poly(VAc-*co*-1-Oct) number average molecular weight (B), dispersity (C) and copolymer composition $F_{1\text{-Oct}}$ (D) with conversion for the VAc/1-Oct polymerization initiated by R-Co(acac)$_2$ in bulk at 40 °C.

The same copolymerization was then carried out under UV irradiation at different temperatures (40, 60 or 80 °C) using a 19.5 µL microflow reactor. The copolymerization was conducted by R-Co(acac)$_2$ (VAc/1-Oct/Co ratio of 383/127/1) in ethyl acetate solution (22.5 vol%) to avoid viscosity effects.

At 40, 60 or 80 °C under UV irradiation, the molar mass of pVAc increased linearly with the monomer conversion and was close to the theoretical value. The dispersity stayed below 1.5 (Figure 4.7).

It is important to note that 1-Oct conversion could again not be determined with sufficient accuracy directly by ^{1}H NMR, due to the dilution and overlapped signals with the solvent (EtOAc). After removing all volatiles under reduced pressure, the 1-Oct content in the copolymer could be precisely determined by ^{1}H NMR. It remained constant with residence times (15-18 mol%) and did not significantly depend on the polymerization temperature.

SEC chromatograms of copolymers produced at 60 and 80 °C presented a bimodal distribution when the conversion was higher than 9 % (Figure 4.8), indicating the occurrence of side reactions under these conditions.

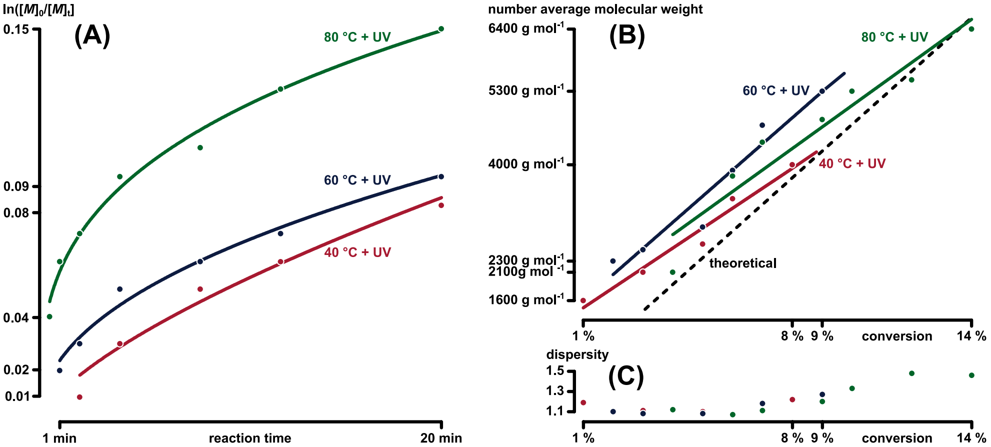

Figure 4.7 Plots of ln([M]$_0$/[M]$_t$) with time (A) and dependence of PVAc number average molecular weight with conversion (B) and dispersity with conversion (C) for the VAc/1-Oct copolymerization initiated by R-Co(acac)2 in a 19.5 µL flow microreactor under UV irradiation at 40 °C, 60 °C or 80 °C.

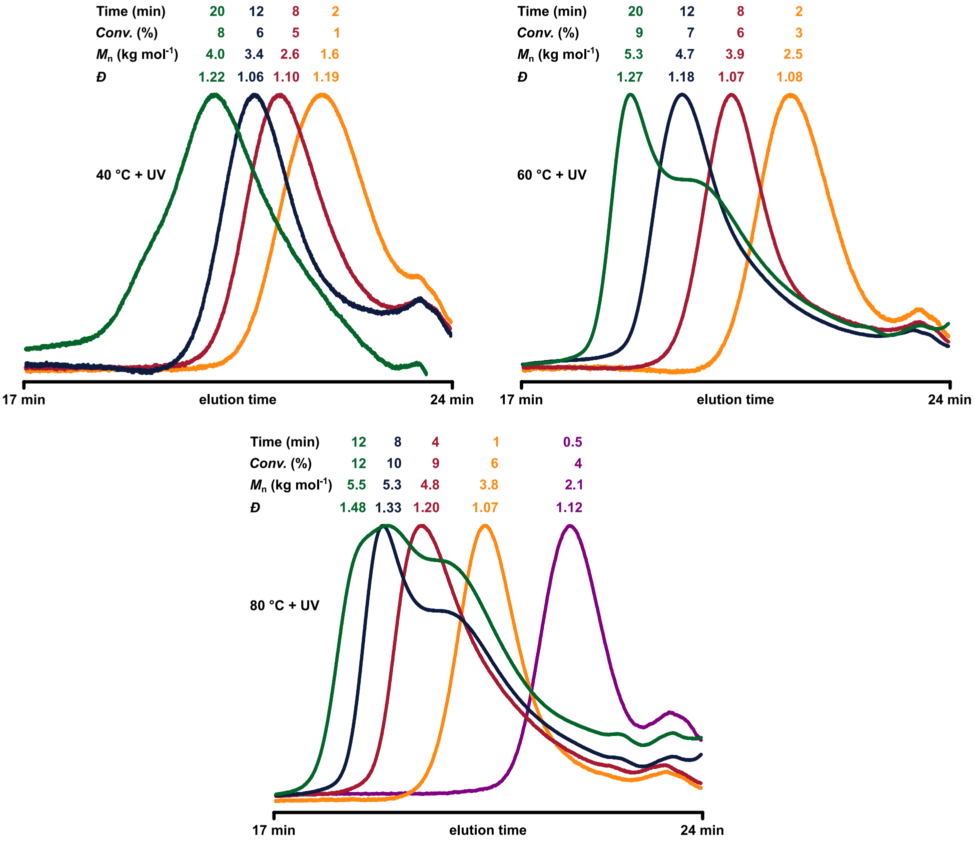

Figure 4.8 SEC traces of poly(VAc-*co*-1-Oct) synthesized in a 19.5 µL flow reactor under UV irradiation at 40 °C, 60 °C and 80 °C.

As reported in the literature, unstabilized radicals, such as α-olefin radicals particular for allylic hydrogens on 1-Oct, lead to a stabilized radical.[252]

Previous studies have demonstrated that the radical homopolymerization of 1-Oct is highly unfavored due to the formation of these stable allylic radicals,[253,252, 254] and coupling reactions between polymer radicals and allylic radicals.[255] These coupling reactions are expected to also occur during the VAc/1-Oct copolymerization.

Since the use of the microflow reactor allows to follow the kinetics of copolymerization at the early stages of the process, thus at low monomer conversions, their use is particularly suitable for determining the reactivity ratios of VAc and 1-Oct under CMRP conditions.

The reactivity ratios (r_{VAc} and $r_{1\text{-}Oct}$) were calculated by employing the terminal model (Mayo-Lewis method)[256, 257] and equations Eq. 4.1 and Eq. 4.2, where f_1 and f_2 are the respective mole fractions of monomers M_1 and M_2 in the reaction feed and F_1 and F_2 are the corresponding mole fractions in the copolymer.[258, 259]

$$\frac{F_1}{F_2} = \frac{f_1(r_1 f_1 + f_2)}{f_2(r_2 f_2 + f_1)} \qquad \textbf{Eq. 4.1}$$

$$F_1 = \frac{\mathrm{r}_1 f_1{}^2 + f_1 f_2}{\mathrm{r}_1 f_1{}^2 + \mathrm{r}_2 f_2{}^2 + 2 f_1 f_2} = 1 - F_2 \qquad \textbf{Eq. 4.2}$$

For that purpose, copolymerizations using different monomer feeds were carried out at 40 °C under UV irradiations for a reaction time of 8 min in order to limit the polymerization to low conversions and to avoid monomer composition drifts (VAc conversion < 5 %). The resulting copolymers were collected from the outlet of the flow reactor, dried overnight at 70 °C under vacuum to remove monomers, and analyzed by ^{1}H NMR to determine their compositions. The results are collated in Table 4.1. The VAc incorporation is in all cases higher than 1-Oct, even for the copolymerization performed with a VAc/1-Oct ratio of 0.09/0.91, indicating the high preference of VAc to propagate compared to 1-Oct.

When fitting the non-linear Mayo-Lewis equation, the following reactivity ratios are obtained: r_{VAc} = 1.73 and $r_{1\text{-}Oct}$ = 0.01 (Figure 4.9). The very low reactivity ratio of 1-Oct confirms the inability of the α-olefin radicals to react with α-olefin monomers,[258] and hence the inability of the α-olefin to homopolymerize via a radical pathway.[255] This is in line with the reactivity ratios determined for the controlled radical copolymerization of 1-Oct with conjugated monomers, e.g. methyl methacrylate or acrylates, by ATRP.[260, 261] Similar conclusions were drawn from the reactivity ratios calculated for free radical acrylate/1-Oct

Table 4.1 Copolymerization of VAc and 1-Oct using various comonomer ratios and initiated by R-Co(acac)$_2$ in a 19.5 μL flow microreactor and experimental and calculated comonomer fractions in poly(VAc-*co*-1-Oct).

f_{Vac}[a]	$f_{1\text{-}Oct}$[a]	F_{Vac}[b]	$F_{1\text{-}Oct}$[b]	Calc F_{Vac}[c]	Calc $F_{1\text{-}Oct}$[c]
0.930	0.070	0.940	0.060	0.960	0.040
0.850	0.150	0.890	0.110	0.915	0.085
0.760	0.240	0.860	0.140	0.865	0.135
0.700	0.300	0.850	0.150	0.835	0.165
0.580	0.420	0.810	0.190	0.770	0.230
0.500	0.500	0.700	0.300	0.730	0.270
0.380	0.620	0.650	0.350	0.670	0.330
0.200	0.800	0.580	0.420	0.580	0.420
0.090	0.910	0.530	0.470	0.520	0.480
0.045	0.955	0.480	0.520	0.480	0.520

[a] Comonomer fractions in feed determined by ^{1}H NMR. [b] Comonomer fractions in poly(VAc-*co*-1-Oct) determined by ^{1}H NMR after elimination of volatiles. [c] Calculated fractions in poly(VAc-*co*-1-Oct) using reactivity ratios r_{VAc} = 1.73 and $r_{1\text{-}Oct}$ = 0.01 (Figure 4.9).

copolymerization.[262] Also in line with the present observation, Gupta *et al.* demonstrated by use of ^{13}C NMR analysis that methyl acrylate/1-Oct copolymers (high 1-Oct content) obtained from radical polymerization featured an almost entirely alternating acrylate/1-Oct copolymer sequence.[263, 264] The use of a RAFT[265] or tellurium-mediated radical polymerization[266] process to synthesize copolymers of 1-Oct with acrylate or methacrylate comonomers resulted likewise in low 1-Oct incorporation and low molar mass copolymers with a moderate dispersity. Importantly, by employing CMRP, copolymers containing up to 50 mol% of 1-Oct can be produced by adjusting the VAc/1-Oct monomer feed ratio (see Figure 4.9).

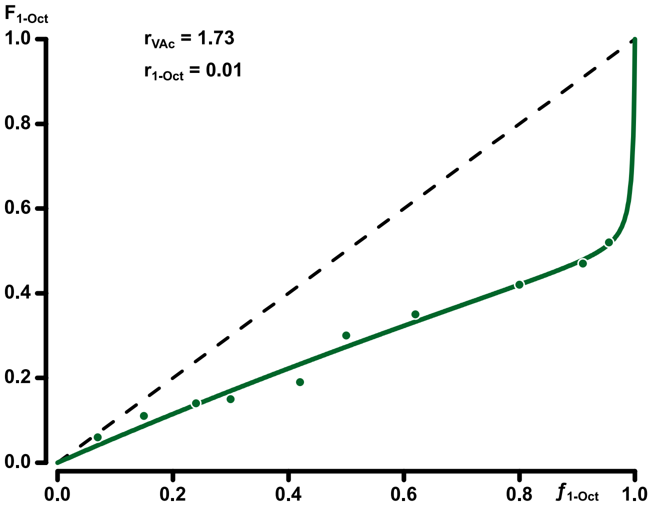

Figure 4.9 Dependence of poly(VAc-*co*-1-Oct) composition (*F*) with monomer ratio (*f*) in feed calculated from reactivity ratios r_{VAc} = 1.73 and $r_{1\text{-Oct}}$ = 0.01.

4.4. Conclusions

UV-activated cobalt-mediated radical polymerization has been investigated under continuous photoflow conditions. Conventional batch synthesis features significant production of broad polymer side products under UV-polymerization conditions. Well-defined monomodal poly(vinyl acetate) is obtained when reactions are carried out in glass-chip (micro)flow reactors. Flow reactor processing allows not only to obtain material with increased purity, but also leads to a significant acceleration of polymerizations. Even in absence of UV-light, a 4-fold increase in the reaction rate is observed when switching from batch to flow operation. A further significant rate increase is obtained with UV-light, mainly because the improved heat transfer capacity of the flow reactor allows for operation at significantly higher temperatures under still isothermal conditions. In contrast, the UV polymerization in batch at temperatures above room temperature yields crosslinked and insoluble polymers. Monomodal distributions in conjunction with overall satisfying molecular weight control are obtained in flow. Polymerizations can thereby be carried out in microflow as well as under milliflow conditions, allowing for a first significant upscale of the reaction, which is important when the process is supposed to be used synthetically. Further upscaling to miniplant conditions are assumed to be unproblematic.[52, 267] This would certainly not be the case for the according batch reaction due to the unavoidable efficiency decrease of UV reactions when increasing reactor (and light pathway) dimensions.[268] The CMRP of VAc is hence a prime example for a scalable UV reaction that is significantly improved when carried out in flow, as not only the product quality can be improved, but also the overall rate of reactions.

Further, the microflow reactor system was used to determine copolymerization parameters of VAc with 1-Oct under CMRP control. Applying the Lewis-Mayo fitting method, $r_{\mathrm{VAc}} = 1.73$ and $r_{\mathrm{1\text{-}Oct}} = 0.01$ were obtained, in agreement with available literature data. Additionally, the flow reactor allowed for largely improved reaction outcomes and could be efficiently used at the same time to screen the copolymerization reaction in detail, underpinning the additional use of microflow reactors in kinetic investigation of radical polymerization processes.

Chapter 5

5. Continuous Microflow PhotoRAFT Polymerizations**

5.1. Abstract

PhotoRAFT (reversible addition fragmentation radical transfer) polymerizations are investigated for reactions induced by conventional radical photoinitiators. As demonstrated, this rather simple photoRAFT reactions show similar outcomes compared to other recently introduced photopolymerizations such as photoiniferter RAFT and photoelectron transfer RAFT. With benzoin as initiator, optimal polymerizations are obtained when the initiator is used in a ratio of 0.25 to the initial RAFT-agent at 60 °C reaction temperature. Chain length of the polymer can be tuned efficiently and block copolymers are accessible from the process despite some slight loss in chain-end fidelity during polymerizations. Additionally, the choice of initiator has a large effect on the polymerization, which can be routed to different decomposition rate constants under the same illumination conditions.

5.2. Introduction

In recent years, a remarkable renaissance of photopolymerization techniques for solution-based synthetic chemistry is observed.[10] While photopolymerizations were only broadly used in coating and film design, and for network formation for example in dental restoratives, only little efforts were made to exploit such reactions in synthesis of materials from solution, despite a broad variety of photoinitiators and processes being available, especially in the realm of free radical polymerization. This lack of interest stemmed mostly from efficiency gaps when performing such reactions and from the general difficulty to upscale photoreactions in an economic way. Still, in the last few years, photo-induced

---

** First published as: "Continuous Microflow PhotoRAFT polymerizations", B. Wenn, T. Junkers, *Macromolecules, in press*.

reaction modes for most controlled radical polymerization techniques have been identified and now developing rapidly. Among several advances in the design of photocatalysts and initiators, research on the performance of photo-initiated reactions in continuous flow reactors is an emerging field in academia as well as industry.[69] To date only few photoreactions are employed in synthesis, most of them being located in the realm of pharmaceutical chemistry where for example photocycloadditions can give access to specific structures that are inaccessible from thermally activated reactions.[54]

Recently, the advantages of photoflow reactors have been picked up in the area of polymer chemistry, in order to perform continuous photo-initiated polymerizations.[10, 160, 269] The main focus in most literature reports is put on reversible deactivation radical polymerization (RDRP) techniques, with photo-induced metal-mediated polymerizations being the most popular choice. Junkers and coworkers reported on the synthesis of acrylate and methacrylate homo- and block copolymers via copper-mediated polymerizations.[91, 100] Melker *et al.* used an iridium complex instead and looked in detail at the influence of different tubing materials on the polymerization.[93] Photo-induced polymerization of vinyl acetate with a cobalt complex was reported by Detrembleur and coworkers.[98] Recently, the first successful photo-initiated reversible addition-fragmentation radical transfer (RAFT) polymerization in a continuous flow reactor using a trithiocarbonate compound as a transfer agent was reported.[99] Gardiner *et al.* recently reported the first real photo-initiated RAFT polymerization in a continuous flow reactor.[172] Yet, classically initiated RAFT polymerizations are sometimes seen as less efficient when compared to recent developments such as photoelectron transfer RAFT (PET-RAFT).[188, 270, 271] The study by Gardiner seemed to confirm that notion as materials with rather large dispersity were obtained. While PET-RAFT certainly displays some fundamental advantages like the ability to choose the wavelength of the incident light, the hypothesis should be tested whether conventional RAFT may not result in similar results.

RAFT differs from the other photoRDRP methods. In principle conventional initiation sources may be used, such as classical radical photoinitiators. However, Qiao and coworkers[272] demonstrated that RAFT-agents and RAFT-polymers may act as radical initiators themselves under UV-irradiation, following a photoiniferter mechanism.[109, 273-276] Typical transfer agents for RAFT polymerizations consist of a stabilizing Z-group and a leaving group (R). Via degenerative transfer, the R-group is commonly released and a dynamic equilibrium between growing chains is established. Under UV-light, the respective carbon sulfur bond can also be broken, without involvement of a transfer reaction. This results in an additional mode of initiation. For RAFT polymerization, dithioesters and trithiocarbonates are most often used, whereby dithioesters strongly absorb UV-light whereas trithiocarbonates are usually associated with lower extinction coefficients and absorption shifted towards higher wavelengths. The RAFT mechanism and its additional iniferter-like radical initiation are summarized in Scheme 5.1.[277] Interestingly, the iniferter initiation pathway creates polymer species which are identical to typical RAFT products, and hence a discrimination between reaction pathways is difficult to achieve. The effect is advantageous at the same time, as it also indicates that the classical features of RDRP are preserved, such as structural integrity and ability to chain extend. In fact, Qiao and coworkers had

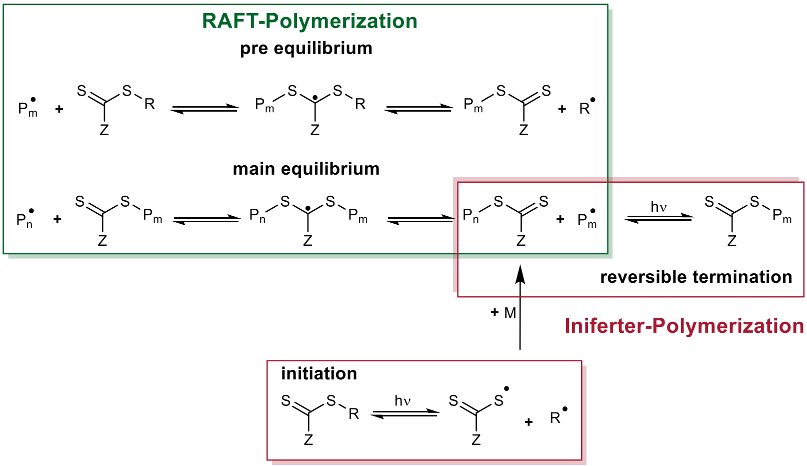

Scheme 5.1 Mechanism of RAFT polymerization as well as the iniferter mechanism.

demonstrated that photoRAFT polymerizations may be reactivated several times in complete absence of any exogenous radical source.

Also, Chen *et al.* polymerized different acrylate monomers via a photoiniferter reaction in two different homemade flow reactors. They reached molecular weights up to 100000 g mol^{-1} with dispersities around 1.2.[99] Using two conventional initiators, so not relying on the iniferter initiation, Gardiner *et al.* polymerized acrylates, methacrylates and acrylamides in a Vapourtec flow reactor setup.[172] In their study, they focused on reaction optimization with respect to the irradiation wavelength leading to high reaction rates, with the purpose to test how photoRAFT can be employed for industrial production. Molecular weights up to 25000 g mol^{-1} were reached with dispersities reaching up to 1.9 in 60 min reaction time.

In here, the use of conventional photoinitiators for continuous flow photoRAFT polymerization is described. Pure iniferter polymerizations are comparatively slow, and hence in principle disadvantageous, even if they are able to deliver products with higher purity due to the lack of R-group exchange reactions that occur when conventional initiators are used.[201] Different initiators are screened to test for the influence of the chosen initiator with respect to reaction rate and product purity. Additionally, polymerizations are compared to the iniferter initiation mechanism in order to elucidate the contribution of the iniferter mechanism to the overall polymerization. In contrast to the study by Gardiner *et al.*, focus is thereby not only put on time/yield correlations, but also on product dispersities. Low dispersities are often seen as a quality mark of RAFT polymers and are required to allow for block copolymer synthesis. In this chapter, the influence of initiator concentration and initiator choice, light intensity and the reaction temperature (an often overlooked factor in photoreactions) is described. Then, block copolymers were synthesized to demonstrate that carefully optimized photoRAFT polymerizations can reach a similar quality as for example copper-mediated radical photopolymerizations.

5.3. Results and Discussion

The usage of flow reactors for photoRDRP reactions is an emerging field in academic research and industry.[160] Fast reaction rates are thereby important for the economic use of flow reactors. A trithiocarbonate was chosen as control agent, as best results have been reported before in flow for these specific RAFT-agents, and because they show no other photodegradation than the supporting iniferter initiation mechanism.[109, 276, 278, 279] All polymerizations were carried out in *n*-butyl acetate (BuAc) as solvent, using 2-(dodecylthiocarbonothioylthio)propionic acid (DoPAT) as RAFT-agent and *n*-butyl acrylate (*n*BA) as monomer. The combination of the used starting materials was based on literature known thermal initiated polymerizations.[102] To screen the reactions conveniently in a broad range of conditions, a Chemtrix Labtrix Start setup with a glass chip microreactor (Reactor volume: 19.5 µL) was employed in all experiments. As light source, an OmniCure S1000 system with a mercury medium pressure lamp (λ_{max} = 365 nm, 100 W) was employed.

5.3.1. Reaction Condition Optimization

First, different ratios between the photoinitiator benzoin and the RAFT-agent DoPAT were screened in order to identify optimal conditions with respect to reaction rate and yield. As standard reaction conditions, a light intensity of 17 mW cm^{-2} and a temperature of 25 °C were set. For the screening, the monomer to RAFT-agent ratio was kept at 80:1 and the photoinitiator ratio varied between 0.05, 0.25, 0.50 and 1.00 with respect to the RAFT-agent. The analysis of the obtained samples showed a broader dispersity with increasing benzoin concentration (Figure 5.1). The measured number average molecular weights follow an increasing linear trend with longer reaction times for the tested DoPAT to benzoin ratios up to 1:0.50. Masses of up to 8700 g mol^{-1} were reached. At the highest initiator concentration, a levelling off at 7000 g mol^{-1} was observed, with dispersities increasing to 1.6. With increasing initiator concentration, faster reaction rates are generally noticed. Monomer conversion went up from 23 % for 1:0.05 via 62 % (1:0.25), 63 % (1:0.50) to 82 % for the 1:1.00 DoPAT to benzoin

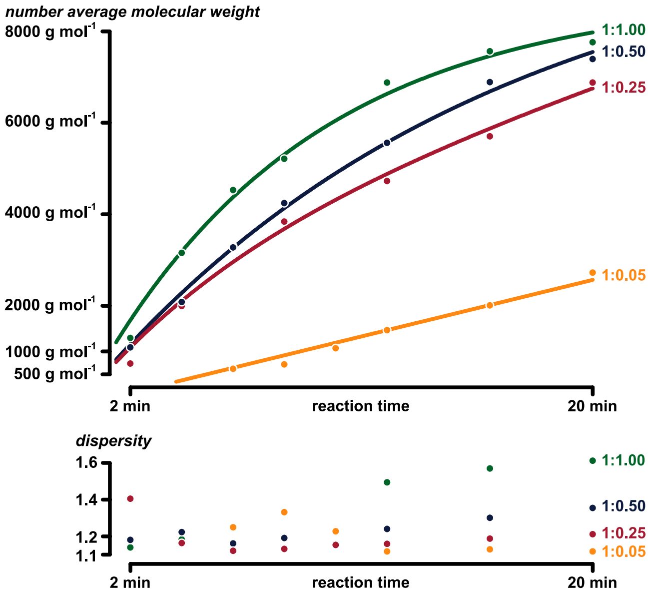

Figure 5.1 Influence of different initiator concentrations on the development of number average molecular weight and dispersities of a photoRAFT polymerization of *n*BA with increasing reaction time. The reactions were carried out at 25 °C with a light intensity of 17 mW cm^{-2} in butyl acetate as solvent. As monomer (*n*BA) to RAFT-agent (DoPAT) ratio, 80:1 was employed with varying the initiator (benzoin) ratios to 0.05, 0.25, 0.50 and 1.00 with respect to the RAFT-agent concentration.

ratio for 20 min maximum reaction time. The ratio of 1:0.25 shows relatively high conversions, and not significantly slower polymerizations compared to the higher initiator concentrations, while retaining reasonable dispersities in the range of 1.2.

For many photoreactions, the influence of temperature is neglected. But for photopolymerizations temperature can have a distinct effect, since the chain growth reaction is essentially thermally activated. Hence, an increase in temperature should directly lead to an increase in the polymerization rate, even if this effect was not directly confirmed for photoCMP reactions.[280] Additionally, polymerizations are exothermic, and UV-light sources often also irradiate heat, which leads in many mesoscale reactors to temperature profiles that are significantly above the set room temperature. To test the exact effect on the photo-initiated RAFT polymerization, the temperature was increased gradually from 25 to 120 °C in the microflow device (note that higher temperatures lead to decomposition of RAFT end groups and hence a breakdown of reaction control). Figure 5.2 depicts the results of this series for DoPAT to benzoin to *n*BA ratios of 1:0.25:80 in BuAc with a light intensity of 17 mW cm^{-2}. The reaction time was 12 minutes for all temperatures. In Figure 5.2, the increasing monomer conversion with higher reaction temperature is clearly confirmed, demonstrating that almost full conversion of the polymerization can be reached at the highest temperature, while room temperature only affords for roughly 32 % conversion in the same time span. As negative side effect, an increase in the dispersity of the obtained polymer was noticed. The dispersities stay below 1.2 for reaction temperatures up to 60 °C. For temperatures above 100 °C, dispersities over 1.3 were measured. The largely increased dispersity at 120 °C is an indication of the onset of trithiocarbonate elimination setting in.[277, 281-283] These dispersity results are in agreement with literature that reports on the behavior of trithiocarbonate controlled RAFT polymerizations.[284] As mentioned above, polymerization was optimized with regard to the precision that can be reached. Hence 60 °C was chosen for the following polymerizations as standard temperature, so as to allow for already increased yields, while maintaining a low overall dispersity.

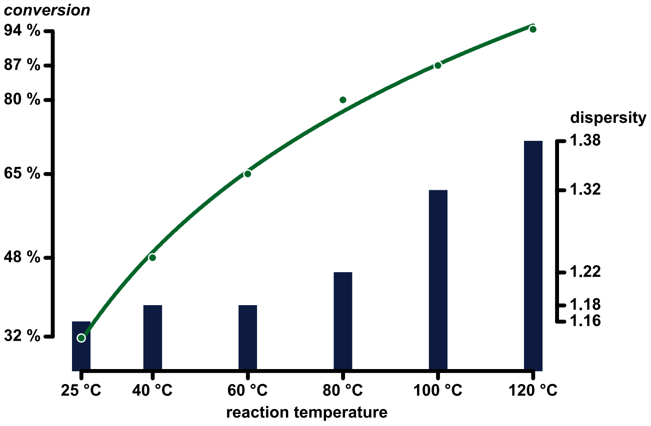

Figure 5.2 Increasing monomer conversion with higher reaction temperatures for a photoRAFT polymerization of *n*BA. Monomer conversion was determined after a reaction time of 12 minutes with a light intensity of 17 mW cm^{-2}. As DoPAT to benzoin to *n*BA ratio 1:0.25:80 was used with butyl acetate as solvent.

For the next optimization step, the influence of the light intensity on the reaction rate was investigated. Monomer conversions with increasing reaction times and light intensities are given in Figure 5.3. Unsurprisingly, an increase in light intensity has advantages on the reaction rate. For an intensity of 5 mW cm^{-2}, only 68 % monomer conversion was reached after 20 minutes reaction time. With increasing intensities, higher conversions can be achieved, reaching 86 % at an intensity of 30 mW cm^{-2} under identical conditions. However, for higher intensities only rather insignificant increases in monomer conversion were observed (70 mW cm^{-2}, 91 %), indicating that 30 mW cm^{-2} marks a point of complete light saturation in the reactor, after which no further significant increase can be observed. Also, from the same light intensity on, deviations from linear first order plots are observed, indicating that an increase of light intensity goes alongside with a change in initiation mechanism over time (see below for a discussion of initiator decay rates). Combining all points of the optimization process, the best reaction conditions are a reaction temperature of 60 °C with a light intensity of 30 mW cm^{-2} and a benzoin molar ratio of 0.25:1 with respect to DoPAT.

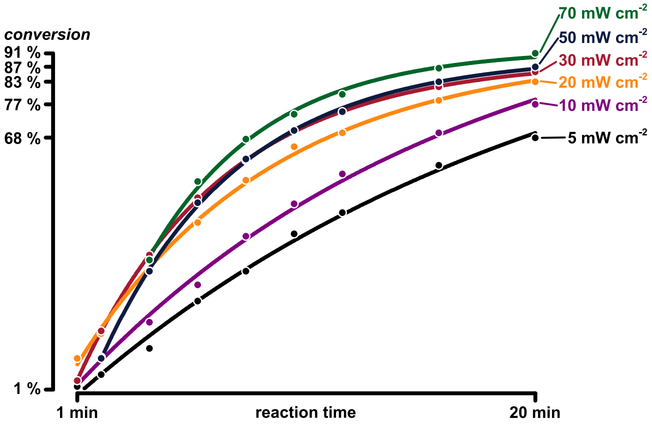

Figure 5.3 Influence of light intensity on the reaction rate of a photo-initiated RAFT polymerization of *n*BA in a microflow reactor. As light source an Omnicure S1000 system with a peak wavelength at 365 nm was used. Ratios of 1:0.25:80 for DoPAT, benzoin and *n*BA were used with BuAc as solvent. All reactions were performed at 60 °C.

5.3.2. Chain Length Variation

To demonstrate the robustness of the photo-induced RAFT polymerization, the RAFT-agent to monomer ratio was changed. Ratios up to 1:160 leading to polymers with a molecular weight around 20000 g mol^{-1} were obtained. These screenings were done for the polymerizations initiated via benzoin as photoinitiator as well as via the photoiniferter mechanism without initiator (Figure 5.4). For both routes, clear increases in the molecular weights were observed, thus underpinning the flexibility that the reaction offers. However, the dispersities of the higher molecular weight polymers from the photo-initiator route show some tailing in the GPC graphs. This was also observed in the increase in dispersity which went up to 1.36. In contrast, the polymer from the photoiniferter route did not show this tailing and the dispersities stayed in the range of 1.10 over the different chain lengths.

5.3.3. Block Copolymer Synthesis

As mentioned above, photoRAFT polymerizations should be able to yield block copolymers if the end group fidelity is not compromised in the reaction. From the above optimizations, it can be seen that the photoinitiator has an influence on

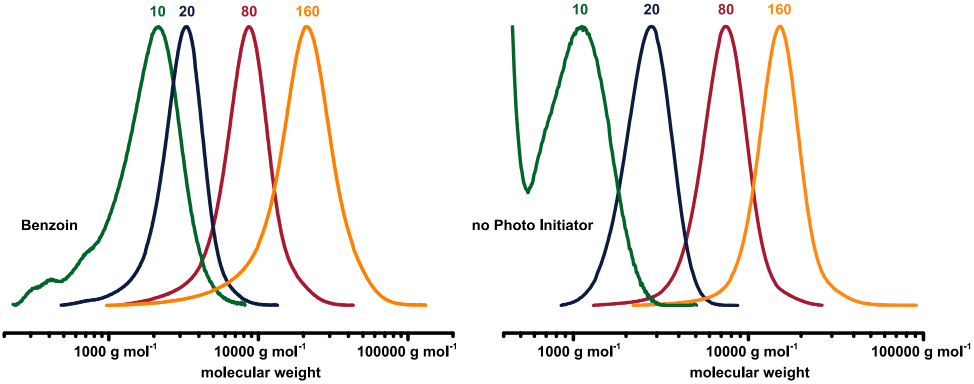

Figure 5.4 The degree of polymerization was varied in *n*BA polymerizations with benzoin (left) as initiator and without initiator (right). Molar ratios of 10, 20, 80 and 160 with respect to the RAFT-agent were polymerized. Reactions were performed at 60 °C in butyl acetate in a microflow reactor with a light intensity of 30 mW cm^{-2}.

dispersity, which is typically associated with a loss of end group fidelity. It should be noted that not only the RAFT end group is of interest, but also the α-chain end, where the RAFT R-group may be replaced by an initiator end group.[285] For block copolymers, the first block represents the R-group in chain extension and R-group replacement leads to a loss of the block structure even if the process is fully living with respect to the trithiocarbonate end group. The structural integrity of the RAFT polymers was then investigated via electrospray ionization mass spectrometry (ESI-MS). A p(*n*BA) sample made in the microflow reactor with optimized reaction conditions was measured and showed a high end group fidelity. Some side products are also visible, which would be less pronounced for an optimized thermal RAFT polymerization.

Yet, fidelity was high enough to approach chain extension, and a *n*BA polymer (M_n = 3000 g mol^{-1}, $Đ$ = 1.18), made via the optimized reaction conditions with benzoin as initiator, was used as macroinitiator for methyl acrylate polymerization with molar rations of 1:0.25:20 for p(*n*BA) to benzoin to MA at 60 °C and with 30 mW cm^{-2} in the microflow reactor setup. A diblock p(*n*BA)-*b*-pMA copolymer with an increased molecular mass of 4000 g mol^{-1} was obtained (Figure 5.5). The

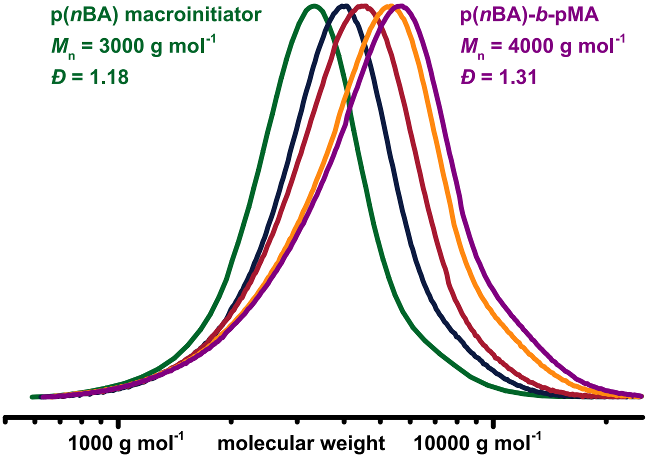

Figure 5.5 Molecular weight distributions for the synthesized p(*n*BA)-*b*-pMA block copolymer via photo-induced RAFT polymerization in a microflow reactor. A shift to higher masses is observed, showing the possibility to reactivate the p(*n*BA) macroinitiator.

reaction reached a monomer conversion of 58 % after 10 minutes reaction time. Theoretical (3990 g mol^{-1}) and measured (4000 g mol^{-1}) molecular masses are in accordance regarding the chain-extended polymer. However, after the chain extension, a slightly higher dispersity of 1.31 was measured, thus demonstrating the limitations of the technique. PhotoRAFT, at least when sustained by conventional photoinitiators, is unlikely to be used for the synthesis of multiblock copolymers.[181, 182] For the synthesis of simple diblock and eventually triblock copolymers, it should be employable, which is typically sufficient for most applications.

5.3.4. Variation of Photoinitiators

After optimal polymerization conditions for the fast synthesis of low dispersity RAFT polymers had been identified, further tests were carried out on the choice of the initiator itself. Thus, a variation of commercially available and commonly used photoinitiators were systematically tested and compared. Beside the before mentioned benzoin, 2,2-dimethoxy-2-phenylacetophenone (DMPA), phenylbis(2,4,6-trimethylbenzoyl)phosphine oxide (Irgacure 819) and 2-hydroxy-4′-(2-hydroxyethoxy)-2-methylpropiophenone (Irgacure 2959) were

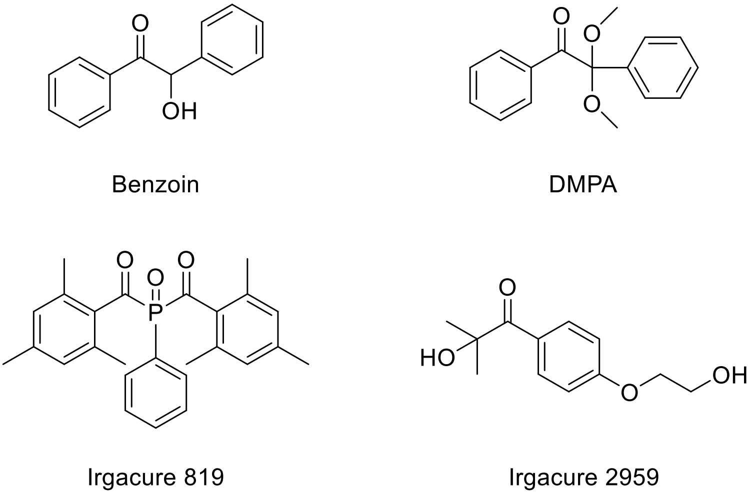

Benzoin

DMPA

Irgacure 819

Irgacure 2959

Scheme 5.2 Chemical structures of the used photoinitiators in this work.

used (Scheme 5.2). Additionally, the pure photoiniferter reaction, in other words RAFT polymerization in absence of any exogenous photoinitiator, was tested as a reference.

The initiators were tested for *n*BA in BuAc under the previously optimized reaction conditions (30 mW cm^{-2}, 60 °C). All initiators were used with a molar ratio of 0.25 to the RAFT-agent. The obtained conversions, number average molecular weights and dispersities are shown in Table 5.1. A strong increase in monomer conversion for the reactions with the various photoinitiators was observed (Figure 5.6). Conversions increased from 61 % for the photoiniferter reaction up to 94 % for Irgacure 2959 within 20 minutes reaction time. Disperties stayed in a range of 1.1 to 1.2 for all reactions apart from the Irgacure 819 initiated one. However, an increase to 1.55 was reported previously and may be explained by the complex dissociation of the Irgacure 819 initiator, which is associated with two photolabile bonds.[172] Consequently, a chain carrying a 819 fragment can act as a macrophotoinitiator, effectively broadening the distribution.[286] Interestingly, for the DMPA and Irgacure 819 initiated reactions, a strong increasing reaction rate is observed in the first minutes of the reaction, after which the first order plot becomes almost linear, indicating a switch in the initiation mechanism. Such change in the mechanism may indicate complete consumption of the initiator, after which the polymerization becomes photoiniferter-controlled (note that the

Table 5.1 Results for the tested photoinitiators and the photoiniferter reaction. All reactions were done in butyl acetate using *n*-butyl acrylate as monomer. Reactions were performed in a microflow reactor at 60 °C with a reaction time of 20 minutes and a light intensity of 30 mW cm^{-2}.

	Initiator	**Molar Ratio M:R:I**	**Conversion**	$M_{n,\,theory}$ **[g mol^{-1}]**	$M_{n,\,GPC}$ **[g mol^{-1}]**	**Đ**
1	-	80:1:0	61 %	7200	6800	1.12
2	Benzoin	20:1:0.25	85 %	2700	3100	1.18
3	DMPA	20:1:0.25	87 %	2800	3000	1.18
4	Irgacure 819	20:1:0.25	88 %	2800	3600	1.55
5	Irgacure 2959	20:1:0.25	94 %	3000	3500	1.20

slope of the linear region does not differ significantly from the pure photoiniferter reaction). In order to understand the differences between benzoin and Irgacure 2959, the decomposition rates were determined at 360 nm for both initiators. For benzoin, a pseudo zeroth order decomposition rate of 8.1 x 10^{-5} M s^{-1} and for Irgacure 2959 of 13.0 x 10^{-5} M s^{-1} was calculated. This corresponds to full decomposition of both initiators within 5-10 minutes under the given conditions. That Irgacure 2959 allows for a faster polymerization is in good agreement with the higher decomposition rate. The reason as to why the reaction proceeds further at high rate even after the initiator was decomposed remains unknown. The connection between fast initiation and fast polymerization is complex (more initiation leads to higher termination rates and thus in principle to lower overall monomer conversions). For the choice of the best photoinitiator the absorption spectrum is one thing to look at. Due to the here used broadband UV-lamps a spectral range between 320 and 500 nm was covered. To have a full view on the initiation step also the reactivity of the different initiator fragments created during

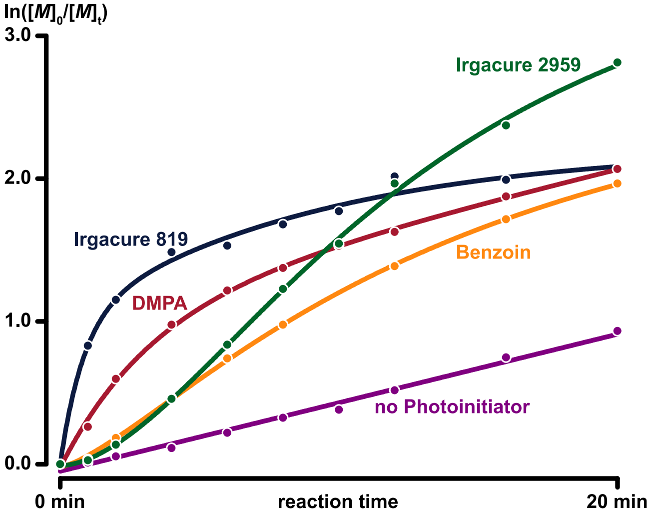

Figure 5.6 Kinetic first-order plot for photoRAFT polymerization of *n*-butyl acrylate in butyl acetate using different initiators. All reactions were performed in a microflow reactor at 60 °C with a light intensity of 30 mW cm^{-2}. The employment of photoinitiators allows for fast reaction rates and reaching monomer conversions above 90 % in 20 minutes.

decomposition need to be considered. More detailed investigations into this phenomenon are currently underway in the Junkers research group.

5.4. Conclusions

PhotoRAFT polymerizations of *n*-butyl acrylate have been studied in depth for polymerizations initiated by conventional radical photoinitiators. As shown in this chapter, polymerizations can be fast, and yield materials that are comparable with regards to chain length control, dispersity and chain end fidelity to conventional RAFT polymerization. Polymerizations can also be comparable to photoRAFT reactions that proceed via a photoiniferter initiation mechanism. The choice of initiator plays a very significant role with respect to the outcome of the polymerization, especially with regards to the overall polymerization rate. The differences seen for the various initiators can be due to the decomposition rate of the initiators, whereby some initiators decay faster than the runtime of a typical polymerization, indicating that the photoiniferter initiation becomes the dominant driver for the polymerizations at a certain point, even if exogenous photoinitiators are added.

Chapter 6

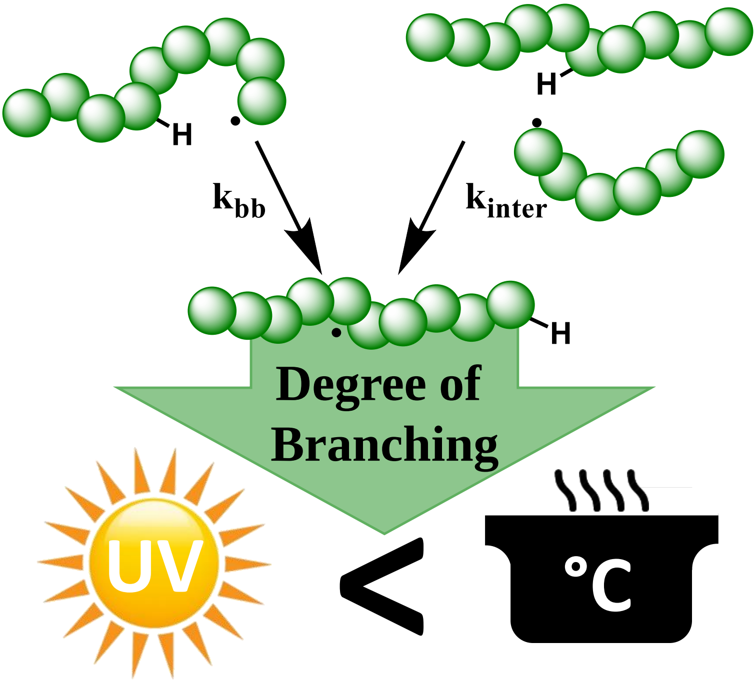

6. Photo-induced Acrylate Polymerization: Unexpected Reduction in Chain Branching[††]

6.1. Abstract

The branching stemming from mid-chain radical formation in *n*-butyl acrylate polymerization was investigated via melt-state ^{13}C NMR measurements. The dependence of the degree of branching on the monomer conversion of the system was examined for photo-induced polymerizations, revealing a steady increase in branching with conversion. For polymerization at moderate light intensities, an increase in branching from 0.03 to 0.37 % was observed at 60 °C, which is fivefold below the level of branching observed in thermally initiated polymerizations under otherwise identical reaction conditions. The reason for this overall reduction in branching remains momentarily unclear, yet, a strong dependence of branching on light intensity was observed. While polymerization under a 1 W LED lamp resulted in branching degrees of 0.22 % at almost full monomer conversion, polymerization under a 400 W lamp yielded 1.81 % of chain branches.

6.2. Introduction

Polyacrylates constitute an important class of polymeric materials. They possess a large variation in physical properties, facile functionalization and, generally, very high polymerization rates. Applications are found in virtually any field ranging from adhesives to drug carriers. Until today, some uncertainties persist regarding their mechanism of polymerization. For a long time, it was believed that acrylates

---

[††] First published partly as "Photoinduced Acrylate Polymerization: Unexpected Reduction in Chain Branching", B. Wenn, G. Reekmans, P. Adriaensens, T. Junkers, *Macromol. Rapid Commun.* 2015, 36, 1479-1485 and

"Chain Branching in Photoinduced Acrylate Polymerization", M. Gomes, L. van Lokeren, B. Wenn, G. Reekmans, P. Adriaensens, T. Junkers, *ongoing research*.

follow a classical radical polymerization behavior. Not too long ago, it was established that the radical polymerization mechanism is overshadowed by extensive transfer-to-polymer reactions.[287-289] The mechanism itself is nowadays presumably well understood and for *n*-butyl acrylate an extensive set of reliable kinetic data has been obtained.[289-294] Key to the specific polymerization behavior of acrylates is the formation of so-called mid-chain radicals (MCR).[289, 295] Mid-chain radicals are formed via two distinct pathways, that is *intra*- or *inter*molecular radical transfer (see Figure 6.1). Secondary propagating radicals (SPR) are readily transformed into the more stabilized MCRs, either via a hydrogen-shift reaction (*intra*molecular, often referred to as backbiting reaction) or via abstraction of a

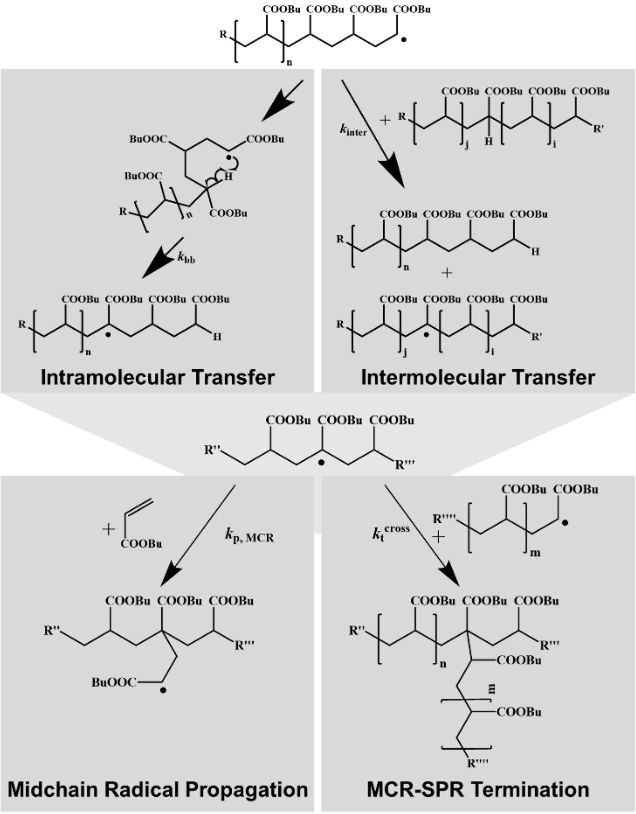

Figure 6.1 Schematic overview of the acrylate polymerization reaction pathways involving mid-chain radicals.

hydrogen atom at a random position of a surrounding polymer chain (*inter*molecular, note that this can in principle also be the radical's own chain in a very specific case of *intra*molecular transfer). Backbiting is an intrinsic problem in acrylate polymerization and its occurrence can – at least this is assumed to date – only be overcome by reducing the polymerization temperature into a regime where backbiting does not occur to significant extend (below room temperature).[296, 297] Interestingly, controlled radical polymerization techniques had been found to yield significantly reduced levels of chain branching.[298] Also by using classical chain transfer agents, a large reduction in branching was observed.[295, 299] Yet, no technique exists to completely avoid mid-chain radical formation at relevant reaction temperatures.

MCRs can react via several reaction channels. Most notably – in the presence of monomer – propagation can occur (at strongly reduced reaction rate compared to SPRs),[300] which will transform the MCR eventually back into a SPR (see Figure 6.1). Alternatively, different termination reactions can occur, either with SPR or other MCR species, from which the second may be regarded as mostly insignificant due to steric hindrance and the foreseeable lower specific cross-termination rate coefficients. Only at high temperature (that is for *n*-butyl acrylate above 80 °C) can scission reactions occur, in which unsaturated polymers are formed alongside a shorter SPR.[301, 302] Thus, as long as polymerizations are carried out at a temperature below the onset temperature of MCR scission, every MCR inevitably results in the formation of a chain branch, either a short chain branch (backbiting followed by MCR propagation or termination) or a long chain branch (random *intra*- or *inter*molecular transfer followed by propagation or termination). The number of quaternary carbon atoms (and thus the overall number of branches) in the polymer product can in principle be used to quantify how many mid-chain radicals were formed during polymerization. The average number of branch points per chain directly translates to the propensity of a growing chain to run through a transfer/propagation or transfer/termination cycle. Such information is important as it is complementary to the kinetic experiments described in literature, where low-conversion pulsed laser techniques are employed.

Quantification of quaternary carbon branch points is in principle performed via conventional liquid state NMR spectroscopy. Different methods have been discussed to quantify the degree of branching in polyacrylates.[288, 303, 304] Gaborieau *et al.* developed a method to measure the degree of branching (DB) in polyacrylates via quantitative melt state ^{13}C NMR spectroscopy.[295, 303] It was shown before that quantitative ^{13}C NMR spectroscopy is a direct way to access DB.[288, 298, 303, 305-307]

In this chapter, melt state ^{13}C NMR spectroscopy was employed to have a closer look on the development of the degree of branching with increasing monomer conversion in *n*-butyl acrylate polymerization. In this way, the cumulative effect of *inter*- and *intra*molecular transfer can be quantified. In principle, from such data, the rate of intermolecular transfer could be estimated using kinetic modelling and literature rate parameters for the other individual reactions. Nikitin *et al.* described previously analytical equations for the analysis of such data.[308] Compared to the previous study by Gaborieau *et al.,* photo-initiation was used rather than thermal polymerization. In this way, reactions can be suddenly stopped in a controlled fashion simply by turning off the UV source. Interestingly – as will be shown in detail below – a drastic reduction in the branching level was observed when employing UV initiation and a strong dependence of the branching content on light intensity is observed. At low light intensities, a steady increase of chain branching with increasing monomer conversion was observed. However, the overall degree of branching remains significantly below the expected threshold reported earlier for pure thermal polymerizations.

6.3. Results and Discussion

The employment of photo-induced free radical acrylate polymerization enables to monitor the development of MCR creation with increasing monomer conversion. Quantitative ^{13}C melt state NMR was used to determine the degree of branching in the synthesized poly(*n*-butyl acrylate) polymers. The degree of branching was calculated with Eq. 6.1, in which $I(C_q)$ is the integral of the quaternary carbon signal around 49 ppm and $I(\text{-}\mathbf{CH_3},\text{CH}_3\text{-}\mathbf{CH_2}\text{-})$ the signal of two side chain carbon atoms (14 and 20 ppm) (Figure 6.2). An example of the spectral integration is given in Figure 6.2. An assignment of all peaks can be found in literature.[303, 304]

$$DB(\%) = \frac{I\left(C_q\right)\cdot 100}{\frac{I\left(-\boldsymbol{CH}_3,\ CH_3-\boldsymbol{CH_2}-\right)}{2}} \qquad \textbf{Eq. 6.1}$$

Table 6.1 summarizes the obtained DB for poly(*n*-butyl acrylate) with monomer conversions from 10 to 99 % in benzoin-initiated UV polymerization in bulk at 60 °C. After an initialization period with up to about 30 % monomer conversion, the degree of branching increases linearly with increasing monomer conversion and reaction time (see Figure 6.4). Normally, at 60 °C for uncontrolled bulk polymerizations, DBs of around 2 % should be obtained at high conversions.[295] Thus, before the present data is discussed further, some remarks must be made on the reliability of the herein used methodology.

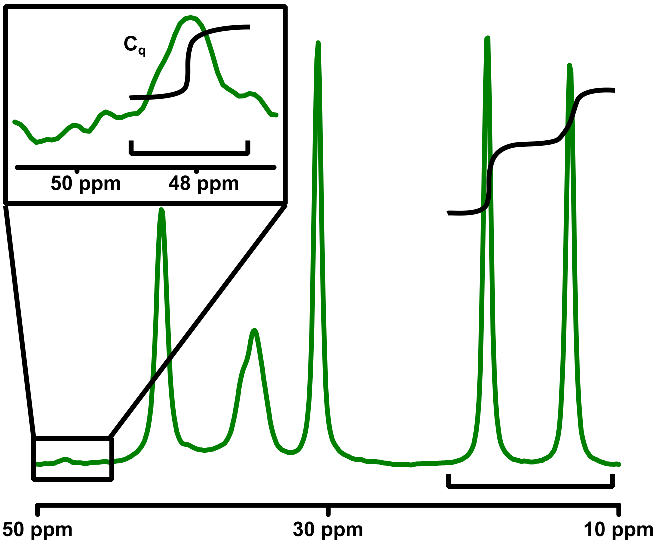

Figure 6.2 Melt-state ^{13}C MAS NMR spectrum of poly(*n*-butyl acrylate) obtained from thermally AIBN-initiated radical polymerization at 60 °C with 93.7 % monomer conversion. The spectrum was recorded at 100 °C (T_g +150 °C). The integration areas for the degree of branching determination are shown.

Polymerizations were carried out at 60 °C to avoid the occurrence of β-scission reactions. When using benzoin, no thermal decomposition occurs. A control experiment where the benzoin-containing sample was left at 60 °C in the dark showed no significant conversion (0.64 % after 5h). Thus, it can be safely assumed that only photoinitiation is active in the system. Further, good

Table 6.1 Monomer conversion and degree of branching (DB) of UV-initiated poly(*n*-butyl acrylate) at 60 °C under variation of the reaction time and light source. S/N = signal to noise

#	**Conversion [%]**	**Reaction time [min]**	**S/N**	**DB [%]**
1	**10.1**[a]	3	2.7	0.03±0.01
2	**22.2**[a]	7	3.5	0.03±0.01
3	**40.2**[a]	8	4.3	0.09±0.02
4	**47.3**[a]	11	4.3	0.14±0.03
5	**60.2**[a]	12	10.7	0.18±0.02
6	**79.4**[a]	18	17.9	0.28±0.02
7	**89.8**[a]	22	13.6	0.34±0.03
8	**98.1**[a]	50	9.9	0.36±0.04
9	**99.8**[a]	360	12.8	0.37±0.03
10	**99.9**[b]	120	9.3	0.22±0.02
11	**99.1**[c]	60	27.2	1.41±0.05
12	**98.6**[d]	60	31.3	1.81±0.06
13	**97.4**[e]	120	32.9	1.75±0.05
14	**98.9**[f]	480	23.6	1.26±0.05
15	**93.7**[g]	480	31.3	1.92±0.06
16	**98.1**[h]	15	-	0.87
17	**98.6**[i]	15	-	1.04

Reaction conditions: [a] 4 x 15 W, λ_{max}= 254 nm, UV-Lamps; [b] 1 W, λ_{max}= 360 nm, UV-LED; [c] 8 x 15 W, λ_{max}= 365 nm, UV-Lamps; [d] 400 W, λ_{max}= 365 nm, UV-Lamp; [e] 8 x 15 W, λ_{max}= 365 nm, UV-Lamps, Initiator: 10^{-3} mol L^{-1} DMPA; [f] 8 x 15 W, λ_{max}= 365 nm, UV-Lamps, Initiator: 10^{-3} mol L^{-1} AIBN; [g] reference sample of thermally-initiated polymerization of *n*-butyl acrylate at 60 °C, Initiator: 10^{-3} mol L^{-1} AIBN; [h] 8 x 15 W, λ_{max}= 365 nm, UV-Lamps, Initiator: 10^{-3} mol L^{-1} Irgacure 819; [i] 8 x 15 W, λ_{max}= 365 nm, UV-Lamps, Initiator: 10^{-3} mol L^{-1} Irgacure 2959.

temperature control was ensured by using an oil bath within a large photoreactor. The used NMR method was adapted from literature. Slight differences in the experimental setup could potentially lead to distorted results. In the present study, Al_2O_3 was used as an inorganic filler material to allow for stable magic angle spinning of the ceramic NMR rotor. Comparison of samples that were measured in the presence and in the absence of the filler showed no significant difference in the integration values and DB. Furthermore, an additional polyacrylate sample from AIBN-initiated polymerization (no UV-light) at 60 °C was measured with the above mentioned NMR method, resulting in a branching degree of close to 2 % (Table 6.1 line 15). This value is in excellent agreement with literature data, meaning that the method is reliable.

The use of UV-initiation leads to moderate polymerization rates. Quantitative conversion was reached after roughly 1 h, thus enabling to obtain samples for very low monomer conversions (10 % after 3 min). The monomer conversion-time evolution shows a steady increase in conversion with time, but scatter in the data is rather high. This scatter can be explained by the different positions of the samples within the UV-reactor, which result in different irradiation doses that reached the samples. Benzoin was chosen as initiator since it decomposes into two equally well-initiating fragments, and hence does not create radicals that may persist for extended life-times in the polymerization mixture.[286] Specific

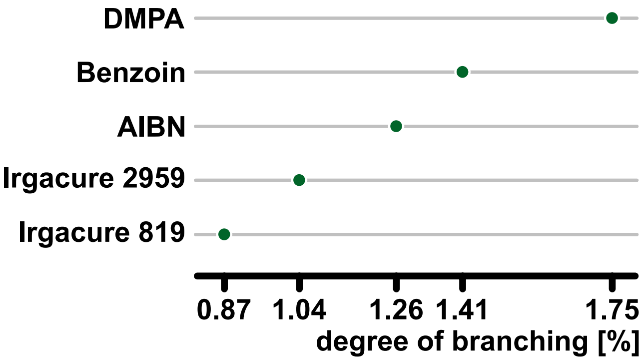

Figure 6.3 Degree of branching for poly(*n*-butyl acrylate) polymerized at 60 °C under UV-light (λ_{max} = 365 nm) initiated with different photo-active initiators and conversions above 93 %.

termination of initiator-derived radicals with MCRs can thus be assumed to be not operational. Other initiators, such as 2,2-dimethoxy-2-phenylacetophenone (DMPA), azobisisobutyronitrile (AIBN) or the industrial used Irgacure 819 or Irgacure 2959, may exhibit such behavior. Comparison of experiments with different initiators shows a clear change in the specific DB for the industrial used Irgacure initiators (Figure 6.3). Compared to thermally-initiated polymerization, the degree of branching in the UV-initiated system is reduced by a factor of five at high conversions. At low conversions (up to 20 %), negligible amounts of branching (DB = 0.03 %) are detected. This low value is very close to the detection limit at which the signal $I(C_q)$ can still be integrated. From 30-40 % of monomer conversion on, the DB increases linearly until a maximum value of 0.37 % is reached at full conversion. Further illumination of the sample for extended periods of time does not lead to a significant increase in the DB, demonstrating that the UV-light alone has, under the chosen conditions, no direct influence on MCR formation or crosslinking. The increase in DB with monomer conversion can be explained on the basis of two mechanisms: (*i*) *inter*molecular transfer scales with the concentration of polymerized monomer units: the amount

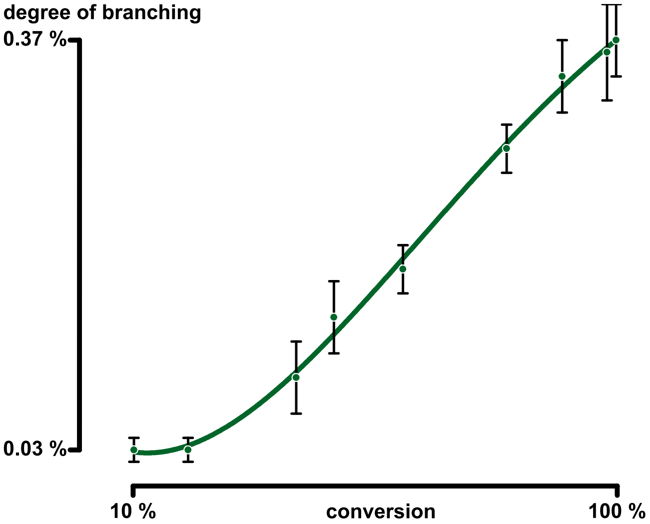

Figure 6.4 Change in degree of branching with increasing monomer conversion for UV-initiated poly(*n*-butyl acrylate) synthesized at 60 °C with four 15 Watt lamps (λ_{max} = 254 nm).

of branching should increase when the polymer concentration increases. This explanation is also in agreement with the onset period seen in Figure 6.4. As long as the polymer solution is still in the diluted regime, no or only little contact between isolated polymer chains occurs. Hence, no *inter*molecular transfer may take place. Only above a critical concentration at which coils start to overlap, effective proton abstractions from chain to chain may happen. (*ii*) Due to the decrease in monomer concentration, the overall rate of propagation is reduced. Since MCR and thus branch formation is dependent on the ratio of *intra*- and *inter*molecular radical transfer over the rate of SPR propagation, an increase in DB is expected from this effect alone. In practice, a combination of the two mechanisms should be responsible for the observed behavior. In principle, the cumulative effect of both mechanisms could be estimated via kinetic modelling using relatively simple acrylate polymerization models. Even though extensive modelling was performed and the qualitative increase in DB with conversion can be well represented in such model, any prediction based on literature backbiting and MCR propagation rate coefficients fails in reproducing the overall low DB observed (in line with previous studies that aimed at modelling DB on the basis of available kinetic data). As seen in this study, lower DB can only be modelled on the basis of significantly reduced backbiting rate coefficients, which stands in strong contrast to the Pulsed-Laser-Polymerization-derived values. As no doubt exists about the validity of these literature rate coefficients, other approaches must be taken to explain the observed branching levels. Differences in termination behavior can also not play a significant role because every transfer step leads to a later chain branch, irrespective of the MCR follow up reaction. Thus, the only remaining explanation is that continuous UV irradiation has a direct influence on the backbiting/transfer reaction itself. For unknown reasons, light seems to favor SPR propagation over backbiting (either speeding one up or slowing the other down). No direct physical reason can be identified whether light incidence should change branching levels. To test the hypothesis, several experiments were carried out, in which the light source, and most notably light intensity were varied. In the above described experiments, rather low intensity lamps were used (in total 60 W, it should be noted that the peak wavelength was well below the UV cut-off of borosilicate so that intensities within the reaction vessel were significantly lower). Further experiments were carried out with 1 W LEDs as well as with high-pressure lamps with intensities up to 400 W. Results from these experiments for high monomer conversions are found in Figure 6.5. A clear dependence of branching levels on light intensity is observed with the lowest DB being observed for the LED and the highest for the 400 W lamp. Overall, for the 400 W lamp, branching levels comparable to the thermally-initiated system at the same temperature are observed. Even though such correlation is evident, it still fails in explaining the overall low branching at low light intensities, and are thus in contradiction to the above hypothesis that light irradiation changes the individual reaction rates. In principle, it is possible that the high energy lamps do not change branching via MCR reactions at all, but favor hydrogen radical abstraction directly by light incidence, and hence cause higher branching levels. This hypothesis is also supported by the predictions made by Nikitin and Hutchinson, who showed that DB should decrease with increasing levels of radical initiation.[309]

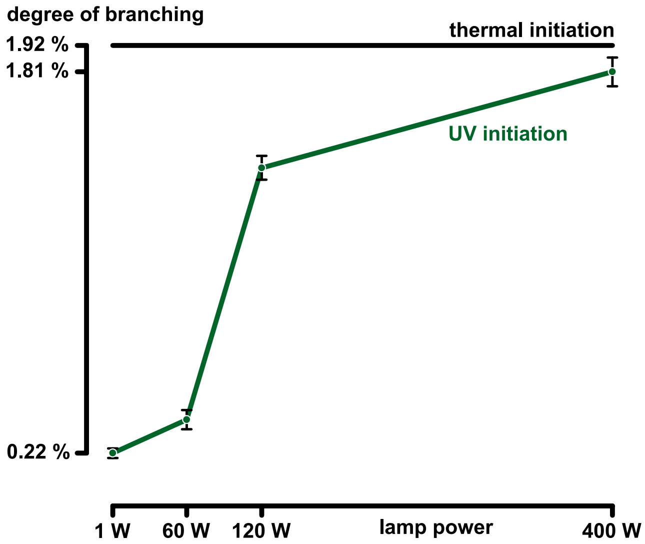

Figure 6.5 Development of degree of branching in UV initiated poly(*n*-butyl acrylate) with monomer conversion above 93 % as a function of increasing lamp power at 60 °C.

6.4. Conclusions

The evolution of the degree of branching with increasing monomer conversion in *n*-butyl acrylate polymerization was investigated via photo-induced polymerization and melt state ^{13}C NMR. A clear dependence of branching on monomer conversion is observed, in line with the theory of *inter*- and *intra*molecular transfer to polymer reactions. Surprisingly, the overall level of branching, even at full monomer conversion, is far below the expected levels when compared to the previously studied thermal polymerizations of *n*BA. The reasons remain unclear. Since each transfer-to-polymer step is inevitably followed by the formation of a chain branch (polymerizations were studied before the onset temperature of chain scission) and the polymerization system is known to show non-significant chain transfer to solvent or monomer, it can be concluded that either backbiting rates are reduced or that propagation rates are increased in the system. However, the two hypotheses seem to be unlikely and further studies need to be carried out to shine further light on this effect. Additionally, secondary reactions involving the initiator fragments may have an influence on the result, even if preliminary data suggest that this influence is small. Further investigations into UV-light intensities reveal a strong dependence of DB on lamp power, and when a 400 W UV lamp is employed, branching levels compared to thermal initiation are obtained.

Chapter 7

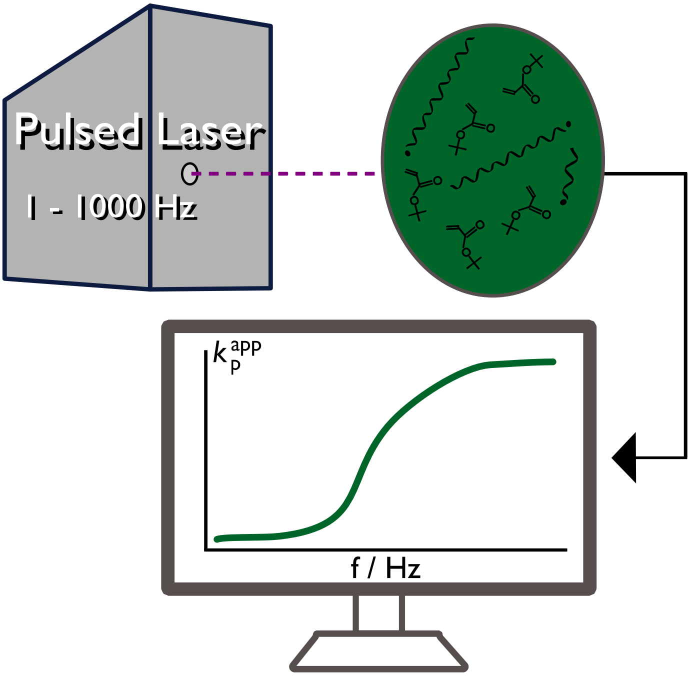

7. Kilohertz Pulsed-Laser-Polymerization: Simultaneous Determination of Backbiting, Secondary and Tertiary Radical Propagation Rate Coefficients for *tert*-Butyl Acrylate[‡‡]

7.1. Abstract

For the first time, a 1000 Hz pulsed-laser has been applied to determine detailed kinetic rate coefficients from pulsed-laser-polymerization – size exclusion chromatography (PLP-SEC) experiments. For the monomer *tert*-butyl acrylate (*t*BA), apparent propagation rate coefficients k_p^{app} have been determined in the temperature range of 0 to 80 °C. k_p^{app} in the range of few hundreds up to 50000 L mol^{-1} s^{-1} were determined for low and high pulse frequencies. The apparent propagation coefficients show a distinct pulse-frequency dependency, which follows a S-shape curve. From these curves, rate coefficients for secondary radical propagation (k_p^{SPR}), backbiting (k_{bb}), mid-chain radical propagation (k_p^{tert}) and the (residual) effective propagation rate (k_p^{eff}) can be deduced via a simple Predici fitting procedure. For k_p^{SPR}, the activation energy was determined to (17.9 ± 0.6) kJ mol^{-1} in excellent agreement with literature data. For k_{bb}, an activation energy of (25.9 ± 2.2) kJ mol^{-1} is deduced.

[‡‡] First published as: “Kilohertz Pulsed-Laser-Polymerization: Simultaneous Determination of Backbiting, Secondary and Tertiary Radical Propagation Rate Coefficients for *tert*-Butyl Acrylate”, B. Wenn, T. Junkers, *Macromol. Rapid Commun.* 2016, 37, 781-787.

7.2. Introduction

The invention of the Pulsed Laser Polymerization (PLP) technique, almost 30 years ago[310, 311], can from today's distance be regarded as one of the biggest revolutions in radical polymerization chemistry. With the ability to measure propagation rate coefficients in a fast and reliable manner, the general understanding of radical polymerization kinetics was largely accelerated. It is not surprising that the development of the first reversible deactivation radical polymerization techniques fell into the same time period or shortly after. Over the years, very reliable propagation rate coefficients for a broad range of monomers were deduced and eventually benchmarked by an IUPAC working party.[312-315] Only acrylate monomers continued to be problematic until the very late 90s, as side reactions blurred the characteristic PLP molecular weight distributions that are used to derive the kinetic coefficients.[290, 316, 317] Today it is well understood that the complications in acrylate k_p determinations stem from the formation of so-called mid-chain radicals (MCRs)[288, 291, 301, 305, 318], which form upon intramolecular backbiting reactions (with the rate coefficient k_bb). These MCRs are of significantly lower reactivity compared to the chain-end secondary propagating radicals (SPRs), and can either add monomer in a MCR propagation step (associated with the kinetic coefficient $k_\mathrm{p}^\mathrm{tert}$), or terminate with surrounding transient radicals.[318] Additionally – when temperature is sufficiently high – also β-scission of the MCRs is possible.[301, 302] Lately, a MCR migration mechanism was confirmed demonstrating that radicals can travel along the backbone of an acrylate.[319-321] The negative impact of the low-reactivity of MCRs on the PLP measurements could be largely overcome by applying higher laser pulse frequencies. While 100 Hz lasers are sufficient to measure most acrylates up to room temperature, 500 Hz lasers have given access to the temperature range up to the point where β-scission adds increasing complexity to the reaction scheme, giving further reason for the failure of the kinetic experiments.[322, 323] Generally, for fast propagating monomers, higher laser pulse frequencies are beneficial and increase the accuracy of the k_p determinations, with limits of the pulse frequency being only of technical

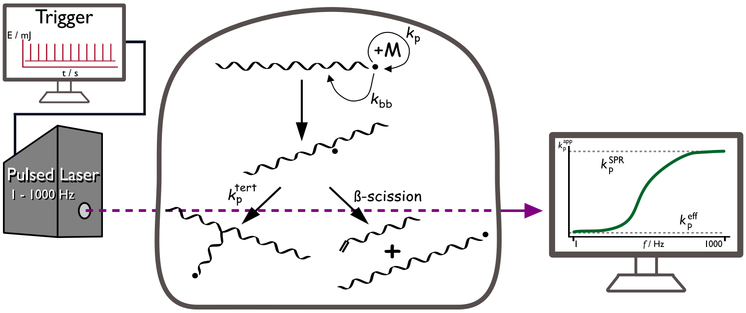

Scheme 7.1 Reaction scheme for the major acrylate-specific reactions complicating the PLP determination of k_p. The graph depicts the typical variation of k_p^{app} determined at increasing laser pulse frequencies.

nature. Lately, kHz excimer laser systems have become available. They are interesting to apply to outstanding dilemmas in acrylate kinetic investigations.

While the propagation rate coefficient for SPR species is available from high frequency PLP, the application of decreasing laser pulse frequencies can also be of interest with regards to acrylate polymerization. As shown already a few years ago, the observable propagation rate coefficient k_p^{app} (deduced from the characteristic inflection point in the molecular weight distribution (MWD) of a PLP distribution under conditions where backbiting has already distorted the result; note that k_p^{app} and k_p^{eff} are not identical) follows a S-shape curve towards lower frequencies (see also Scheme 7.1).[300] Unsurprisingly, the upper plateau in this S-curve represents the SPR k_p. The lower plateau is a measure for the effective propagation rate, which is derived from the equation:[291, 304]

$$k_p^{eff} = k_p^{SPR} - \frac{k_p^{SPR} - k_p^{tert}}{1 + \frac{k_p^{tert}[M]}{k_{bb}}} \qquad \textbf{Eq. 7.1}$$

The fall-off of the curve is then a measure for k_{bb} and k_p^{tert}, which are interconnected via the above equation and can be seen as a pair of parameters. Nikitin *et al.* were the first to exploit this characteristic of the frequency-dependent k_p^{app} to determine backbiting and MCR propagation rate parameters for the monomer *n*BA.[300] To reach this aim, they used a simulation approach, in which PLP-derived MWD structures were simulated based on different k_{bb}. These were subsequently compared to the experimental distributions. Unfortunately, this first study was not followed by further publications and the procedure requires a large number of simulations to determine accurate rate coefficients. This lack of further data can be explained by the relatively small range of conditions that could be accessed with the then employed 100 Hz laser system. With access to high frequency lasers, a much higher accuracy can be reached (exact determination of k_p^{SPR} is crucial for the procedure), and as it will be shown below, kHz pulsing is of significant advantage for this purpose.

To the best of my knowledge, this is the first report on kHz-PLP measurements. The variation of the apparent propagation rate coefficients with the pulse frequency in *tert*-butyl acrylate polymerization was studied. As described above, such studies require knowledge of apparent k_p at very high pulse frequencies in order to observe the entire effect of the MCR influence. *t*BA polymerization was studied in the temperature range from 0 to 80 °C. From this data Arrhenius relations for the SPR propagation rate coefficient (k_p^{SPR}), backbiting rate coefficients (k_{bb}), MCR propagation (k_p^{tert}) and effective propagation rate coefficients (k_p^{eff}) were deduced.

7.3. Results and Discussion

Overall, in the approach of Nikitin *et al.*, the authors exploited the fact that k_{bb} and k_p^{tert} are interlinked via Eq. 7.1. Via simplification and rearrangement of the equation one receives:[300]

$$k_{bb} = [M]\left(\frac{k_p^{SPR}}{k_p^{eff}} - 1\right)k_p^{tert} \qquad \textbf{Eq. 7.2}$$

To fit the data, k_p^{SPR}, k_p^{eff} and [M] are required as input parameters, and fitting of only one parameter (either k_{bb} or k_p^{tert}) is sufficient, which largely simplifies the modelling exercise to be performed. Nikitin *et al.* simulated full MWDs and compared those to the experimental data. This approach is time-consuming and requires the assumption of a number of other rate coefficients, such as termination or transfer-to-monomer rate coefficients. Also, SEC-band broadening must be accounted for to identify comparable inflection points between experiment and simulation. It is relatively unclear whether such procedure constitutes a true fitting procedure, since rate parameters are rather guessed than fitted. Consequently, it was opted for the development of a simplified procedure that is easier to apply, avoids issues related to band-broadening in simulations and is broadly applicable. Therefore, a standardized procedure was followed. k_p^{SPR} and k_p^{eff} were estimated via a sigmoidal fit of the experimental data, as shown in Figure 7.1 for *t*BA at 20 °C. It should be noted that such a procedure necessarily underestimates k_p^{eff} as the apparent k_p drops off to almost zero at hypothetically infinitely small pulse frequency. This was also described by Nikitin, who then always assumed k_p^{eff} to be significantly larger than the lower plateau value.[300] Unfortunately, no clear rule can be deduced about how much larger k_p^{eff} should be, and hence for the sake of this study the (also slightly overestimated) values of the fitting procedure were taken. Next, these data were used as input

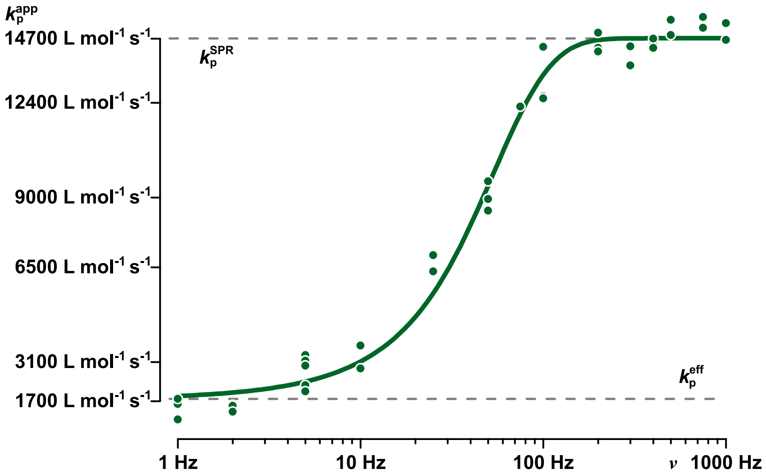

Figure 7.1 *t*BA k_p^{app} at 20 °C in the frequency range 1 < *f* < 1000 Hz with a sigmoidal fit of the data to estimate k_p^{SPR} and k_p^{eff}.

parameters for a Predici model. Within the model, no full PLP-characteristic distributions were calculated. The model assumes a monodisperse growth of propagating radicals in time, an assumption that certainly holds true for short delays between two laser pulses. From M_n of the radical distribution at any given point in time, a k_p^{app} can be directly calculated, allowing to obtain a full S-curve within a single simulation run. With this approach, it is ignored that k_p^{app} is determined from the first inflection point of the PLP structure rather than the maximum of the peak molecular weight. Since radical distributions are used, this approach is justified. Within the model, only k_p^{tert} is left as variable parameter, and k_{bb} is internally calculated based on Eq. 7.2. Hence, in order to fit the experimental data, k_p^{tert} was varied. It is clear that the variation of k_p^{tert} leads to a side-shift of the S-curve, with a delay of the onset of increasing apparent propagation rate coefficients with accelerating MCR propagation. To quantify the shift, the pulse frequency was determined for an arbitrarily chosen k_p^{app} reference point, ideally in a range where the shift of the curves is most significant (close to the inflection point). This data is then fitted and from the experimentally derived pulse frequency at the reference point, k_p^{tert} (and hence also k_{bb}) for the experimental series is determined. This procedure was thoroughly tested and was found to be very robust. Crucial for the result is, however, to choose k_p^{SPR} and k_p^{eff} correctly. While k_p^{SPR} is with high-frequency pulsing sufficiently accessible (which alone is a significant improvement since the early study), k_p^{eff} is more difficult to assess (see above), and the error in k_p^{eff} is directly reflected in the error of k_p^{tert}.

To test the validity of this approach, first k_p^{app} for *n*-butyl acrylate at 20 °C between 1 and 1000 Hz was measured. For *n*BA, k_{bb} and k_p^{tert} were determined before,[292, 300] which allowed to test this method. From the above sketched procedure, k_{bb} was determined experimentally at 20 °C to 106 s^{-1} and k_p^{tert} to 1.50 L mol^{-1} s^{-1}. Extrapolation of the data of Nikitin *et al.* yields a k_{bb} of 109 s^{-1} and k_p^{tert} of 10.8 L mol^{-1} s^{-1}.[300] Thus, while k_{bb} matched almost perfectly, k_p^{tert} differed by almost one order of magnitude. This is explained by the vast difference in the assumption of k_p^{eff}. While here a value of 1204 L mol^{-1} s^{-1} was used, Nikitin assumed an almost five-fold higher value, which is then directly reflected in k_p^{tert}. Using the five-fold higher value, an almost identical k_p^{tert} was obtained from Eq. 7.2 for the here obtained data. In an independent approach, Barth *et al.* determined k_{bb} and k_p^{tert} from ESR measurements, where for the same conditions a k_{bb} of 105 s^{-1} and a k_p^{tert} of 8.3 L mol^{-1} s^{-1} were found.[292] It can be concluded that with this procedure k_{bb} is very well estimated, while k_p^{tert} is associated with a certain error that is currently difficult to quantify. It should be noted, that k_p^{tert} can be, however, easily recalculated when another k_p^{eff} is inserted, thus when independent k_p^{eff} data becomes available (for example from steady-state polymerization experiments).

After the method is validated (fully for k_{bb} and partially for k_p^{tert}), the *t*BA system can be discussed in detail.

Figure 7.2 depicts the experimental data obtained in the temperature range from 0 to 80 °C alongside with the simulated S-curves from Predici for the optimized k_p^{tert} / k_{bb} pair. Note that the lower plateau shows only very little temperature variation, and almost all simulated curves converge at practically 0 L mol^{-1} s^{-1} at

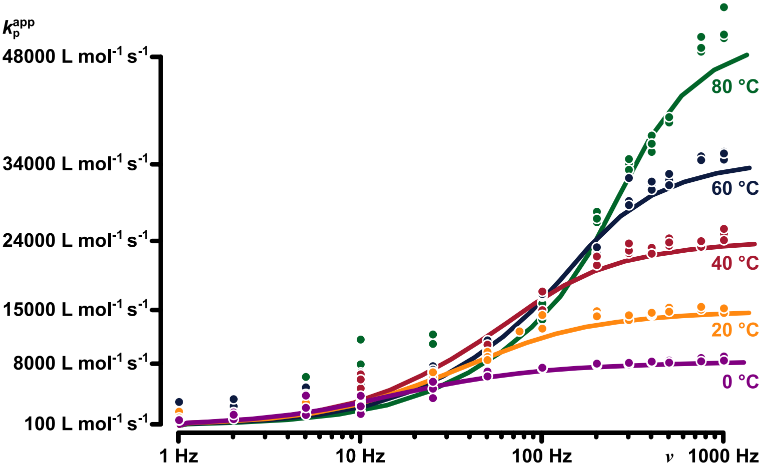

Figure 7.2 Experimental k_p^{app} for *t*BA in the temperature range of 0 to 80 °C for pulse frequencies between 1 and 1000 Hz. The curves depict the S-curves for optimized kinetic parameters as derived from Predici modelling based on the parameters given in Table 7.1.

low frequencies irrespective of the k_p^{eff} chosen. Interestingly, even though k_p^{SPR} was always chosen practically as an average of the k_p^{app} of the highest frequency data, the fit increasingly underestimates the high plateau with increasing temperature, indicating that even at 1000 Hz the final plateau may not yet be fully reached. The full set of kinetic rate coefficients for the different fits are completed in Table 7.1. The deduced data for k_p^{SPR} are almost identical to the data derived from classical 500 Hz PLP,[324] again underpinning the high quality and statistical robustness of the present data. Unsurprisingly, k_p^{eff} shows a much smaller variation than k_p^{SPR}. k_{bb} varies from 51 s^{-1} to 720 s^{-1} and k_p^{tert} changes from 1.5 to 12 L mol^{-1} s^{-1} in the same temperature range.

Arrhenius plots for the data are given in Figure 7.3 and resulting frequency factors and activation energies are given in Table 7.2 (linear best fits of data taking a weighted error of 20 % into account). For k_p^{SPR}, an activation energy of (17.9 ± 0.6) kJ mol^{-1} was obtained. Previously, with 500 Hz PLP, this value was determined to 17.5 kJ mol^{-1}. Both values are hence in very good agreement. It should be noted that fitting non-linear Arrhenius data might yield refined values, but for the sake of comparison, linear least square fitting is sufficient. Also Couvreur *et al.* had previously determined the activation energy to 17.7 kJ mol^{-1} for low-temperature conditions, employing 100 Hz laser technology.[300] While this agreement is satisfying, it is not so surprising as in the previous PLP studies –

Table 7.1 Experimentally determined rate coefficients for the data given in Figure 7.2.

T [°C]	**k_p^{eff} [L mol^{-1}]**	**k_p^{SPR} [L mol^{-1}]**	**k_{bb} [s^{-1}]**	**k_p^{tert} [L mol^{-1}]**	**c_M [mol L^{-1}]**
0	1390	8230	51	1.5	7.05
20	1780	14710	108	2.2	6.89
40	2640	23640	201	3.8	6.73
60	4110	33920	349	7.3	6.57
80	4810	49870	718	12.0	6.41

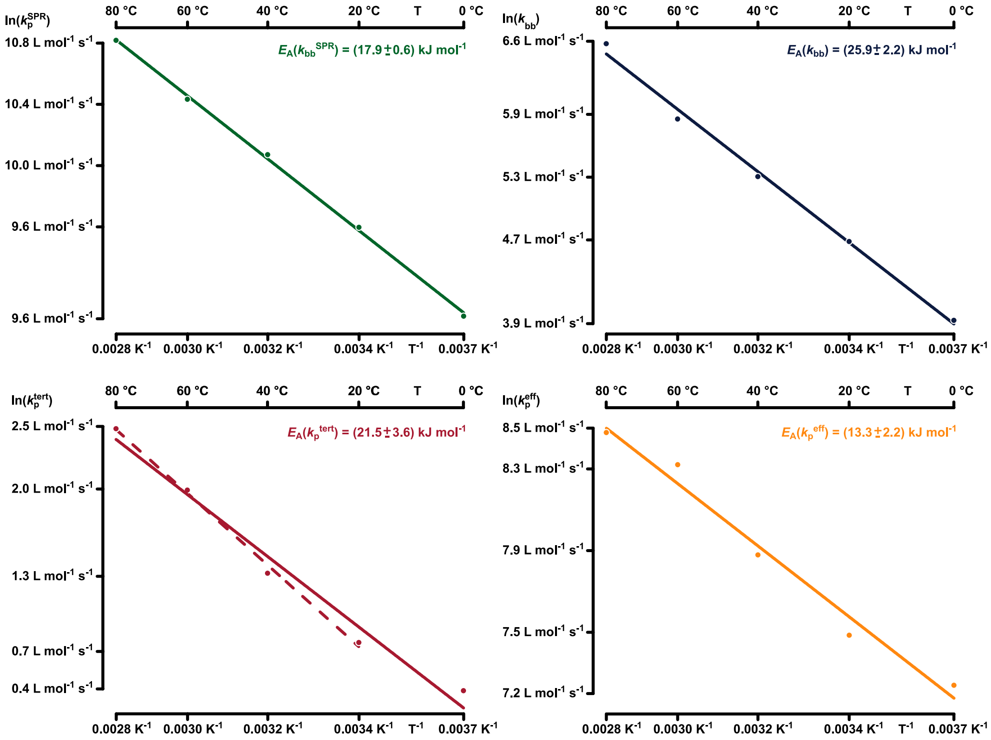

Figure 7.3 Arrhenius plots for the four different rate coefficients determined for *t*BA.

while only focusing on k_p^{SPR} – were of high quality and no doubts on the accuracy of data existed.

For backbiting, a relatively low activation energy of (25.9 ± 2.2) kJ mol^{-1} was deduced. The Arrhenius relation features excellent linearity, and at room temperature k_{bb} is almost identical to *n*BA. Yet, for *n*BA, an E_A of 31.7 kJ mol^{-1} (PLP method)[300] and 34.7 kJ mol^{-1} (ESR method)[292] were reported as the most reliable reference values available for any acrylate in literature. This lowered activation energy is, however, well in line with the observation that PLP structures can be more clearly identified at higher temperatures in case of *t*BA compared to *n*BA. This indicates that the *t*BA system is somewhat less affected by MCR formation. For MCR monomer addition, an activation energy of

Table 7.2 Frequency factors and activation energies for the rate coefficients determined herein. For k_p^{tert}, an alternative value is given for the limited fit as presented in Figure 7.3.

	E_A [kJ mol^{-1}]	ln(A) [L mol^{-1} s^{-1}]
k_p^{SPR}	17.9 ± 0.6	16.91 ± 0.14
k_{bb}	25.9 ± 2.2	15.23 ± 0.42
k_p^{tert}	21.5 ± 3.6	9.73 ± 0.70
	(24.9 ± 2.2)	(10.94 ± 0.40)
k_p^{eff}	13.3 ± 2.2	13.01 ± 0.43

(21.5 ± 3.6) kJ mol^{-1} is obtained, which is also significantly below the reported values for *n*BA polymerization (in the range of 28 kJ mol^{-1}). Interestingly, the data obtained at 0 °C seem to be less consistent with the entire dataset. This might be associated with problems indicated above to reliably determine k_p^{eff}. If the temperature range between 20 and 80 °C is only fitted, a value close to 25 kJ mol^{-1} is determined, which is within error limits in agreement with the *n*BA value. While changes in the activation energy can be foreseen in the backbiting reaction with the more rigid *tert*-butyl ester, similar (but not identical) activation energies should be observed for the monomer addition, also according to general experience with family behavior in acrylate polymerization.[317] Most interestingly, k_p^{eff} shows (as already indicated above) the lowest activation energy, namely 13.3 kJ mol^{-1}. While this value should be treated with some care, it is certainly a significant observation that the high activation energies for backbiting and tertiary radical monomer addition result in an overall lowered temperature dependence of the effective propagation (and thereby overall polymerization) rate. Until this date, usually only SPR propagation rates have been discussed for acrylate monomers in literature, and reactivity comparisons have been made on this basis. Often, such data is directly extrapolated to estimate overall polymerization rates, which may not hold true as is seen in the present example. As already mentioned above, independent confirmation of the k_p^{eff} values is still required, but should in the future certainly be included in discussions of reactivity within the acrylate monomer family, as k_p^{eff} is in simple modelling approaches (when backbiting is not explicitly taken into account) of very high practical relevance.

7.4. Conclusions

A comprehensive PLP-SEC study has been provided for the monomer *tert*-butyl acrylate in the temperature range of 0 to 80 °C, employing for the first time a kHz pulsed laser system in scientific literature (for any acrylate monomer). This very fast pulsing action allows to study not only the propagation kinetics of the chain-end secondary propagating radicals, but also the rate of backbiting and monomer addition to the hereby resulting mid-chain radicals. To evaluate the kinetics of the backbiting reaction, a simplified Predici simulation procedure has been developed, that allows for fast evaluation of the data without complex simulation of full molecular weight distributions or requirement of detailed knowledge of rate coefficients.

For SPR propagation, an activation energy for k_p^{SPR} has been determined to (17.9 ± 0.6) kJ mol^{-1}, in excellent agreement with literature data, underpinning the high quality of the herein deduced data ($\ln(A$ / L mol^{-1} s$^{-1}) = 16.91 \pm 0.14$). For backbiting, an activation energy of (25.9 ± 2.2) kJ mol^{-1} is deduced ($\ln(A$ / L mol^{-1} s$^{-1}) = 15.23 \pm 0.42$), which is somewhat lower than the values reported before for *n*BA. For MCR propagation, data evaluation may be associated with a somewhat higher error due to imperfect determination of k_p^{eff} from the individual apparent k_p variation plots, but the activation energy is believed to be in the range of 20 - 28 kJ mol^{-1}. Interestingly, the combined action of backbiting and MCR propagation results in an overall decreased activation energy for the average propagation, namely 13.3 kJ mol^{-1}.

As detailed knowledge on kinetic rate coefficients on the backbiting reaction (and its follow up processes) is almost entirely unavailable, with the exception of *n*BA polymerization, further investigations in this direction can be triggered from this work. Increasing the knowledge on this parameter for a series of monomers is of uttermost importance as to date almost all kinetic predictions on functional acrylates are made on the basis of *n*BA, even though pronounced ester side chain effects may occur, similar as to the variation typically identified for linear and branched alkyl acrylates[325-327] or for k_p of alkyl acrylates in solution.[328-330]

Chapter 8

8. Experimental Section

8.1. Analytical Equipment

Liquid State NMR ^{1}H NMR spectra were recorded in deuterated chloroform applying a pulse delay of 12 s with two NMR spectrometers (300 and 400 MHz) from Oxford Instruments Ltd. using a Varian probe (9 mm-4-nucleus AutoSWPFG).

Solid State NMR The quantitative ^{13}C MAS NMR spectra were acquired on an Agilent Inova 400 wide bore spectrometer (9.4 T) in 7 mm ceramic Si_3N_4 rotors at 100 °C (T_g + 150 °C). Magic angle spinning (MAS) was performed at 2.3 kHz. The aromatic signal of hexamethylbenzene was used to calibrate the carbon chemical shift scale to 132.1 ppm. Acquisition parameters used were: a spectral width of 40 kHz, a 90° pulse length of 4.8 μs, an acquisition time of 35 ms, a recycle delay time of 10 s and 20.000-50.000 accumulations, depending on the degree of branching. High power proton dipolar decoupling during the acquisition time was set to 65 kHz. In order to obtain a stable magic angle spinning, the polymers were mixed with about 10 wt% Al_2O_3 powder.

Size Exclusion Chromatography Analytical SEC (Size Exclusion Chromatography) was performed on a Tosoh EcoSEC HLC-8320GPC, comprising an autosampler, a PSS guard column SDV (50 x 7.5 mm), followed by three PSS SDV analytical linear XL (5 µm, 300 x 7.5 mm) columns thermostated at 40 °C (column molecular weight range: $1 \times 10^{2} – 1 \times 10^{6}$ g mol^{-1}), and a differential refractive index detector (Tosoh EcoSEC RI) using THF as the eluent with a flow rate of 1 mL min^{-1}. Toluene was used as a flow marker. Calibration was performed using linear narrow polystyrene (PS) standards from PSS Laboratories in the range of 470 - 7.5×10^{6} g mol^{-1}.

In Chapter 4 a Malvern chromatograph equipped with a Viscotek TDA 305 triple detection (refractometer, viscosimeter and low angle laser light scattering (LALLS)) as well as Agilent columns (three PL-gel 5 µm columns: 10^{4}, 10^{3} and

10^2 Å) was used to measure number average molecular weights and dispersities. The columns were stored at 45 °C and THF as solvent was pumped with a flow rate of 0.7 mL min^{-1}.

Electrospray ionization mass spectrometry Electrospray ionization mass spectrometry (ESI-MS) was performed on an LCQ Fleet mass spectrometer (ThermoFischer Scientific) equipped with an atmospheric pressure ionization source operating in the nebulizer-assisted electrospray mode. The instrument was calibrated in the *m/z* range 220-2000 using a standard solution containing caffeine; MRFA, and Ultramark 1621. A constant spray voltage of 5 kV was used, and nitrogen at a dimensionless auxiliary gas flow rate of 3 and a dimensionless sheath gas flow rate of 3 were applied. The capillary voltage, the tube lens offset voltage, and the capillary temperatures were set to 25 V, 120 V, and 275 °C, respectively. A 250 µL aliquot of polymer solution with a concentration of 10 µg ml^{-1} was injected. A mixture of THF and methanol (THF:MeOH = 3:2), all HPLC grade, was used as solvent.

Dynamic light scattering Dynamic light scattering (DLS) measurements were done with a Brookhaven Instruments ZetaPALS system.

8.2. Experimental Equipment

Microflow reactor set-up. As microflow reactor set-up, a Labtrix Start R2.2 system (Chemtrix BV), equipped with a glass microreactor (3227, reactor volume = 19.5 µL, width channel = 300 µm, depth channel = 120 µm) was used. Two gas-tight 1 mL syringes (SGE, Trajan Scientific Australia Pty Ltd.) in a Fusion 100 classic syringe pump (Chemyx Inc.) were used to deliver the reaction solutions into the reactor. Reaction times (residence times) are controlled by setting different flow rates. A thermoelectric cooler temperature controller MTTC1410 (Melcor Thermal Solutions, temperature range -15 to 195 °C) was used to control and regulate the reaction temperature. For the UV-light, a OMNICURE Series 1000 system, equipped with a 100 W high pressure mercury vapor short arc lamp (spectral emission: 320-500 nm, maximum 365 nm) was employed. The reactor running was 1.5 times the residence time before each sample recovery.

2 mL flow reactor set-up The 2 mL flow reactor is a FlowSyn mixer block (Uniqsis Ltd.), which consists out of a borosilicate glass chip reactor with an internal volume of 2 mL (channel diameter = 1 mm). For heating the chip is mounted on an aluminum block which is heated by an ADS-HP-NT heating plate (Asynt Ltd.), equipped with a ADS-TC-NT thermocouple (Asynt Ltd.) to control the temperature. A Fusion 100 classic syringe pump (Chemyx Inc.) with a 10 mL SGE gas tight glass syringe (Trajan Scientific Australia Pty Ltd.) was used to transport the reaction solution into the reactor and to control the reactions (residence times). The reactor was operated under a pressure of 75 psi. As UV-light source a combination of an OMNICURE Series 2000 system (200 W high pressure mercury vapor short arc lamp, spectral emission: 250-500 nm, maximum 365 nm) and a Lot Oriel system (200 W Hg(Xe), spectral emission: 320-390 nm) was used. The reactor running was 1.5 times the residence time before each sample recovery.

Continuous tubular reactor setup For the continuous tubular photoflow reactor, a PFA tubing (outer diameter 1/16", inner diameter 0.75 mm) is wrapped tightly around a UV-light source. As UV-light sources a 400 W medium pressure UV-lamp (λ_{max} = 365 nm) inside a quartz cooling mantle (Photochemical Reactors Ltd., UK) or a 15 W Vilbour-Lourmant UV-light tube (λ_{max} = 365 nm) were used.

The whole tubing was irradiated equally by the UV-Lamp. To deliver the degassed reaction solutions HPLC (Knauer BlueShadow 20P) or syringe pumps (Chemyx Fusion 100) were used.

Coupled photoflow reactors For the coupled reactors, 2.3 m and 3.5 m PFA tubing (Advanced Polymer Tubing GmbH, outer diameter 1/16”, inner diameter 0.75 mm, reactor volume 1 mL and 1.5 mL respectively) were wrapped around a 15 W UV-light tube (Vilbour Lurmant, λ_{max} = 365 nm). The reaction solutions were loaded into two NormJect plastic syringes and a Chemyx Fusion 100 syringe pump was used to deliver the solutions. For fast reaction solution mixing, a static mixer (Upchurch Scientific) was added in the lines before entering the reactor. The exit of the first reactor was coupled to a second static mixer. In this mixer also the second monomer solution was supplied via a NormJect syringe and a Chemyx pump. The lamp created a reaction temperature between 50 and 55 °C.

Pulsed Laser Polymerization. The sealed sample vials were purged with nitrogen to remove the oxygen. Before polymerization the samples were placed in an aluminum sample holder. A thermostat (VWR AD15R-30) was used to bring the sample to desired reaction temperature with a temperature sensor directly at the sample. Before initiating the samples via laser pulsing they were allowed to equilibrate in temperature for about 3 minutes. An ATL ATLEX 1000i Excimer Laser at 351 nm (XeF-Gas) with repetition rates up to 1000 Hz was used as laser source. The energy was set to 1.5 mJ per pulse hitting the sample from the bottom.

8.3. Experimental Part for Chapter 2 -. Photo-Induced Copper-Mediated Polymerization of (Meth)Acrylates in Continuous Flow Reactors

Materials. Ethyl 2-bromoisbutyrate (EBiB, Alfa Aesar, 98+ %), copper(II) bromide ($CuBr_2$, Sigma-Aldrich, 99 %), *N,N,N',N'',N''*-Pentamethyl-diethylenetriamine (PMDETA), dimethyl formamide (DMF, VWR, pro analysis), methanol (MeOH, VWR, technical), ethanol (EtOH, VWR, technical) and dimethyl sulfoxide (DMSO, Merck, pro analysis) were all used as received. Tris[2-(dimethylamino)ethyl]amine (Me_6TREN)[331] and 2-hydroxyethyl-2`-methyl-2`bromopropionate (HMB)[332] were synthesized according to a literature procedure. Methyl acrylate (MA, Acros, 99 %), *n*-butyl acrylate (*n*BA, Acros, 99 %), ethyl acrylate (EA, Acros, 99.5%), di(ethylene glycol) ethyl ether acrylate (DEGA, TCI, 98%) and 2-hydroxyethyl acrylate (HEA, TCI, 95%) were deinhibited over a column of activated basic alumina, prior to use. Additionally, 2-hydroxyethyl acrylate (HEA, TCI, 95%) was purified by distillation.

General polymerization procedure using the continuous photoflow reactor. EBiB (1 eq.), $CuBr_2$ (0.02 eq.) and Me_6TREN (0.12 eq.) were mixed in a 20 mL amber volumetric flask which was filled up with DMSO. 20 mL monomer (25 – 500 eq.) was filled into a separate amber volumetric flask and both were purged with nitrogen gas for approximately 15 minutes. The solutions were transferred into Normject plastic syringes and placed in the syringe pump. Different reaction times were screened via adjusting the flow rate (between 0.025 and 1 mL min^{-1}).

Polymerization of DEGA in a water/ethanol mixture. Before purging for 15 minutes with nitrogen gas, one amber volumetric flask was filled with DEGA (25 – 100 eq.) and another one with HMB (1 eq.), $CuBr_2$ (0.02 eq.) and Me_6TREN (0.12 eq.) and a 50/50 vol% H_2O/EtOH mixture. The oxygen free solutions were loaded into two Normject syringes and a syringe pump was used to deliver the solutions into the reactor. By changing the flow rates several reaction times were screened.

General procedure for the synthesis of pMMA-Br using the continuous tubular reactor setup. In a 100 mL amber volumetric flask, 1.903 g (9.76 mmol, 1 eq) EBiB, 0.043 g (0.19 mmol, 0.02 eq) $CuBr_2$, 0.106 g (0.61 mmol, 0.06 eq) PMDETA and 18.912 g (188.89 mmol, 19 eq.) MMA were mixed and 25 mL methanol was added. The volumetric flask was filled with DMF. Before purging with nitrogen for 30 minutes, the mixture was transferred into a 100 mL amber laboratory bottle with a GL-45 screw cap. The flow reaction proceeded at 40 °C

Procedure for the synthesis of pMA using the microflow reactor setup. Methyl acrylate (0.415 g, 44 eq., 4.82 mmol), EBiB (0.021 g, 1 eq., 0.11 mmol), $CuBr_2$ (0.001 g, 0.02 eq., 0.01 mmol) and Me_6TREN (0.003 g, 0.12 eq., 0.01 mmol) were mixed in a 5 mL volumetric flask and filled up to a volume of 5 mL with DMSO. The polymerization targeted a number average molecular weight (M_n) of 3800 g mol^{-1}. Prior to use, the mixture was purged with nitrogen for 3 min and then transferred into two 1 mL gas tight syringes and inserted into the syringe pump.

Procedure for the synthesis of a pMA-*b*-pBA block-copolymer using the microflow reactor setup. Poly(methyl acrylate) (0.105 g, 1 eq., 0.03 mmol, $Đ = 1.1$, $M_n = 3100$ g mol^{-1}) was used as macroinitiator and mixed with $CuBr_2$ (0.001 g, 0.02 eq., 0.01 mmol) and Me_6TREN (0.001 g, 0.12 eq., 0.01 mmol) in a 5 mL volumetric flask and filled up to a volume of 5 mL with DMSO. The polymerization targeted a number average molecular weight of 7500 g mol^{-1}. Prior to use the mixture was purged with nitrogen for 3 min and then transferred into two 1 mL gas tight syringes and inserted into the syringe pump.

General procedure for the synthesis of pMMA-*b*-pMA-*Br* using the continuous tubular reactor setup. 0.336 g pMMA-Br macroinitiator (2600 g mol^{-1}, 0.13 mmol, 1 eq.), 0.001 g $CuBr_2$ (0.01 mmol, 0.08 eq), 0.010 g Me_6TREN (0.04 mol, 0.31 eq), 1.343 g MA (15.60 mmol, 120 eq) and 5 mL DMF were mixed in a 25 mL volumetric flask and filled up with DMSO. The solution was purged for 15 min with nitrogen in an amber laboratory bottle before the reaction was started by pumping the solution into the reactor.

One step chain extension of DEGA in a water/ethanol mixture. In a 10 mL amber volumetric flask, 0.42 g (2.16 mmol, 1 eq.) HMB, 0.01 g (0.04 mmol, 0.02 eq.) $CuBr_2$ and 0.06 g (0.26 mmol, 0.12 eq.) Me_6TREN were dissolved in a 50/50 vol% H_2O/EtOH mixture. This solution as well as 10 mL DEGA were purged for 10 minutes with nitrogen and transferred into two syringes. For the second monomer addition, 5 mL DEGA was mixed with 5 mL 50/50 vol% H_2O/EtOH mixture, purged with N_2 for 10 minutes and loaded into a syringe.

8.4. Experimental Part for Chapter 3 - Efficient Multiblock Star Polymer Synthesis from Photo-Induced Copper-Mediated Polymerization with up to 21 Arms

Materials. Copper(II) bromide ($CuBr_2$, Sigma-Aldrich, 99%), *β*-cyclodextrin (98%, Acros Organics), triethylamine (99%, Acros Organics), 2-bromopropionyl bromide (97%, Alfa Aesar), trifluoroacetic acid (TFA, 99% Acros Organics), dichloromethane (DCM, VWR Prolabo Chemicals), diethyl ether (VWR Prolabo Chemicals), chloroform ($CHCl_3$, VWR Prolabo Chemicals), *n*-hexane (VWR Prolabo Chemicals), tetrahydrofuran (THF, VWR Prolabo Chemicals) and dimethyl sulfoxide (DMSO, Merck, pro analysis) were all used as received. Tris[2-(dimethylamino)ethyl]amine (Me_6TREN)[331], pentaerythritol tetrakis (2-bromoisobutyrate) ($4Br^iBu$)[193], dipentaerythritol hexakis (2-bromoisobutyrate) ($6Br^iBu$)[193] and 2,3,6-tri-O-(2-bromo-2-methylpropionyl]-ß-cyclodextrin)[333] were synthesized according to literature procedures. Methyl acrylate (MA, Acros, 99%), *n*-butyl acrylate (*n*BA, Acros, 99 %), *tert*-butyl acrylate (*t*BA, Alfa Aesar, 99%) and di(ethylene glycol) ethyl ether acrylate (DEGA, Acros, 99%) were deinhibited over columns of activated basic alumina prior to use.

4-arm star block copolymer synthesis with IR probe. 43.5 mg (5.9×10^{-2} mmol, 1 eq.) $4Br^iBu$ (macro)initiator, 0.5 mg (2.4×10^{-3} mmol, 0.04 eq.) $CuBr_2$, 4.1 mg (1.8×10^{-2} mmol, 0.30 eq.) Me_6TREN and 475 mg (5.5 mmol, 93 eq.) MA are weighted into a 5 mL volumetric flask. The flask is filled with DMSO and the reaction mixture is transferred into a 100 mL three-neck round bottom flask. Through one neck a Mettler Toledo TM15 in-situ FTIR probe is introduced into the reaction mixture. After sealing the flask the solution is purged with nitrogen for 5 minutes. The reaction is started by switching on the Omnicure S1000 system (spectral emission: 320-500 nm, peak at 365 nm) at an iris opening of 100%. After reaching a monomer conversion of 95% the lamp is switched off and a sample for analysis is taken before 437.6 mg (5.5 mmol, 93 eq.) *t*BA is added. The solution is purged again with nitrogen for 5 minutes and the reaction reinitiated by switching on the UV lamp. The same experimental setup was used by Chuang *et al.* and more detailed information can be found there.[181]

General polymerization procedure in the flow reactor. Reactions were carried out in a Labtrix Start microflow reactor (Chemtrix, Geleen, NL). Before filling a 10 mL volumetric flask with DMSO, 1 eq. 4Br^{i}Bu, 0.30 eq. Me_6TREN and 93 eq. MA are added. $CuBr_2$ is added accordingly to the different tested concentrations (0.02, 0.04, 0.08 and 0.20 eq.). Before filling the gas tight 1 mL glass syringes, the solution was purged with nitrogen for 5 minutes. Via the flow rate the reaction time (residence time) in the reactor is controlled and changed. Two times the residence time was waited to stabilize the reaction conditions before the samples were taken.

General polymerization procedure. Initiator (4Br^{i}Bu, 6Br^{i}Bu or 21BrCD), Me_6TREN, monomer and $CuBr_2$ were added to an amber volumetric flask which was then filled with DMSO. The ratios are 0.04 eq $CuBr_2$, 0.075 eq Me_6TREN and 23 eq monomer per initiating group CH-Br. The mixture was ultrasonicated until a homogeneous solution was obtained before being transferred to an erlenmeyer flask of the appropriate volume. The solution was shielded from light and purged with N_2-gas for 15-45 minutes, depending on the volume of the solution. Afterwards it was placed in a Multilamp Reactor MLU 18 (Photochemical Reactor Ltd.) equipped with ten 15 Watt lamps (Vilber Lourmat) with a peak emission of 365 nm. Before extracting the polymer solution 3 times with 25 mL $CHCl_3$, 25 mL H_2O was added. Afterwards the organic phase was washed twice with 25 mL H_2O and the solvent was removed under reduced pressure. The polymer product was then filtered through a silica filter into an amber glass vial. Next, the vial was placed in the vacuum oven overnight for drying.

4-arm star block copolymer synthesis. The general polymerization procedure was carried out with the following equivalence ratios: 1 eq. 4Br^{i}Bu (macro)initiator, 0.04 eq. $CuBr_2$ and 0.30 eq. Me_6TREN. MA, *t*BA, *n*BA and DEGA equivalence ratios were appropriately adjusted in order to obtain varying target molecular weights per arm. The received products were each time used as macroinitiator for further block synthesis.

6-arm star block copolymer synthesis. The general polymerization procedure was carried out using the following equivalence ratios: 1 eq. 6Br^{i}Bu (macro)initiator, 0.06 eq. $CuBr_2$, 0.45 eq. Me_6TREN. The equivalence ratios of MA and *t*BA were adjusted in order to obtain different arm lengths. The received products were each time utilized as macroinitiator for further block synthesis.

21-arm star block copolymer synthesis. The following equivalence ratios were used for each reaction: 1 eq. 21BrCD (macro)initiator, 0.21 eq. $CuBr_2$, 1.58 eq. Me_6TREN. Different arm lengths were obtained by varying the equivalence ratios of MA and *t*BA. The received products were each time used as macroinitiator for further block synthesis.

General procedure for the degradation of *t*BA to acrylic acid. After dissolving around 100 mg of each polymer containing *t*BA in roughly 2 mL DCM and 2 mL TFA, they were stirred overnight. The DCM and TFA were removed under reduced pressure.

Average size determination. 100 mg of the star polymers were dissolved in 1 mL ethanol which was then diluted with 9 mL water. Before the DLS measurement the solution was ultrasonicated for 15 seconds.

8.5. Experimental Part for Chapter 4 - Improved Photo-Induced Cobalt-Mediated Radical Polymerization in Continuous Photoflow Reactors

Materials. Vinyl acetate (VAc, >99 %, Aldrich) was dried over calcium hydride, degassed by several freeze-pump-thawing cycles before distillation under reduced pressure and stored under argon. Bis(acetylacetonato)cobalt(II) ($Co(acac)_2$) (>98%, Acros) was stored under argon and used as received. 2,2,6,6-tetramethylpiperidine-1-oxy (TEMPO, 98%, Aldrich) was used as received. 2,2′-azobis(4-methoxy-2,4-dimethylvaleronitrile) (V-70, 96%, Wako) was stored at -20 °C and used as received. Ethyl acetate (EtOAc) and 1-octene (1-Oct, 98%, Aldrich) were dried over molecular sieves and degassed by bubbling argon for 30 min. The alkyl-cobalt(III) adduct initiator ($[Co(acac)_2(CH(OAc)\text{-}CH_2)_{<4}R_0]$, R_0 being the primary radical generated by 2,2′-azo-bis(4-methoxy-2,4-dimethyl valeronitrile) (V-70, Wako) was prepared as described previously and stored as a CH_2Cl_2 solution at -20 °C under argon.[248]

Cobalt-mediated radical polymerization of VAc in a 20 vol% EtOAc solution. A solution of alkyl–cobalt(III) initiator ($[Co(acac)_2(CH(OAc)\text{-}CH_2)_{<4}R_0]$, R-$Co(acac)_2$) in CH_2Cl_2 was introduced under argon in a round bottom flask (0.5 mL of a 0.041 M stock solution, 0.0205 mmol) and evaporated to dryness under reduced pressure, after which the reactor was filled with argon. Degassed EtOAc (4 mL) and then VAc (1 mL, 10.85 mmol) were added to the alkyl–cobalt(III) initiator. The polymerization mixture was stirred in an oil bath at 40 °C. Samples were regularly withdrawn from the medium by using an argon flushed syringe. The monomer conversion was evaluated by ^1H NMR analysis in $CDCl_3$. Molecular parameters M_n and M_w/M_n were determined by SEC-THF using a PS calibration after adding TEMPO to the sample solution.

Cobalt-mediated radical copolymerization of VAc and 1-Oct (75/25 mol%) in bulk. The same procedure as before for cobalt-mediated radical polymerization of VAc in a 20% EtOAc solution was applied. Reagents: Alkyl–cobalt(III) initiator ($[Co(acac)_2(CH(OAc)\text{-}CH_2)_{<4}R_0]$, R-$Co(acac)_2$) in CH_2Cl_2

(1.5 mL of a 0.092 M stock solution, 0.14 mmol), VAc (5 mL, 54.23 mmol) and 1-Oct (2.8 mL, 17.85 mmol).

Cobalt-mediated radical polymerization of VAc in a flow reactor. Under argon, 10 mL of VAc (108.47 mmol) and 40 mL of EtOAc (405.86 mmol) were added into a Schlenk tube to prepare a 20vol% VAc in EtOAc stock solution. For a typical VAc polymerization in a flow reactor, 1.0 mL of alkyl–cobalt(III) initiator ([Co(acac)$_2$(CH(OAc)-CH$_2$)$_{<4}$R$_0$], R-Co(acac)$_2$) in CH_2Cl_2 (0.041 M stock solution, 0.041 mmol) was added under argon into a Schlenk tube and evaporated to dryness under reduced pressure. A volume of 10.0 mL of the 20vol% VAc solution in EtOAc (VAc/EtOAc 1/4 V/V) was added to the alkyl–cobalt(III) initiator under argon. The reaction solution was filled into a 10 mL gas tight glass syringe and inserted into the 2 mL glass-chip flow reactor. For different reaction times and reaction temperatures samples were collected and analyzed. Some TEMPO was added to the SEC samples to stop the reaction.

Cobalt-mediated radical polymerization of VAc in a microflow reactor. The reaction solution for polymerization in the microflow reactor consists of 200 µL of alkyl–cobalt(III) initiator ([Co(acac)$_2$(CH(OAc)-CH$_2$)$_{<4}$R$_0$], R-Co(acac)$_2$) in CH_2Cl_2 (0.041 M stock solution, 0.008 mmol) and 2.0 mL of the 20% VAc in EtOAc stock solution which were mixed under argon in a Schlenk tube (VAc/Co = 529). Before adding the stock solution, the CH_2Cl_2 was evaporated under reduced pressure from the tube. The solution was transferred into two 1 mL gas tight glass syringes and inserted into the microflow reactor. Samples at different reaction times and temperatures were taken for analysis. TEMPO was added to the SEC samples to stop the reaction immediately.

Cobalt-mediated radical copolymerization of VAc and 1-Oct (75/25 mol%) in a microflow reactor. A solution of 7.5 mL of VAc (81.3 mmol), 4.2 mL of 1-Oct (27.1 mmol, VAc/1-Oct = 75/25 mol%) and 40 mL of EtOAc (concentration of 22.5 vol%) was prepared under argon atmosphere in a schlenk tube. To prepare the reaction mixture, 200 µL of alkyl–cobalt(III) initiator solution ([Co(acac)$_2$(CH(OAc)-CH$_2$)$_{<4}$R$_0$], R-Co(acac)$_2$) in CH_2Cl_2 (0.041

M stock solution, 0.008 mmol) were transferred in a Schlenk and CH_2Cl_2 was removed under vacuum. Then 2.0 mL of the prepared VAc/1-Oct solution (3.1 mmol of VAc, 1.05 mmol of 1-Oct, VAc/1-Oct/R-Co molar ratio of 383/127/1) in EtOAc was added under argon. The reaction mixture was injected into the reactor by using two 1 mL gas tight glass syringes. For ^1H NMR in $CDCl_3$ and SEC-THF (PS calibration) analysis, samples were taken at different reaction times and with different reaction temperatures. To prevent further polymerization in the sample containers, TEMPO was added to the SEC samples.

Determination of reactivity ratios for VAc/1-Oct copolymerization in a microflow reactor. The solutions of VAc and 1-Oct in EtOAc (1 g of comonomers in 4 mL of EtOAc) were prepared under argon atmosphere with various VAc/1-Oct ratios. The solutions were analyzed by ^1H NMR to determine precisely the VAc and 1-Oct fractions in the feed (f_{VAc} and $f_{1\text{-}Oct}$). To prepare the reaction solutions, the procedure from the cobalt-mediated radical copolymerization of VAc and 1-Oct (75/25 mol%) in a microflow reactor was used, varying the VAc/1-Oct concentrations. The copolymerization was performed at 40 °C under UV irradiation and with a reaction time of 8 minutes. Copolymers were collected and dried at 70 °C under reduced pressure to eliminate all volatiles and analyzed by ^1H NMR to determine VAc and 1-Oct fractions (F_{VAc} and $F_{1\text{-}Oct}$).

8.6. Experimental Part for Chapter 5 – Continuous Microflow PhotoRAFT Polymerization

Materials. The monomers *n*-butyl acrylate (*n*BA, Acros, 99%) and methyl acrylate (MA, Acros, 99%) were purified over a basic alumina column prior to use. *n*-Butyl acetate (Acros, 99%), benzoin (Janssen Chimica, 98%), 2,2-dimethoxy-2-phenylacetophenone (DMPA, Acros, 99%), phenylbis(2,4,6-trimethylbenzoyl)phosphine oxide (IRGACURE 819, Tokyo Chemica Industry, 96%) and 2-hydroxy-4′-(2-hydroxyethoxy)-2-methylpropiophenone (IRGACURE 2959, Sigma Aldrich, 98%) were used as received. 2-([(Dodecylsulfanyl)carbonothioyl]sulfanyl) propanoic acid (DoPAT) was synthesized as reported in literature.[334]

General polymerization procedure. For all polymerizations the monomer *n*BA was added into an amber glass vial. In another amber glass vial the photoinitiator, the RAFT-agent (DoPAT) and the solvent (BuAc) were mixed. The vials were degassed using nitrogen and purged for 4 minutes. Afterwards, two gas-tight glass syringes were filled with the reagents. The reagents were inserted into the microflow reactor using a syringe pump. Different reaction times (residence times) were screened.

Synthesis of p*n*BA at different temperatures. The general polymerization procedure was applied by using the following amounts: 7.02 mmol (0.90 g, 20 eq.) *n*BA, 0.0878 mmol (0.02 g, 0.25 eq.) Benzoin, 0.35 mmol (0.12 g, 1 eq.) DoPAT and 1.0 mL of BuAc. Different temperatures were screened with a residence time of 12 minutes and a light intensity of 30 mW cm^{-2}.

Influence of light intensity. The reaction was performed at 60 °C with varying light intensities, following the general polymerization procedure with these values: 7.02 mmol (0.90 g, 20 eq.) *n*BA, 0.0878 mmol (0.02 g, 0.25 eq.) benzoin, 0.35 mmol (0.12 g, 1 eq.) DoPAT and 1.0 mL of BuAc.

Reactions for different photo-initators. 7.02 mmol (0.90 g, 20 eq.) *n*BA, 0.25 eq. photoinitiator, 0.35 mmol (0.12 g, 1 eq.) DoPAT and 1.0 mL BuAc were prepared, following the general polymerization procedure and using different photoinitiators (benzoin, DMPA, Irgacure 819 and Irgacure 2959). One reaction was done without adding a photoinitiator. All reactions were done at 60 °C with a light intensity of 30 mW cm^{-2}.

Synthesis of pnBA-b-pMA block copolymers. Poly(*n*-butyl acrylate) (0.0784 mmol, 0.2312 g, 1 eq., $Đ$ = 1.18, M_n = 2900 g mol^{-1}) was synthesized following the general polymerization procedure and used as a macroinitiator. It was mixed in an amber glass vial with 0.0196 mmol (0.0042 g, 0.25 eq.) benzoin and 0.4 mL BuAc. In another amber glass vial 1.5681 mmol (0.1350 g, 20 eq.) MA and 0.25 mL BuAc were mixed. Both vials were purged with nitrogen for 4 minutes. Reaction conditions of 60 °C and 30 mW cm^{-2} were set to perform the chain extension.

8.7. Experimental Part for Chapter 6 – Photo-induced Acrylate Polymerization: Unexpected Reduction in Chain Branching

Materials. *n*-Butyl acrylate (*n*BA, Acros, 99%) was used after de-inhibition over an activated basic alumina column. Azobisisobutyronitrile (AIBN, Acros, 99%) was recrystallized two times in ethanol before usage. Benzoin (Janssen Chemica), 2,2-dimethoxy-2-phenylacetophenone (DMPA, Acros, 99%), phenylbis(2,4,6-trimethylbenzoyl)phosphine oxide (IRGACURE 819, Tokyo Chemical Industry, 96%) and 2-hydroxy-4′-(2-hydroxyethoxy)-2-methylpropiophenone (IRGACURE 2959, Sigma Aldrich, 98%) were used as received.

Photo-initiated polymerization of *n*-butyl acrylate. Before filling a 50 mL amber volumetric flask with *n*BA, 50 mg (0.24 mmol, 5×10^{-3} mol L^{-1}) of the initiator was added. For each sample around 2 mL of the solution was put into a clear 5 mL glass vial with a stir bar and sealed with a rubber septum, parafilm and metal wire. The vials were purged 5 minutes with nitrogen, before they were hanged into a borosilicate beaker containing a 60 °C silicon oil bath. After 5 minutes the samples were exposed to UV-light using a Photochemical Reactor Ltd. Multilamp Reactor MLU 18 equipped with four 15 Watt lamps (Vilber Lourmat) with a peak emission of 254 nm. After the reaction the samples were quenched in an ice bath and exposed to air. The conversion was determined gravimetrically after removing the residual monomer at 40 °C under reduced pressure for three days. The reaction was also carried out with eight 15 Watt Vilber Lourmat lamps (λ_{max} = 365 nm), with 18 LEDs (λ_{max} = 360 nm) and a 400 W medium pressure UV-lamp (λ_{max} = 365 nm, Photochemical Reactors Ltd.).

Thermal-initiated polymerization of *n*-butyl acrylate. Two mL of a 5×10^{-3} mol L^{-1} AIBN solution in *n*BA was filled into a clear 5 mL glass vial, equipped with a stir bar. Before degassing for 5 minutes with nitrogen, the vial was sealed with a rubber septum, parafilm and metal wire. The sample was quenched in an ice bath and exposed to air after a reaction time of 8 hours in a 60 °C oil bath. The conversion was determined gravimetrically after removing the residual monomer at 40 °C under reduced pressure for three days.

8.8. Experimental Part for Chapter 7 - Kilohertz Pulsed-Laser-Polymerization: Simultaneous Determination of Backbiting, Secondary and Tertiary Radical Propagation Rate Coefficients for *tert*-Butyl Acrylate

Materials. The monomers *tert*-butyl acrylate (*t*BA, Alfa Aesar, 99%) and *n*-butyl acrylate (*n*BA, Acros, 99%) were deinhibited by passing over a basic alumina column. As initiator 2,2-dimethoxy-2-phenylacetophenone (DMPA, Sigma Aldrich, 99%) was used as received.

Pulsed Laser Polymerization. 0.5 mL of the bulk polymerization solutions containing 5×10^{-3} mol L^{-1} initiator were placed in the sample vials. The vials were sealed with rubber septa and purged for 2 minutes with nitrogen to remove oxygen. Before polymerization the samples were placed in an aluminum sample holder. A thermostat (VWR AD15R-30) was used to bring the samples to the desired reaction temperature with a temperature sensor directly at the sample. Before initiating the samples via laser pulsing they were allowed to equilibrate in temperature for about 3 minutes. An ATL ATLEX 1000i Excimer Laser at 351 nm (XeF-Gas) with repetition rates up to 1000 Hz was used as laser source. The energy was set to 1.5 mJ per pulse hitting the sample from the bottom. Before drying the samples in a vacuum oven, hydroquinone/THF was added. The monomer conversion was determined gravimetric and was for all samples between 0.5 and 4.0 %. Monomer densities were calculated via $\rho/\mathrm{g\ mL^{-1}} = 0.90382-0.00103\cdot\theta/°\mathrm{C}$ for *t*BA and $\rho/\mathrm{g\ mL^{-1}} = 0.91771-0.00095\cdot\theta/°\mathrm{C}$ for *n*BA.[328]

Chapter 9

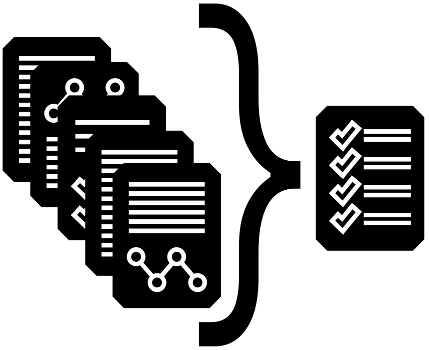

9. General Conclusions

9.1. Summary

In summary, continuous flow production of high precision polymer materials is highly advantageous. A significant advantage is even observed when switching flow reactors from thermal to photochemical mode. Photoreactions benefit from flow processing in a way that easily surpasses the batch reaction effects. Flow photoreactions allow for enormous increases in reaction rates and are able to eliminate side product formation significantly. This effect is not routed to isothermicity, but is due to the excellent light illumination that is reached when internal flow diameters are kept low.

PhotoRDRP has only recently received significant attention, even in classical batch chemistry. The interest in these methods is rapidly growing, owing to the high efficiencies that can be achieved with ease. As described above, the reaction efficiencies can be further increased when switching to photoflow processes. Additionally photoflow offers the engineering advantage that products can be synthesized in significant amounts without the requirement of expensive equipment.

A comparison between photobatch and photoflow synthesis of polymers via RDRP mechanisms shows the enormous advantages of using continuous photoflow reactors (see Table 9.1). For all photoRDRP methods used in this thesis, a clear increase of the polymerization rate was observed.

Photo-induced copper-mediated polymerizations of acrylates as well as methacrylates were faster by a factor of 4 to 5, yielding identical polymers as the batch reactions. The possibility to synthesize complex structures, such as block copolymers or star-shaped systems, was successfully demonstrated. Additionally, photoCMP was carried out in a H_2O/EtOH to take a first step towards “green” polymerizations. Here, a reactor cascade was built to obtain chain-extended polymers without intermediate purification. The synthesized star polymers were

Table 9.1 Comparison between photoflow and photobatch synthesis of precision polymers made via the most common reversible deactivation radical polymerization techniques.

#ref	Method	Reactor	Monomer	Reaction time [min]	Conv. [%]	M_n [g mol^{-1}]	Đ
1[98]	Co-mediated	Batch	Vinyl acetate	1800	26	18500	1.33
2[98]	Co-mediated	Flow	Vinyl acetate	60	30	14200	1.28
3[38]	Cu-mediated	Batch	Methyl acrylate	90	95	4500	1.05
4[91]	Cu-mediated	Flow	Methyl acrylate	20	79	3100	1.10
5[100]	Cu-mediated	Batch	Methyl methacrylate	420	88	2900	1.23
6[100]	Cu-mediated	Flow	Methyl methacrylate	60	48	3100	1.24
7[13]	photoiniferter	Batch	*n*-Butyl acrylate	3000	46	20700	1.12
8[335]	photoiniferter	Flow	*n*-Butyl acrylate	20	61	6800	1.12
9[336]	photoRAFT	Batch	Methyl acrylate	240	92	11400	1.10
10[335]	photoRAFT	Flow	*n*-Butyl acrylate	20	94	3500	1.20

chain extended up to eight times with different acrylate monomers. This allowed to create thermal as well as pH-responsive materials.

Performance of photo-induced cobalt-mediated radical polymerizations in continuous flow reactors reduced reaction times from days to hours or minutes. For photoCMRP it was the first time a significant increase in yield quality was observed by switching from batch to flow processing. High molecular weight crosslinked polymer structures were not seen in the flow product, while resulted in a strongly reduced dispersity.

Besides transition metal-mediated polymerizations, RAFT polymerizations were carried out in continuous photoflow reactors as well. Here, both iniferter without additional photo-initiator as well as real photoRAFT polymerizations with extra photo-initiator were realized. Like for the other reactions, an increase in polymerization rate was observed in photoflow reactors. Both polymerization types yielded precise polymers with narrow dispersities and different molecular weights. Tests with different photo-initiators showed possibilities to influence the polymerization performance.

In this thesis, the kinetics of acrylate polymerizations were investigated. An unexpected reduction in mid-chain branching during photo-induced free radical polymerization was discovered. Depending on the UV-light source, the measured degree of branching was up to 5 times lower than a similar thermally driven polymerization. Also an increase in branching with increasing monomer conversion during photopolymerization was found.

Pulsed-Laser-Polymerization (PLP) was used to determine *tert*-radical propagation and backbiting rates for *t*BA, based on data obtained from experiments.

With the eminent advantages of photoflow, it can be speculated that most laboratories will switch (or extend) to flow processing in future. This is not only due to the reasons stated above, but also because flow offers general benefits to precision polymer design. First studies have already been carried out, in which complex macromolecular architectures such as star, brush or cyclic polymers are also targeted. Furthermore, flow processes can be conveniently combined with (dark) thermal reactions, thus allowing for sequential modification. In future λ–orthogonal reactions may also come in the focus of photoflow material design, expanding the tool box from RDRP to the realm of photo*click* reactions.[337]

The combination of photoRDRP, photoclick and thermal polymer modification reactions (in conjunction with in-line purification) will give access to highly complex material synthesis, virtually in one-step procedures. The polymer chemistry community – outside classical polymer reaction engineering – is only at the beginning of implementing flow techniques to the synthesis portfolio. As an infant research topic in the polymer community, photoflow will give a further boost to flow adoption due to its obvious benefits. With certainty, the above described data are only the beginning of a rapid development, and the full potential of photoflow precision polymer material design and synthesis will soon unfold.

9.2. Outlook

During the 4 years of research, the field of photoRDRP in continuous flow reactors developed rapidly. It gained a lot of interest from research groups around the world who have started to use the technique. Research on photoRDRP will further expand in the future, and a lot of new techniques and methods will be developed.

One well known RDRP method has not yet been translated to continuous photoflow reactors, namely nitroxide-mediated polymerization (NMP). Literature on nitroxide-mediated radical photopolymerization (NMP^2) is only available for batch reactions.[187] NMP in batch and thermal processes is already one of the fastest RDRP methods and can probably still benefit from the usage of continuous photoflow reactors. Now the components of NMP^2 and photoflow polymerizations have to be put together to show the benefits of photoflow processing.

So far, no pure free radical polymerization was performed in a continuous photoflow reactor. Only some reports on the usage of FRP in segmented photoflow systems for particle are available. The main challenge in this research area will be the high molecular weights created during these uncontrolled reactions. As discussed earlier, high molecular weights lead to an increased viscosity, which could cause reactor fouling and blocking. Probably the only way to overcome this would be to work in high dilutions and to accept the drawbacks that the reaction rate decreases and that the solvent needs to be removed from the final polymer.

In continuous flow processing, inline purification methods are developing. Devices for different applications become commercially available and thus easier to use. At the moment, several research groups, mainly at the MIT, are working on continuous inline purification in organic synthesis. Polymer chemists can also benefit from inline purification and basic research needs to be done. One interesting field could be the in situ block copolymer synthesis. Inline purification could simplify block copolymer synthesis and lead to high value materials via a one step process. The challenge here is to drive the polymerization to full monomer conversion. If this is not possible, the unreacted monomer needs to be removed after the first reaction step before the second monomer is added. Filtration over a specific membrane could perform this task. The development of these membranes is the highest hurdle to take in the field of inline purification for the synthesis of block copolymers.

Combined with inline continuous flow purification, a higher automatization of flow reactors can also be investigated. Especially for synthetic chemists, it would be an advantageous and time saving process to test several reaction conditions automatically. Some automated systems are commercially available, but show a lot of disadvantages in the flexibility and specific reactor design.

Further research also needs to be conducted on the synthesized star polymers. In this work, exclusively the basic analysis about micelle formation in different media was investigated. To discover the full potential of precise star polymers for biomedical applications and nanomedicine, a full and detailed study needs to be carried out.

Modelling of the obtained data for the mid-chain branching in free radical photopolymerization could give some insights to understand and explain the low degree of branching. Besides, the influence of the irradiation wavelength, intensity and maybe the reaction temperature would be interesting aspects to be investigated.

The developed method to determine different kinetic parameters from pulsed-laser-polymerization measurements should be used in combination with additional monomers. A lot of polymerizations can benefit from the extended knowledge about the mechanism and the reaction kinetics gained from this method.

9.3. Nederlandse Samenvatting

In het algemeen zijn doorstroomreactoren een betere keuze voor de productie van hoge-precisie polymeren dan batch-reactoren. Het verschil wordt zelfs nog groter als niet thermische maar fotochemische reacties bestudeerd worden. De voordelen van doorstroomreactoren voor fotochemische processen overstijgen dan ook met gemak die van batch-reactoren. Zo zal de reactiesnelheid enorm toenemen en kunnen nevenreacties significant beter vermeden worden. Dit is niet het gevolg van de isothermiciteit van de doorstroomreactor, maar wel van een superieure belichting en bestraling van de reactor, in het bijzonder wanneer de interne diameter klein wordt gehouden.

Hoewel de initiële aandacht voor foto-RDRP eerder beperkt was, is de interesse recent sterk toegenomen, niet alleen in doorstroomreactoren, maar ook in klassieke batch-chemie. Het grote voordeel van doorstroomreactoren, de hoge efficiëntie die op eenvoudige wijze gehaald kan worden, wordt zelfs nog groter voor fotochemische processen. Bovendien kunnen in doorstroomreactoren grote hoeveelheden polymeren geproduceerd worden zonder specifieke of dure apparatuur.

Een vergelijkende studie tussen fotochemische RDRP-reacties in batch of in doorstroomreactor toont het enorme voordeel van doorstroomreactoren. Voor alle foto-RDRP-polymerizatiereacties die in deze doctoraatsthesis besproken worden werd een significant hogere reactiesnelheid vastgesteld.

Door de vele voordelen van doorstroomreactoren voor fotochemische reacties zou men kunnen verwachten dat de meeste laboratoria in de toekomst zullen overstappen of tenminste toch uitbreiden naar doorstroomreactoren. Deze beslissing wordt immers niet alleen ingegeven door de hoger genoemde voordelen, doorstroomreactoren bieden immers tal van voordelen voor het ontwerpen en synthetiseren van precisie-polymeren. Polymeren met een complexe macromoleculaire architectuur zoals ster-, borstel- en cyclische polymeren werden reeds geëxploreerd. Een ander belangrijk voordeel is dat in doorstroomreactoren optische processen eenvoudig kunnen gecombineerd (en afgewisseld) worden met thermische processen, wat op zijn beurt weer sequentiemodificatie mogelijk maakt. In de toekomst kunnen bijvoorbeeld ook λ-orthogonale reacties bestudeerd worden voor materiaalontwikkeling, wat de RDRP-toolbox zou uitbreiden met foto-*click*-reacties.[337]

De combinatie van foto-RDRP-, foto-*click*- en thermische polymerisatiereacties voor de ontwikkeling en productie van polymere materialen, samen met de mogelijkheid tot in-line zuivering, openen de deur naar ontwerp en synthese van uiterst complexe materialen in vrij eenvoudige, virtuele een-staps-processen. Polymeerchemici en polymerisatiereactie-ingenieurs staan slechts aan het begin van de implementatie van doorstroomreactoren in hun arsenaal van synthesetechnieken. Bovendien staan optische doorstroomreacties nog in hun kinderschoenen, maar de fenomenale voordelen beloven nu reeds de implementatie van doorstroomreactoren in productieprocessen een enorme boost te geven. De resultaten gepresenteerd in dit doctoraat zijn slechts het begin van de ontwikkeling van hoge-precisiepolymeren en de bijhorende synthese- en productietechnieken. In de (nabije) toekomst zullen de kracht en de mogelijkheden van optische doorstroomreactoren voor de ontwikkeling en productie van precisie-polymeren geëxploiteerd worden.

List of Publications

"Facile design of degradable poly(β-thioester)s with tunable structure and functionality"
N. Zaquen, **B. Wenn**, K. Ranieri, J. Vandenbergh, T. Junkers, *J. Polym. Sci., Part A: Polym. Chem.* 2014, 52, 178-187.

- Synthesis of the RAFT initiator and polymers
- Not presented in this thesis

"Photo-Induced Copper-Mediated Polymerization of Methyl Acrylate in Continuous Flow Reactors"
B. Wenn, M. Conradi, A. D. Carreiras, D. M. Haddleton, T. Junkers, *Polym. Chem.* **2014**, 5, 3053-3060.

- Article writing
- All synthetic work, characterization and analysis
- ESI-MS measurement and analysis: Matthias Conradi

"Solvent Effects on Acrylate kp in Organic Media?—A Systematic PLP–SEC Study"
A. P. Haehnel, **B. Wenn**, K. Kockler, T. Bantle, A. M. Misske, F. Fleischhaker, T. Junkers, C. Barner-Kowollik, *Macromol. Rapid Commun.* 2014, 35, 2029-2037.

- Partyl synthetic work, characterization and analysis
- Not presented in this thesis

“Solvent Effects on Acrylate kp in Organic Media?: Statement to the Response”
A. P. Haehnel, **B. Wenn**, K. Kockler, T. Bantle, A. M. Misske, F. Fleischhaker, T. Junkers, C. Barner-Kowollik, *Macromol. Rapid Commun.* 2015, 36, 1984-1986.

- Not presented in this thesis

“Photoinduced Acrylate Polymerization: Unexpected Reduction in Chain Branching”
B. Wenn, G. Reekmans, P. Adriaensens, T. Junkers, *Macromol. Rapid Commun.* 2015, 36, 1479-1485.

- Article writing

- All synthetic work

- NMR measurements and analysis: Gunter Reekmans

“Improved photo-induced cobalt-mediated radical polymerization in continuous flow photoreactors”
A. Kermagoret, **B. Wenn**, A. Debuigne, C. Jerome, T. Junkers, C. Detrembleur, *Polym. Chem.* 2015, 6, 3847-3857.

- Partly synthetic work, characterization and analysis

- Partly article writing

"Ligand Switch in Photoinduced Copper-Mediated Polymerization: Synthesis of methacrylate-acrylate block copolymers"
Y.-M. Chuang, **B. Wenn**, S. Gielen, A. Ethirajan, T. Junkers, *Polym. Chem.* 2015, 6, 6488-6497.

- Article writing about flow polymerizations
- Synthetic work, characterization and analysis of the flow polymerizations

"Continuous Photoflow Synthesis of Precision Polymers‟
T. Junkers, **B. Wenn**, *React. Chem. Eng.*, 2016, 1, 60-64.

- Literature Research
- Partly article writing

"Efficient multiblock star polymer synthesis from photo-induced copper-mediated polymerization with up to 21 arms"
B. Wenn, A. C. Martens, Y.-M. Chuang, J. Gruber, T. Junkers, *Polym. Chem.* 2016, 7, 2720-2727.

- Article writing
- All synthetic work, characterization and analysis

"Kilohertz Pulsed-Laser-Polymerization: Simultaneous Determination of Backbiting, Secondary, and Tertiary Radical Propagation Rate Coefficients for *tert*-Butyl Acrylate"
B. Wenn, T. Junkers, *Macromol. Rapid Commun.* 2016, 37, 781-787.

- Article writing
- All synthetic work, characterization and analysis

"Photo-Induced Copper-Mediated Acrylate Polymerization in Continuous Flow Reactors"
S. Railian, **B. Wenn**, T. Junkers, *J. Flow Chem.* 2016, DOI: 10.1556/1846.2016.00018*.*

- Article writing
- Partly synthetic work, characterization and analysis

"Continuous Microflow PhotoRAFT polymerization"
B. Wenn, T. Junkers, *Macromolecules, in press*.

- Article writing
- All synthetic work, characterization and analysis

Chapter: "Photoflow Material Synthesis"
B. Wenn, T. Junkers in *Photochemical processes in continuous-flow reactors: From engineering principles to chemical applications*, T. Noël Ed., Imperial College Press. 2016, *submitted.*

- Literature Research
- Chapter writing

List of Conference Presentations

Oral Presentations

“Photo-Initiated Copper-Mediated Polymerization - A Fast and Efficient Pathway to Complex Sequential Polymer Architectures”
B. Wenn, J. Laun, Y.-M. Chuang, J. Vandenbergh, T. Junkers, 21th Annual Meeting of the Belgian Polymer Group, May **2015**, Houffalize (Belgium).

“Photo-Initiated Copper-Mediated Polymerization - A Fast and Efficient Pathway to Complex Sequential Polymer Architectures”
B. Wenn, J. Laun, Y.-M. Chuang, J. Vandenbergh, T. Junkers, IUPAC 11th International Conference on Advanced Polymers via Macromolecular Engineering, October **2015**, Yokohama (Japan).

"Continuous Photoflow Synthesis of Precision Polymers"
B. Wenn, Flow Chemistry Workshop, January **2016**, Hasselt (Belgium).

Poster Presentations

"Nitroxide-Mediated Polymerization in Flow Microreators"
B. Wenn, J. Vandenbergh, T. Junkers, 19th Annual Meeting of the Belgian Polymer Group, May **2013**, Houffalize (Belgium).

"Photo-Induced Copper-Mediated Polymerization of Methyl Acrylate in Continuous Flow Reactors"
B. Wenn, M. Conradi, A. D. Carreiras, D. M. Haddleton, T. Junkers, ChemCYS 12th Chemistry Conference for Young Scientists, February **2014**, Blankenberge (Belgium).

"Photo-Induced Copper-Mediated Polymerizations in Continuous Flow Reactors"
B. Wenn, M. Conradi, A. D. Carreiras, D. M. Haddleton, T. Junkers, 20th Annual Meeting of the Belgian Polymer Group, May **2014**, Gent (Belgium).

"Photo-Induced Copper-Mediated Polymerizations in Continuous Flow Reactors"
B. Wenn, T. Junkers, FlowMaster Class, September **2014**, Hasselt (Belgium).

"Photo-Induced Copper-Mediated Polymerizations in Continuous Flow Reactors"
B. Wenn, T. Junkers, Annual Scientific Meeting IAP P7/05 FS2, September **2014**, Louvain-la-Neuve (Belgium).

"Cobalt-Mediated Radical Polymerization in Continuous Flow Reactors for Vinyl Acetate and 1-Octene Copolymerization"
A. Kermagoret, **B. Wenn**, A. Debuigne, C. Jérôme, T. Junkers, C. Detrembleur, Annual Scientific Meeting IAP P7/05 FS2, September **2014**, Louvain-la-Neuve (Belgium).

"Photo-Initiated Copper-Mediated Polymerization - A Fast and Efficient Pathway to Complex Sequential Polymer Architectures"
B. Wenn, J. Laun, Y.-M.- Chuang, J. Vandenbergh, T. Junkers, Annual Scientific Meeting IAP P7/05 FS2, September **2015**, Hasselt (Belgium).

"Photo-Initiated Copper-Mediated Polymerization - A Fast and Efficient Pathway to Complex Sequential Polymer Architectures"
B. Wenn, J. Laun, Y.-M.- Chuang, J. Vandenbergh, T. Junkers, Makromolekulares Kolloqium, February **2016**, Freiburg (Germany).

"Photo-Induced Copper-Mediated Acrylate Polymerization in Continuous Flow Reactors"
S. Railian, **B. Wenn**, T. Junkers, 22nd Annual Meeting of the Belgian Polymer Group, May **2016**, Hasselt (Belgium).

"Functionalized thermo-responsive star polymers – A novel smart material for nanomedicine"
J. Vrijsen, **B. Wenn**, J. Salaklang, T. Junkers, 22nd Annual Meeting of the Belgian Polymer Group, May **2016**, Hasselt (Belgium).

"Functionalized thermo-responsive star polymers – A novel smart material for nanomedicine"
J. Vrijsen, **B. Wenn**, J. Salaklang, T. Junkers, 20th MOSA Conference, June **2016**, Maastricht (Netherlands).

References

1. H. Staudinger, *Berichte der deutschen chemischen Gesellschaft (A and B Series)*, 1920, **53**, 1073-1085.
2. A. D. Jenkins, P. Kratochvíl, R. F. T. Stepto and U. W. Suter, *Pure Appl. Chem.*, 1996, **68**, 2287.
3. S. Penczek and G. Moad, *Pure Appl. Chem.*, 2008, **80**, 2163.
4. C. Geacintov, J. Smid and M. Szwarc, *J. Am. Chem. Soc.*, 1962, **84**, 2508-2514.
5. S. Aoshima and S. Kanaoka, *Chem. Rev.*, 2009, **109**, 5245-5287.
6. P. J. Flory, *Principles of Polymer Chemistry*, Cornell University Press, 1953.
7. C. Barner-Kowollik, P. Vana and T. P. Davis, in *Handbook of Radical Polymerization*, John Wiley & Sons, Inc., 2003, DOI: 10.1002/0471220450.ch4, pp. 187-261.
8. T. Otsu, T. Matsunaga, T. Doi and A. Matsumoto, *Eur. Polym. J.*, 1995, **31**, 67-78.
9. T. Otsu, M. Yoshida and T. Tazaki, *Makromol. Chem., Rapid Commun.*, 1982, **3**, 133-140.
10. X. Pan, M. A. Tasdelen, J. Laun, T. Junkers, Y. Yagci and K. Matyjaszewski, *Prog. Polym. Sci.*, 2016, DOI: 10.1016/j.progpolymsci.2016.06.005.
11. J. Chiefari, Y. K. Chong, F. Ercole, J. Krstina, J. Jeffery, T. P. T. Le, R. T. A. Mayadunne, G. F. Meijs, C. L. Moad, G. Moad, E. Rizzardo and S. H. Thang, *Macromolecules*, 1998, **31**, 5559-5562.
12. C. H. Hornung, C. Guerrero-Sanchez, M. Brasholz, S. Saubern, J. Chiefari, G. Moad, E. Rizzardo and S. H. Thang, *Org. Process Res. Dev.*, 2011, **15**, 593-601.
13. Y.-Z. You, C.-Y. Hong, R.-K. Bai, C.-Y. Pan and J. Wang, *Macromol. Chem. Phys.*, 2002, **203**, 477-483.
14. T. Junkers, A. Theis, M. Buback, T. P. Davis, M. H. Stenzel, P. Vana and C. Barner-Kowollik, *Macromolecules*, 2005, **38**, 9497-9508.
15. S. Muthukrishnan, E. H. Pan, M. H. Stenzel, C. Barner-Kowollik, T. P. Davis, D. Lewis and L. Barner, *Macromolecules*, 2007, **40**, 2978-2980.
16. W. Jakubowski and K. Matyjaszewski, *Angew. Chem. Int. Ed.*, 2006, **45**, 4482-4486.
17. K. Matyjaszewski, W. Jakubowski, K. Min, W. Tang, J. Y. Huang, W. A. Braunecker and N. V. Tsarevsky, *Proc. Natl. Acad. Sci. U. S. A.*, 2006, **103**, 15309-15314.
18. A. J. D. Magenau, N. C. Strandwitz, A. Gennaro and K. Matyjaszewski, *Science*, 2011, **332**, 81-84.
19. C. M. R. Abreu, P. V. Mendonça, A. n. C. Serra, A. V. Popov, K. Matyjaszewski, T. Guliashvili and J. F. J. Coelho, *ACS Macro Lett.*, 2012, **1**, 1308-1311.
20. D. Konkolewicz, Y. Wang, M. Zhong, P. Krys, A. A. Isse, A. Gennaro and K. Matyjaszewski, *Macromolecules*, 2013, **46**, 8749–8772.
21. T. Guliashvili, P. V. Mendonça, A. C. Serra, A. V. Popov and J. F. J. Coelho, *Chem. Eur. J.*, 2012, **18**, 4607-4612.

22. V. Percec, T. Guliashvili, J. S. Ladislaw, A. Wistrand, A. Stjerndahl, M. J. Sienkowska, M. J. Monteiro and S. Sahoo, *J. Am. Chem. Soc.*, 2006, **128**, 14156-14165.
23. X. Pan, M. Lamson, J. Yan and K. Matyjaszewski, *ACS Macro Lett.*, 2015, **4**, 192-196.
24. N. J. Treat, H. Sprafke, J. W. Kramer, P. G. Clark, B. E. Barton, J. R. de Alaniz, B. P. Fors and C. J. Hawker, *J. Am. Chem. Soc.*, 2014, **136**, 16096-16101.
25. K. Matyjaszewski, *Macromolecules*, 2012, **45**, 4015-4039.
26. Y. Wang and K. Matyjaszewski, *Macromolecules*, 2010, **43**, 4003-4005.
27. A. Debuigne, R. Poli, C. Jérôme, R. Jérôme and C. Detrembleur, *Prog. Polym. Sci.*, 2009, **34**, 211-239.
28. M. Kato, M. Kamigaito, M. Sawamoto and T. Higashimura, *Macromolecules*, 1995, **28**, 1721-1723.
29. S. Yamago, Y. Ukai, A. Matsumoto and Y. Nakamura, *J. Am. Chem. Soc.*, 2009, **131**, 2100-2101.
30. W. A. Braunecker, Y. Itami and K. Matyjaszewski, *Macromolecules*, 2005, **38**, 9402-9404.
31. G. Lligadas, B. M. Rosen, M. J. Monteiro and V. Percec, *Macromolecules*, 2008, **41**, 8360-8364.
32. V. Percec, A. V. Popov, E. Ramirez-Castillo, M. Monteiro, B. Barboiu, O. Weichold, A. D. Asandei and C. M. Mitchell, *J. Am. Chem. Soc.*, 2002, **124**, 4940-4941.
33. B. M. Rosen and V. Percec, *Chem. Rev.*, 2009, **109**, 5069-5119.
34. A. Debuigne, M. Schoumacher, N. Willet, R. Riva, X. Zhu, S. Rutten, C. Jérôme and C. Detrembleur, *Chem. Commun.*, 2011, **47**, 12703-12705.
35. Y. Zhao, M. Yu and X. Fu, *Chem. Commun.*, 2013, **49**, 5186-5188.
36. L. D. Arvanitopoulos, M. P. Greuel, B. M. King, A. K. Shim and J. H. Harwood, in *Controlled Radical Polymerization*, American Chemical Society, 1998, vol. 685, ch. 20, pp. 316-331.
37. J. Mosnáček and M. Ilčíková, *Macromolecules*, 2012, **45**, 5859-5865.
38. A. Anastasaki, V. Nikolaou, Q. Zhang, J. Burns, S. R. Samanta, C. Waldron, A. J. Haddleton, R. McHale, D. Fox, V. Percec, P. Wilson and D. M. Haddleton, *J. Am. Chem. Soc.*, 2014, **136**, 1141-1149.
39. D. Konkolewicz, K. Schröder, J. Buback, S. Bernhard and K. Matyjaszewski, *ACS Macro Lett.*, 2012, **1**, 1219-1223.
40. M. A. Tasdelen, M. Uygun and Y. Yagci, *Macromol. Chem. Phys.*, 2011, **212**, 2036-2042.
41. B. P. Fors and C. J. Hawker, *Angew. Chem. Int. Ed.*, 2012, **51**, 8850-8853.
42. J. Lalevée, N. Blanchard, M.-A. Tehfe, M. Peter, F. Morlet-Savary and J. P. Fouassier, *Macromol. Rapid Commun.*, 2011, **32**, 917-920.
43. W. Ma, D. Chen, L. Wang, Y. Ma, C. Zhao and W. Yang, *J. Macromol. Sci., Part A: Pure Appl. Chem.*, 2015, **52**, 761-769.
44. K. Iwai, M. Uesugi and F. Takemura, *Polym. J.*, 1985, **17**, 1005-1011.
45. G. Zhang, I. Y. Song, K. H. Ahn, T. Park and W. Choi, *Macromolecules*, 2011, **44**, 7594-7599.

46. N. V. Alfredo, N. E. Jalapa, S. L. Morales, A. D. Ryabov, R. Le Lagadec and L. Alexandrova, *Macromolecules*, 2012, **45**, 8135-8146.
47. X. Pan, N. Malhotra, J. Zhang and K. Matyjaszewski, *Macromolecules*, 2015, **48**, 6948-6954.
48. Z. Xue, N. T. B. Linh, S. K. Noh and W. S. Lyoo, *Angew. Chem. Int. Ed.*, 2008, **47**, 6426-6429.
49. G.-X. Wang, M. Lu, Z.-H. Hou, Y. Gao, L.-C. Liu and H. Wu, *J. Macromol. Sci., Part A: Pure Appl. Chem.*, 2014, **51**, 565-571.
50. B. B. Wayland, G. Poszmik, S. L. Mukerjee and M. Fryd, *J. Am. Chem. Soc.*, 1994, **116**, 7943-7944.
51. A. Debuigne, J.-R. Caille and R. Jérôme, *Angew. Chem. Int. Ed.*, 2005, **44**, 1101-1104.
52. C. Wiles and P. Watts, *Eur. J. Org. Chem.*, 2008, **2008**, 1655-1671.
53. V. Hessel, *Chem. Eng. Technol.*, 2009, **32**, 1655-1681.
54. M. Oelgemöller and O. Shvydkiv, *Molecules*, 2011, **16**, 7522-7550.
55. J.-i. Yoshida, H. Kim and A. Nagaki, *ChemSusChem*, 2011, **4**, 331-340.
56. C. Tonhauser, A. Natalello, H. Löwe and H. Frey, *Macromolecules*, 2012, **45**, 9551-9570.
57. A. Cholette and L. Cloutier, *Can. J. Chem. Eng.*, 1959, **37**, 105-112.
58. M. Harada, K. Tanaka, W. Eguchi and S. Nagata, *J. Chem. Eng. Jpn.*, 1968, **1**, 148-152.
59. B. D. A. Hook, W. Dohle, P. R. Hirst, M. Pickworth, M. B. Berry and K. I. Booker-Milburn, *J. Org. Chem.*, 2005, **70**, 7558-7564.
60. J. Vandenbergh and T. Junkers, *Polym. Chem.*, 2012, **3**, 2739-2742.
61. N. Zaquen, E. Baeten, J. Vandenbergh, L. Lutsen, D. Vanderzande and T. Junkers, *Chem. Eng. Technol.*, 2015, **38**, 1749-1757.
62. D. T. McQuade and P. H. Seeberger, *J. Org. Chem.*, 2013, **78**, 6384-6389.
63. J. H. Bannock, S. H. Krishnadasan, M. Heeney and J. C. de Mello, *Mater. Horiz.*, 2014, **1**, 373-378.
64. J. J. Haven, J. Vandenbergh and T. Junkers, *Chem. Commun.*, 2015, **51**, 4611-4614.
65. Y. Su, K. Kuijpers, V. Hessel and T. Noel, *React. Chem. Eng.*, 2016, **1**, 73-81.
66. J. P. Knowles, L. D. Elliott and K. I. Booker-Milburn, *Beilstein J. Org. Chem.*, 2012, **8**, 2025-2052.
67. L. D. Elliott, J. P. Knowles, P. J. Koovits, K. G. Maskill, M. J. Ralph, G. Lejeune, L. J. Edwards, R. I. Robinson, I. R. Clemens, B. Cox, D. D. Pascoe, G. Koch, M. Eberle, M. B. Berry and K. I. Booker-Milburn, *Chem. Eur. J.*, 2014, **20**, 15226-15232.
68. E. E. Coyle and M. Oelgemoller, *Photochem. Photobiol. Sci.*, 2008, **7**, 1313-1322.
69. M. Oelgemoeller, *Chem. Eng. Technol.*, 2012, **35**, 1144-1152.
70. H. Trommsdorff, *Annalen der Pharmacie*, 1834, **11**, 190-207.
71. N. Hoffmann, *Chem. Rev.*, 2008, **108**, 1052-1103.
72. T. Bach and J. P. Hehn, *Angew. Chem. Int. Ed.*, 2011, **50**, 1000-1045.
73. J. Iriondo-Alberdi and M. F. Greaney, *Eur. J. Org. Chem.*, 2007, **2007**, 4801-4815.

74. K.-H. Pfoertner, in *Ullmann's Encyclopedia of Industrial Chemistry*, Wiley-VCH Verlag GmbH & Co. KGaA, 2000, DOI: 10.1002/14356007.a19_573.
75. D. Cambié, C. Bottecchia, N. J. W. Straathof, V. Hessel and T. Noël, *Chem. Rev.*, 2016, DOI: 10.1021/acs.chemrev.5b00707.
76. C. M. Doede; and C. A. Walker, *Chem. Eng.*, 1955, **62**, 159-178.
77. K. Ueno, F. Kitagawa and N. Kitamura, *Lab Chip*, 2002, **2**, 231-234.
78. H. Lu, M. A. Schmidt and K. F. Jensen, *Lab Chip*, 2001, **1**, 22-28.
79. S. Landgraf, *Spectrochim. Acta, Part A*, 2001, **57**, 2029-2048.
80. T. Aillet, K. Loubière, L. Prat and O. Dechy-Cabaret, *AlChE J.*, 2015, **61**, 1284-1299.
81. D. H. Waldeck, *Chem. Rev.*, 1991, **91**, 415-436.
82. S. Erbas-Cakmak, D. A. Leigh, C. T. McTernan and A. L. Nussbaumer, *Chem. Rev.*, 2015, **115**, 10081-10206.
83. J. Broichhagen, J. A. Frank and D. Trauner, *Acc. Chem. Res.*, 2015, **48**, 1947-1960.
84. W. Szymański, J. M. Beierle, H. A. V. Kistemaker, W. A. Velema and B. L. Feringa, *Chem. Rev.*, 2013, **113**, 6114-6178.
85. H. D. Rauter, R. Seliger, S. Werner and F. D. Wissmann, *Chem. Abstrs.*, 2009, **150**, 376721.
86. J. A. Burns, C. Houben, A. Anastasaki, C. Waldron, A. A. Lapkin and D. M. Haddleton, *Polym. Chem.*, 2013, **4**, 4809-4813.
87. P. Derboven, P. H. M. Van Steenberge, J. Vandenbergh, M.-F. Reyniers, T. Junkers, D. R. D'Hooge and G. B. Marin, *Macromol. Rapid Commun.*, 2015, **36**, 2149-2155.
88. T. Fukuyama, Y. Kajihara, I. Ryu and A. Studer, *Synthesis*, 2012, **44**, 2555-2559.
89. N. Chan, M. F. Cunningham and R. A. Hutchinson, *J. Polym. Sci., Part A: Polym. Chem.*, 2013, **51**, 3081-3096.
90. T. Noda, A. J. Grice, M. E. Levere and D. M. Haddleton, *Eur. Polym. J.*, 2007, **43**, 2321-2330.
91. B. Wenn, M. Conradi, A. D. Carreiras, D. M. Haddleton and T. Junkers, *Polym. Chem.*, 2014, **5**, 3053-3060.
92. Y. Shen and S. Zhu, *AlChE J.*, 2002, **48**, 2609-2619.
93. A. Melker, B. P. Fors, C. J. Hawker and J. E. Poelma, *J. Polym. Sci., Part A: Polym. Chem.*, 2015, **53**, 2693–2698.
94. E. Baeten, B. Verbraeken, R. Hoogenboom and T. Junkers, *Chem. Commun.*, 2015, **51**, 11701-11704.
95. J. Haven, J. Vandenbergh, R. Kurita, J. Gruber and T. Junkers, *Polym. Chem.*, 2015, **6**, 5752-5765.
96. M. Conradi and T. Junkers, *J. Photochem. Photobiol., A*, 2013, **259**, 41-46.
97. M. Conradi and T. Junkers, *Macromolecules*, 2014, **47**, 5578-5585.
98. A. Kermagoret, B. Wenn, A. Debuigne, C. Jérôme, T. Junkers and C. Detrembleur, *Polym. Chem.*, 2015, **6**, 3847-3857.
99. M. Chen and J. A. Johnson, *Chem. Commun.*, 2015, **51**, 6742-6745.
100. Y.-M. Chuang, B. Wenn, S. Gielen, A. Ethirajan and T. Junkers, *Polym. Chem.*, 2015, **6**, 6488-6497.

101. D. Wilms, J. Klos and H. Frey, *Macromol. Chem. Phys.*, 2008, **209**, 343-356.
102. J. Vandenbergh, T. de Moraes Ogawa and T. Junkers, *J. Polym. Sci., Part A: Polym. Chem.*, 2013, **51**, 2366-2374.
103. M. Janata, L. Lochmann, P. Vlček, J. Dybal and A. H. E. Müller, *Die Makromolekulare Chemie*, 1992, **193**, 101-112.
104. K. Iida, T. Q. Chastek, K. L. Beers, K. A. Cavicchi, J. Chun and M. J. Fasolka, *Lab Chip*, 2009, **9**, 339-345.
105. J. Vandenbergh, T. Tura, E. Baeten and T. Junkers, *J. Polym. Sci., Part A: Polym. Chem.*, 2014, **52**, 1263-1274.
106. A. Nagaki, Y. Takahashi, K. Akahori and J.-i. Yoshida, *Macromol. React. Eng.*, 2012, **6**, 467-472.
107. E. Yoshida, *Colloid. Polym. Sci.*, 2010, **288**, 73-78.
108. J. F. Quinn, L. Barner, C. Barner-Kowollik, E. Rizzardo and T. P. Davis, *Macromolecules*, 2002, **35**, 7620-7627.
109. S. H. Qin and K. Y. Qiu, *Eur. Polym. J.*, 2001, **37**, 711-717.
110. M. A. Tasdelen, M. Uygun and Y. Yagci, *Macromol. Rapid Commun.*, 2011, **32**, 58-62.
111. T. Junkers, *Eur. Polym. J.*, 2015, **62**, 273-280.
112. C.-H. Yeh and Y.-C. Lin, *Microfluid Nanofluid*, 2009, **6**, 277-283.
113. W. J. Jeong, J. Y. Kim, J. Choo, E. K. Lee, C. S. Han, D. J. Beebe, G. H. Seong and S. H. Lee, *Langmuir*, 2005, **21**, 3738-3741.
114. D. K. Hwang, D. Dendukuri and P. S. Doyle, *Lab Chip*, 2008, **8**, 1640-1647.
115. D. Dendukuri, K. Tsoi, T. A. Hatton and P. S. Doyle, *Langmuir*, 2005, **21**, 2113-2116.
116. K. P. Yuet, D. K. Hwang, R. Haghgooie and P. S. Doyle, *Langmuir*, 2010, **26**, 4281-4287.
117. C.-H. Chen, R. K. Shah, A. R. Abate and D. A. Weitz, *Langmuir*, 2009, **25**, 4320-4323.
118. Z. Nie, W. Li, M. Seo, S. Xu and E. Kumacheva, *J. Am. Chem. Soc.*, 2006, **128**, 9408-9412.
119. Y. Hennequin, N. Pannacci, C. P. de Torres, G. Tetradis-Meris, S. Chapuliot, E. Bouchaud and P. Tabeling, *Langmuir*, 2009, **25**, 7857-7861.
120. M. T. Gokmen, W. Van Camp, P. J. Colver, S. A. F. Bon and F. E. Du Prez, *Macromolecules*, 2009, **42**, 9289-9294.
121. R. A. Prasath, M. T. Gokmen, P. Espeel and F. E. Du Prez, *Polym. Chem.*, 2010, **1**, 685-692.
122. M. T. Gokmen, B. Dereli, B. G. De Geest and F. E. Du Prez, *Part. Part. Syt. Charact.*, 2013, **30**, 438-444.
123. M. T. Gokmen, B. G. De Geest, W. E. Hennink and F. E. Du Prez, *ACS Appl. Mater. Interfaces*, 2009, **1**, 1196-1202.
124. M. Moreno-Mañas and R. Pleixats, *Acc. Chem. Res.*, 2003, **36**, 638-643.
125. P. Mukherjee, C. R. Patra, A. Ghosh, R. Kumar and M. Sastry, *Chem. Mater.*, 2002, **14**, 1678-1684.
126. R. M. Crooks, M. Zhao, L. Sun, V. Chechik and L. K. Yeung, *Acc. Chem. Res.*, 2001, **34**, 181-190.

127. A. Knauer, S. Schneider, F. Möller, A. Csáki, W. Fritzsche and J. M. Köhler, *Chem. Eng. J.*, 2013, **227**, 80-89.
128. S. Link and M. A. El-Sayed, *J. Phys. Chem. B*, 1999, **103**, 4212-4217.
129. G. Schmid and L. F. Chi, *Adv. Mater.*, 1998, **10**, 515-526.
130. L. Hafermann and J. M. Köhler, *Chem. Eng. Technol.*, 2015, **38**, 1138-1143.
131. L. Hafermann and J. Michael Köhler, *J. Nanopart. Res.*, 2015, **17**, 1-8.
132. A. Knauer and J. M. Koehler, *Nanotechnology Reviews*, 2014, **3**, 5.
133. M. Wörner, *Microfluid Nanofluid*, 2012, **12**, 841-886.
134. A. Knauer, A. Csáki, F. Möller, C. Hühn, W. Fritzsche and J. M. Köhler, *J. Phys. Chem. C*, 2012, **116**, 9251-9258.
135. Z. Wan, W. Luan and S.-t. Tu, *J. Phys. Chem. C*, 2011, **115**, 1569-1575.
136. A. Knauer, A. Thete, S. Li, H. Romanus, A. Csáki, W. Fritzsche and J. M. Köhler, *Chem. Eng. J.*, 2011, **166**, 1164-1169.
137. A. B. Theberge, F. Courtois, Y. Schaerli, M. Fischlechner, C. Abell, F. Hollfelder and W. T. S. Huck, *Angew. Chem. Int. Ed.*, 2010, **49**, 5846-5868.
138. J. Wagner and J. M. Köhler, *Nano Lett.*, 2005, **5**, 685-691.
139. Y. Tonbul, M. Zahmakiran and S. Özkar, *Appl. Catal., B*, 2014, **148–149**, 466-472.
140. S. M. Humphrey, M. E. Grass, S. E. Habas, K. Niesz, G. A. Somorjai and T. D. Tilley, *Nano Lett.*, 2007, **7**, 785-790.
141. M. Liu, J. Zhang, J. Liu and W. W. Yu, *J. Catal.*, 2011, **278**, 1-7.
142. J. C. Scaiano, K. G. Stamplecoskie and G. L. Hallett-Tapley, *Chem. Commun.*, 2012, **48**, 4798-4808.
143. S. Silvestrini, T. Carofiglio and M. Maggini, *Chem. Commun.*, 2013, **49**, 84-86.
144. S. Chen and D. L. Carroll, *Nano Lett.*, 2002, **2**, 1003-1007.
145. R. Jin, Y. Cao, C. A. Mirkin, K. L. Kelly, G. C. Schatz and J. G. Zheng, *Science*, 2001, **294**, 1901-1903.
146. X. Wu, P. L. Redmond, H. Liu, Y. Chen, M. Steigerwald and L. Brus, *J. Am. Chem. Soc.*, 2008, **130**, 9500-9506.
147. C. Xue, G. S. Métraux, J. E. Millstone and C. A. Mirkin, *J. Am. Chem. Soc.*, 2008, **130**, 8337-8344.
148. M. Maillard, P. Huang and L. Brus, *Nano Lett.*, 2003, **3**, 1611-1615.
149. B. Adhikari and S. Majumdar, *Prog. Polym. Sci.*, 2004, **29**, 699.
150. R. F. Gibson, *Composite Struct.*, 2010, **92**, 2793.
151. D. W. Hatchett and M. Josowicz, *Chem. Rev.*, 2008, **108**, 746.
152. Y. Ofir, B. Samanta and V. M. Rotello, *Chem. Soc. Rev.*, 2008, **37**, 1814.
153. J. F. Tressler, S. Alkoy, A. Dogan and R. E. Newnham, *Composites, Parts A*, 1999, **4**, 477.
154. K. S. Iyer, B. Zdyrko, S. Malynych, G. Chumanov and I. Luzinov, *Soft Matter*, 2011, **7**, 2538.
155. J. I. Park, A. Saffari, S. Kumar, A. Guenther and E. Kumacheva, *Annu. Rev. Mater. Res.*, 2010, **40**, 415.
156. S. Q. Xu, Z. H. Nie, M. Seo, P. Lewis, E. Kumacheva, H. A. Stone, P. Garstecki, D. B. Weibel, I. Gitlin and G. M. Whitesides, *Angew. Chem., Int. Ed.*, 2005, **44**, 724.

157. C. A. Serra and Z. Chang, *Chem. Eng. Technol.*, 2008, **31**, 1099.
158. J. M. Köhler, A. März, J. Popp, A. Knauer, I. Kraus, J. Faerber and C. Serra, *Anal. Chem.*, 2013, **85**, 313-318.
159. Y. Su, N. J. W. Straathof, V. Hessel and T. Noël, *Chem. - Eur. J.*, 2014, **20**, 10562-10589.
160. T. Junkers and B. Wenn, *React. Chem. Eng.*, 2016, **1**, 60-64.
161. J. Nicolas, Y. Guillaneuf, C. Lefay, D. Bertin, D. Gigmes and B. Charleux, *Prog. Polym. Sci.*, 2013, **38**, 63-235.
162. C. Boyer, N. A. Corrigan, K. Jung, D. Nguyen, T.-K. Nguyen, N. N. M. Adnan, S. Oliver, S. Shanmugam and J. Yeow, *Chem. Rev.*, 2016, **116**, 1803-1949.
163. V. Coessens, T. Pintauer and K. Matyjaszewski, *Prog. Polym. Sci.*, 2001, **26**, 337-377.
164. D. M. Haddleton, M. C. Crossman, K. H. Hunt, C. Topping, C. Waterson and K. G. Suddaby, *Macromolecules*, 1997, **30**, 3992-3998.
165. Y. Guillaneuf, D. Bertin, D. Gigmes, D.-L. Versace, J. Lalevée and J.-P. Fouassier, *Macromolecules*, 2010, **43**, 2204-2212.
166. C. Detrembleur, D.-L. Versace, Y. Piette, M. Hurtgen, C. Jérôme, J. Lalevée and A. Debuigne, *Polym. Chem.*, 2012, **3**, 1856-1866.
167. E.-X. Liang, M. Zhong, Z.-H. Hou, Y. Huang, B.-H. He, G.-X. Wang, L.-C. Liu and H. Wu, *J. Macromol. Sci., Part A: Pure Appl. Chem.*, 2016, **53**, 210-214.
168. N. J. Treat, B. P. Fors, J. W. Kramer, M. Christianson, C.-Y. Chiu, J. R. d. Alaniz and C. J. Hawker, *ACS Macro Lett.*, 2014, **3**, 580-584.
169. E. Frick, A. Anastasaki, D. M. Haddleton and C. Barner-Kowollik, *J. Am. Chem. Soc.*, 2015, **137**, 6889-6896.
170. J. Laun, M. Vorobii, A. de los Santos Pereira, O. Pop-Georgievski, V. Trouillet, A. Welle, C. Barner-Kowollik, C. Rodriguez-Emmenegger and T. Junkers, *Macromol. Rapid Commun.*, 2015, **36**, 1681-1686.
171. J. Vandenbergh, G. Reekmans, P. Adriaensens and T. Junkers, *Chem. Sci.*, 2015, **6**, 5753-5761.
172. J. Gardiner, C. H. Hornung, J. Tsanaktsidis and D. Guthrie, *Eur. Polym. J.*, 2016, **80**, 200-207.
173. E. Baeten, S. Vanslambrouck, C. Jérôme, P. Lecomte and T. Junkers, *Eur. Polym. J.*, 2016, **80**, 208-218.
174. A. Anastasaki, V. Nikolaou, A. Simula, J. Godfrey, M. X. Li, G. Nurumbetov, P. Wilson and D. M. Haddleton, *Macromolecules*, 2014, **47**, 3852-3859.
175. J. Mosnacek, A. Eckstein-Andicsova and K. Borska, *Polym. Chem.*, 2015, **6**, 2523-2530.
176. J. Mosnacek, A. Eckstein-Andicsova and K. Borska, *Polymer Chemistry*, 2015, DOI: 10.1039/C4PY01807A.
177. T. Zhang, T. Chen, I. Amin and R. Jordan, *Polym. Chem.*, 2014, **5**, 4790.
178. N. Bortolamei, A. A. Isse, A. J. D. Magenau, A. Gennaro and K. Matyjaszewski, *Angew. Chem. Int. Ed.*, 2011, **50**, 11391-11394.
179. J. Mosnacek, A. Kundys and A. Andicsova, *Polymers*, 2014, **6**, 2862-2874.
180. C. H. Hornung, X. Nguyen, S. Kyi, J. Chiefari and S. Saubern, *Aust. J. Chem.*, 2013, **66**, 192-198.

181. Y.-M. Chuang, A. Ethirajan and T. Junkers, *ACS Macro Lett.*, 2014, **3**, 732-737.
182. A. Anastasaki, V. Nikolaou, N. W. McCaul, A. Simula, J. Godfrey, C. Waldron, P. Wilson, K. Kempe and D. M. Haddleton, *Macromolecules*, 2015, **48**, 1404-1411.
183. Y. Yagci, S. Jockusch and N. J. Turro, *Macromolecules*, 2010, **43**, 6245-6260.
184. K. Matyjaszewski, T. E. Patten and J. H. Xia, *J. Am. Chem. Soc.*, 1997, **119**, 674-680.
185. K. Matyjaszewski and J. H. Xia, *Chem. Rev.*, 2001, **101**, 2921-2990.
186. V. Percec, A. V. Popov, E. Ramirez-Castillo and O. Weichold, *J. Polym. Sci., Part A: Polym. Chem.*, 2003, **41**, 3283-3299.
187. D.-L. Versace, J. Lalevée, J.-P. Fouassier, Y. Guillaneuf, D. Bertin and D. Gigmes, *Macromol. Rapid Commun.*, 2010, **31**, 1383-1388.
188. S. Shanmugam, J. T. Xu and C. Boyer, *Macromolecules*, 2014, **47**, 4930-4942.
189. A. Anastasaki, V. Nikolaou, G. S. Pappas, Q. Zhang, C. Wan, P. Wilson, T. P. Davis, M. R. Whittaker and D. M. Haddleton, *Chem. Sci.*, 2014, **5**, 3536-3542.
190. N. Hadjichristidis, A. Guyot and L. J. Fetters, *Macromolecules*, 1978, **11**, 668-672.
191. S. Jacob, I. Majoros and J. P. Kennedy, *Macromolecules*, 1996, **29**, 8631-8641.
192. C. Boyer, A. Derveaux, P. B. Zetterlund and M. R. Whittaker, *Polym. Chem.*, 2012, **3**, 117-123.
193. K. Matyjaszewski, P. J. Miller, J. Pyun, G. Kickelbick and S. Diamanti, *Macromolecules*, 1999, **32**, 6526-6535.
194. N. Hadjichristidis, H. Iatrou, M. Pitsikalis and J. Mays, *Prog. Polym. Sci.*, 2006, **31**, 1068-1132.
195. S. Kobben, A. Ethirajan and T. Junkers, *J. Polym. Sci., Part A: Polym. Chem.*, 2014, **52**, 1633-1641.
196. C.-H. Lu, J.-H. Wang, F.-C. Chang and S.-W. Kuo, *Macromol. Chem. Phys.*, 2010, **211**, 1339-1347.
197. C. Waldron, A. Anastasaki, R. McHale, P. Wilson, Z. D. Li, T. Smith and D. M. Haddleton, *Polym. Chem.*, 2014, **5**, 892-898.
198. R. Aksakal, M. Resmini and C. R. Becer, *Polym. Chem.*, 2016, **7**, 171-175.
199. H. Wei, S. Perrier, S. Dehn, R. Ravarian and F. Dehghani, *Soft Matter*, 2012, **8**, 9526-9528.
200. W. Radke, J. Gerber and G. Wittmann, *Polymer*, 2003, **44**, 519-525.
201. G. Gody, P. B. Zetterlund, S. Perrier and S. Harrisson, *Nat. Commun.*, 2016, **7**, 10514.
202. C. A. Lipinski, *J. Pharmacol. Toxicol. Methods*, 2000, **44**, 235-249.
203. K. Knop, G. M. Pavlov, T. Rudolph, K. Martin, D. Pretzel, B. O. Jahn, D. H. Scharf, A. A. Brakhage, V. Makarov, U. Mollmann, F. H. Schacher and U. S. Schubert, *Soft Matter*, 2013, **9**, 715-726.
204. S. Huebschmann, D. Kralisch, V. Hessel, U. Krtschil and C. Kompter, *Chem. Eng. Technol.*, 2009, **32**, 1757-1765.

205. V. Hessel, P. Loeb and H. Loewe, in *Industrial microreactor process development up to production*, Wiley-VCH Verlag GmbH & Co. KGaA, 2008, DOI: 10.1002/9783527622856.ch5, pp. 211-275.

206. F. Bally, C. A. Serra, V. Hessel and G. Hadziioannou, *Chem. Eng. Sci.*, 2011, **66**, 1449-1462.

207. L. Malet-Sanz and F. Susanne, *J. Med. Chem.*, 2012, **55**, 4062-4098.

208. D. T. McQuade and P. H. Seeberger, *J. Org. Chem.*, 2013, **78**, 6384-6389.

209. B. P. Mason, K. E. Price, J. L. Steinbacher, A. R. Bogdan and D. T. McQuade, *Chem. Rev.*, 2007, **107**, 2300-2318.

210. J.-i. Yoshida, A. Nagaki and T. Yamada, *Chem. - Eur. J.*, 2008, **14**, 7450-7459.

211. J.-i. Yoshida, A. Nagaki, T. Iwasaki and S. Suga, *Chem. Eng. Technol.*, 2005, **28**, 259-266.

212. R. L. Hartman, J. P. McMullen and K. F. Jensen, *Angew. Chem., Int. Ed.*, 2011, **50**, 7502-7519.

213. F. Bally, C. A. Serra, V. Hessel and G. Hadziioannou, *Macromol. React. Eng.*, 2010, **4**, 543-561.

214. V. Hessel, C. Sera, H. Loewe and G. Hadziioannou, *Chem. Ing. Tech.*, 2005, **77**, 1693-1710, 1712-1714.

215. D. Wilms, J. Klos and H. Frey, *Macromol. Chem. Phys.*, 2008, **209**, 343-356.

216. B. Dervaux, T. Junkers, C. Barner-Kowollik and F. E. Du Prez, *Macromol. React. Eng.*, 2009, **3**, 529-538.

217. N. Chan, M. F. Cunningham and R. A. Hutchinson, *J. Polym. Sci., Part A: Polym. Chem.*, 2013, **51**, 3081-3096.

218. J. A. Burns, C. Houben, A. Anastasaki, C. Waldron, A. A. Lapkin and D. M. Haddleton, *Polym. Chem.*, 2013, **4**, 4809-4813.

219. C. H. Hornung, K. von Känel, I. Martinez-Botella, M. Espiritu, X. Nguyen, A. Postma, S. Saubern, J. Chiefari and S. H. Thang, *Macromolecules*, 2014, **47**, 8203-8213.

220. R. J. J. Jachuck and V. Nekkanti, *Macromolecules*, 2008, **41**, 3053-3062.

221. L. E. N. Allan, M. R. Perry and M. P. Shaver, *Prog. Polym. Sci.*, 2012, **37**, 127-156.

222. C.-H. Peng, T.-Y. Yang, Y. Zhao and X. Fu, *Org. Biomol. Chem.*, 2014, **12**, 8580-8587.

223. M. Hurtgen, C. Detrembleur, C. Jérôme and A. Debuigne, *Polym. Rev.*, 2011, **51**, 188-213.

224. A. Debuigne, R. Poli, C. Jérôme, R. Jérôme and C. Detrembleur, *Prog. Polym. Sci.*, 2009, **34**, 211-239.

225. R. Poli, *Angew. Chem., Int. Ed.*, 2006, **45**, 5058-5070.

226. A. Debuigne, C. Michaux, C. Jérôme, R. Jérôme, R. Poli and C. Detrembleur, *Chem.-Eur. J.*, 2008, **14**, 7623-7637.

227. M. Hurtgen, A. Debuigne, C. Jérôme and C. Detrembleur, *Macromolecules*, 2010, **43**, 886-894.

228. A. Debuigne, J.-R. Caille and R. Jérôme, *Angew. Chem., Int. Ed.*, 2005, **44**, 1101-1104.

229. Y. Piette, A. Debuigne, C. Jérôme, V. Bodart, R. Poli and C. Detrembleur, *Polym. Chem.*, 2012, **3**, 2880-2891.

230. A. Kermagoret, K. Mathieu, J.-M. Thomassin, C.-A. Fustin, R. Duchène, C. Jérôme, C. Detrembleur and A. Debuigne, *Polym. Chem.*, 2014, **5**, 6534-6544.
231. A. Debuigne, A. N. Morin, A. Kermagoret, Y. Piette, C. Detrembleur, C. Jérôme and R. Poli, *Chem.-Eur. J.*, 2012, **18**, 12834-12844.
232. D. Cordella, A. Kermagoret, A. Debuigne, R. Riva, I. German, M. Isik, C. Jérôme, D. Mecerreyes, D. Taton and C. Detrembleur, *ACS Macro Lett.*, 2014, **3**, 1276-1280.
233. A. Kermagoret, A. Debuigne, C. Jérôme and C. Detrembleur, *Nat. Chem.*, 2014, **6**, 179-187.
234. R. Bryaskova, N. Willet, P. Degée, P. Dubois, R. Jérôme and C. Detrembleur, *J. Polym. Sci., Part A: Polym. Chem.*, 2007, **45**, 2532-2542.
235. L. S. Boffa and B. M. Novak, *Chem. Rev.*, 2000, **100**, 1479-1493.
236. J. Demarteau, A. Kermagoret, C. Jérôme, C. Detrembleur and A. Debuigne, in *Controlled Radical Polymerization: Materials*, American Chemical Society, 2015, vol. 1188, ch. 4, pp. 47-61.
237. S. Yamago and Y. Nakamura, *Polymer*, 2013, **54**, 981-994.
238. S. Dadashi-Silab, M. Atilla Tasdelen and Y. Yagci, *J. Polym. Sci., Part A: Polym. Chem.*, 2014, **52**, 2878-2888.
239. J. Xu, K. Jung and C. Boyer, *Macromolecules*, 2014, **47**, 4217-4229.
240. N. J. Treat, H. Sprafke, J. W. Kramer, P. G. Clark, B. E. Barton, J. Read de Alaniz, B. P. Fors and C. J. Hawker, *J. Am. Chem. Soc.*, 2014, **136**, 16096-16101.
241. T. G. Ribelli, D. Konkolewicz, S. Bernhard and K. Matyjaszewski, *J. Am. Chem. Soc.*, 2014, **136**, 13303-13312.
242. *US Pat.,* US5468785A, 1995.
243. A. Debuigne, M. Schoumacher, N. Willet, R. Riva, X. Zhu, S. Rütten, C. Jérôme and C. Detrembleur, *Chem. Commun.*, 2011, **47**, 12703-12705.
244. Y. Zhao, M. Yu and X. Fu, *Chem. Commun.*, 2013, **49**, 5186-5188.
245. X. Miao, W. Zhu, Z. Zhang, W. Zhang, X. Zhu and J. Zhu, *Polym. Chem.*, 2014, **5**, 551-557.
246. Y. Zhao, M. Yu, S. Zhang, Y. Liu and X. Fu, *Macromolecules*, 2014, **47**, 6238-6245.
247. C. Detrembleur, D.-L. Versace, Y. Piette, M. Hurtgen, C. Jérôme, J. Lalevée and A. Debuigne, *Polym. Chem.*, 2012, **3**, 1856-1866.
248. A. Debuigne, Y. Champouret, R. Jérôme, R. Poli and C. Detrembleur, *Chem.- Eur. J.*, 2008, **14**, 4046-4059.
249. A. Nakamura, S. Ito and K. Nozaki, *Chem. Rev.*, 2009, **109**, 5215-5244.
250. A. Berkefeld and S. Mecking, *Angew. Chem., Int. Ed.*, 2008, **47**, 2538-2542.
251. N. M. G. Franssen, J. N. H. Reek and B. de Bruin, *Chem. Soc. Rev.*, 2013, **42**, 5809-5832.
252. A. Rudin and P. Choi, in *The Elements of Polymer Science and Engineering*, ed. Elsevier, Academic Press New York, 3rd edn., 2012, ch. 8, pp. 341-389.
253. H. Zipse, *Top. Curr. Chem.*, 2006, **263**, 163-189.
254. E. S. Huyser, *J. Org. Chem.*, 1961, **26**, 3261-3264.
255. G. A. Mortimer and L. C. Arnold, *J. Polym. Sci. A*, 1964, **2**, 4247-4253.

256. F. R. Mayo and F. M. Lewis, *J. Am. Chem. Soc.*, 1944, **66**, 1594-1601.
257. M. L. Coote and T. P. Davis, *Prog. Polym. Sci.*, 2000, **24**, 1217-1251.
258. A. Rudin and P. Choi, in *The Elements of Polymer Science and Engineering*, ed. Elsevier, Academic Press New York, 3rd edn., 2012, ch. 9, pp. 391-425.
259. A.-M. Zorn, T. Junkers and C. Barner-Kowollik, *Macromolecules*, 2011, **44**, 6691-6700.
260. R. Venkatesh and B. Klumperman, *Macromolecules*, 2004, **37**, 1226-1233.
261. R. Venkatesh, S. Harrisson, D. M. Haddleton and B. Klumperman, *Macromolecules*, 2004, **37**, 4406-4416.
262. Z. Fu, Y. Fan and Z. Fan, *Iran. Polym. J.*, 2011, **20**, 223-235.
263. S. Kaur, G. Singh and V. K. Gupta, *J. Polym. Sci., Part A: Polym. Chem.*, 2009, **47**, 2156-2162.
264. S. Kaur, G. Singh, A. V. Kothari and V. K. Gupta, *J. Appl. Polym. Sci.*, 2009, **111**, 87-93.
265. R. Venkatesh, B. B. P. Staal and B. Klumperman, *Chem. Commun.*, 2004, 1554-1555.
266. E. Mishima, T. Tamura and S. Yamago, *Macromolecules*, 2012, **45**, 8998-9003.
267. C. Wiles and P. Watts, *Green Chem.*, 2014, **16**, 55-62.
268. B. D. A. Hook, W. Dohle, P. R. Hirst, M. Pickworth, M. B. Berry and K. I. Booker-Milburn, *J. Org. Chem.*, 2005, **70**, 7558-7564.
269. M. Chen, M. Zhong and J. A. Johnson, *Chem. Rev.*, 2016, DOI: 10.1021/acs.chemrev.5b00671.
270. J. Xu, S. Shanmugam, H. T. Duong and C. Boyer, *Polym. Chem.*, 2015, **6**, 5615-5624.
271. K. Jung, J. Xu, P. B. Zetterlund and C. Boyer, *ACS Macro Lett.*, 2015, **4**, 1139-1143.
272. T. G. McKenzie, Q. Fu, E. H. H. Wong, D. E. Dunstan and G. G. Qiao, *Macromolecules*, 2015, **48**, 3864-3872.
273. J. Lalevée, N. Blanchard, M. El-Roz, X. Allonas and J. P. Fouassier, *Macromolecules*, 2008, **41**, 2347-2352.
274. J. Lalevée, X. Allonas and J. P. Fouassier, *Macromolecules*, 2006, **39**, 8216-8218.
275. B. de Boer, H. K. Simon, M. P. L. Werts, E. W. van der Vegte and G. Hadziioannou, *Macromolecules*, 2000, **33**, 349-356.
276. T. Otsu and M. Yoshida, *Makromol. Chem., Rapid Commun.*, 1982, **3**, 127-132.
277. G. Moad, E. Rizzardo and S. H. Thang, *Polymer*, 2008, **49**, 1079-1131.
278. M.-k. Ham, J. HoYouk, Y.-K. Kwon and Y.-J. Kwark, *J. Polym. Sci., Part A: Polym. Chem.*, 2012, **50**, 2389-2397.
279. X. M. Yang and K. Y. Qiu, *J. Macromol. Sci., Part A: Pure Appl. Chem.*, 1997, **34**, 315-325.
280. S. Railian, B. Wenn and T. Junkers, *J. Flow Chem.*, 2016, DOI: 10.1556/1846.2016.00018.
281. G. Moad, E. Rizzardo and S. H. Thang, *Austral. J. Chem.*, 2005, **58**, 379.
282. H. Willcock and R. K. O'Reilly, *Polym. Chem.*, 2010, **1**, 149-157.

283. A. Postma, T. P. Davis, G. Moad and M. S. O'Shea, *Macromolecules*, 2005, **38**, 5371-5374.
284. C. H. Hornung, A. Postma, S. Saubern and J. Chiefari, *Polymer*, 2014, **55**, 1427-1435.
285. J. Vandenbergh and T. Junkers, *Macromolecules*, 2014, **47**, 5051-5059.
286. Z. Szablan, T. Junkers, S. P. S. Koo, T. M. Lovestead, T. P. Davis, M. H. Stenzel and C. Barner-Kowollik, *Macromolecules*, 2007, **40**, 6820-6833.
287. G. E. Scott and E. Senogles, *J. Polym. Sci., Part A: Polym. Chem.*, 1970, **4**, 1105-1117.
288. N. M. Ahmad, F. Heatley and P. A. Lovell, *Macromolecules*, 1998, **31**, 2822-2827.
289. T. Junkers and C. Barner-Kowollik, *J. Polym. Sci., Part A: Polym. Chem.*, 2008, **46**, 7585-7605.
290. J. M. Asua, S. Beuermann, M. Buback, P. Castignolles, B. Charleux, R. G. Gilbert, R. A. Hutchinson, J. R. Leiza, A. N. Nikitin, J.-P. Vairon and A. M. van Herk, *Macromol. Chem. Phys.*, 2004, **205**, 2151-2160.
291. A. N. Nikitin, P. Castignolles, B. Charleux and J.-P. Vairon, *Macromol. Rapid Commun.*, 2003, **24**, 778-782.
292. J. Barth, M. Buback, P. Hesse and T. Sergeeva, *Macromolecules*, 2010, **43**, 4023-4031.
293. J. Barth, M. Buback, G. T. Russell and S. Smolne, *Macromol. Chem. Phys.*, 2011, **212**, 1366-1378.
294. T. Junkers and C. Barner-Kowollik, *Macromol. Theory Simul.*, 2009, **18**, 421-433.
295. M. Gaborieau, S. P. S. Koo, P. Castignolles, T. Junkers and C. Barner-Kowollik, *Macromolecules*, 2010, **43**, 5492-5495.
296. R. X. E. Willemse, A. M. van Herk, E. Panchenko, T. Junkers and M. Buback, *Macromolecules*, 2005, **38**, 5098-5103.
297. M. Buback, P. Hesse, T. Junkers, T. Sergeeva and T. Theis, *Macromolecules*, 2007, **41**, 288-291.
298. N. M. Ahmad, B. Charleux, C. Farcet, C. J. Ferguson, S. G. Gaynor, B. S. Hawkett, F. Heatley, B. Klumperman, D. Konkolewicz, P. A. Lovell, K. Matyjaszewski and R. Venkatesh, *Macromol. Rapid Commun.*, 2009, **30**, 2002-2021.
299. T. Junkers, S. P. S. Koo, T. P. Davis, M. H. Stenzel and C. Barner-Kowollik, *Macromolecules*, 2007, **40**, 8906-8912.
300. A. N. Nikitin, R. A. Hutchinson, M. Buback and P. Hesse, *Macromolecules*, 2007, **40**, 8631-8641.
301. J. Chiefari, J. Jeffery, R. T. A. Mayadunne, G. Moad, E. Rizzardo and S. H. Thang, *Macromolecules*, 1999, **32**, 7700-7702.
302. T. Junkers, F. Bennet, S. P. S. Koo and C. Barner-Kowollik, *J. Polym. Sci., Part A: Polym. Chem.*, 2008, **46**, 3433-3437.
303. P. Castignolles, R. Graf, M. Parkinson, M. Wilhelm and M. Gaborieau, *Polymer*, 2009, **50**, 2373-2383.
304. C. Plessis, G. Arzamendi, J. R. Leiza, H. A. S. Schoonbrood, D. Charmot and J. M. Asua, *Macromolecules*, 2000, **33**, 5041-5047.
305. N. M. Ahmad, F. Heatley, D. Britton and P. A. Lovell, *Macromol. Symp.*, 1999, **143**, 231-241.

306. F. Heatley, P. A. Lovell and T. Yamashita, *Macromolecules*, 2001, **34**, 7636-7641.
307. N. Ballard, J. C. de la Cal and J. M. Asua, *Macromolecules*, 2015, **48**, 987-993.
308. A. N. Nikitin, R. A. Hutchinson, G. A. Kalfas, J. R. Richards and C. Bruni, *Macromol. Theory Simul.*, 2009, **18**, 247-258.
309. A. N. Nikitin and R. A. Hutchinson, *Macromolecules*, 2005, **38**, 1581-1590.
310. A. Aleksandrov, V. Genkin, M. Kitay, I. Smirnova and V. Sokolov, *Kvant. electron.*, 1977, **4**, 976-981.
311. O. F. Olaj, I. Bitai and F. Hinkelmann, *Die Makromolekulare Chemie*, 1987, **188**, 1689-1702.
312. M. Buback, R. G. Gilbert, R. A. Hutchinson, B. Klumperman, F.-D. Kuchta, B. G. Manders, K. F. O'Driscoll, G. T. Russell and J. Schweer, *Macromol. Chem. Phys.*, 1995, **196**, 3267-3280.
313. S. Beuermann, M. Buback, T. P. Davis, R. G. Gilbert, R. A. Hutchinson, O. F. Olaj, G. T. Russell, J. Schweer and A. M. van Herk, *Macromol. Chem. Phys.*, 1997, **198**, 1545-1560.
314. S. Beuermann, M. Buback, T. P. Davis, R. G. Gilbert, R. A. Hutchinson, A. Kajiwara, B. Klumperman and G. T. Russell, *Macromol. Chem. Phys.*, 2000, **201**, 1355-1364.
315. S. Beuermann, M. Buback, T. P. Davis, N. García, R. G. Gilbert, R. A. Hutchinson, A. Kajiwara, M. Kamachi, I. Lacík and G. T. Russell, *Macromol. Chem. Phys.*, 2003, **204**, 1338-1350.
316. S. Beuermann, M. Buback, P. Hesse, F.-D. Kuchta, I. Lacík and M. van Herk Alex, *Pure Appl. Chem.*, 2007, **79**, 1463.
317. C. Barner-Kowollik, S. Beuermann, M. Buback, P. Castignolles, B. Charleux, M. L. Coote, R. A. Hutchinson, T. Junkers, I. Lacík, G. T. Russell, M. Stach and A. M. van Herk, *Polym. Chem.*, 2014, **5**, 204-212.
318. C. Barner-Kowollik and S. Perrier, *J. Polym. Sci., Part A: Polym. Chem.*, 2008, **46**, 5715-5723.
319. J. Vandenbergh and T. Junkers, *Macromolecules*, 2012, **45**, 6850-6856.
320. J. Vandenbergh and T. Junkers, *Macromolecules*, 2013, **46**, 3324-3331.
321. D. Cuccato, E. Mavroudakis, M. Dossi and D. Moscatelli, *Macromol. Theory Simul.*, 2013, **22**, 127-135.
322. C. Barner-Kowollik, F. Günzler and T. Junkers, *Macromolecules*, 2008, **41**, 8971-8973.
323. K. B. Kockler, A. P. Haehnel, T. Junkers and C. Barner-Kowollik, *Macromol. Rapid Commun.*, 2016, **37**, 123-134.
324. B. Dervaux, T. Junkers, M. Schneider-Baumann, F. E. Du Prez and C. Barner-Kowollik, *J. Polym. Sci., Part A: Polym. Chem.*, 2009, **47**, 6641-6654.
325. A. P. Haehnel, M. Schneider-Baumann, K. U. Hiltebrandt, A. M. Misske and C. Barner-Kowollik, *Macromolecules*, 2013, **46**, 15-28.
326. A. P. Haehnel, M. Schneider-Baumann, L. Arens, A. M. Misske, F. Fleischhaker and C. Barner-Kowollik, *Macromolecules*, 2014, **47**, 3483-3496.

327. K. B. Kockler, A. P. Haehnel, F. Fleischhaker, M. Schneider-Baumann, A. M. Misske and C. Barner-Kowollik, *Macromol. Chem. Phys.*, 2015, **216**, 1573-1582.
328. L. Couvreur, G. Piteau, P. Castignolles, M. Tonge, B. Coutin, B. Charleux and J.-P. Vairon, *Macromol. Symp.*, 2001, **174**, 197-208.
329. A. P. Haehnel, B. Wenn, K. Kockler, T. Bantle, A. M. Misske, F. Fleischhaker, T. Junkers and C. Barner-Kowollik, *Macromol. Rapid Commun.*, 2014, **35**, 2029-2037.
330. A. P. Haehnel, B. Wenn, K. Kockler, T. Bantle, A. M. Misske, F. Fleischhaker, T. Junkers and C. Barner-Kowollik, *Macromol. Rapid Commun.*, 2015, **36**, 1984-1986.
331. L. Feng, J. W. Hu, Z. L. Liu, F. B. Zhao and G. J. Liu, *Polymer*, 2007, **48**, 3616-3623.
332. Z. Yin, C. Koulic, C. Pagnoulle and R. Jérôme, *Macromolecules*, 2001, **34**, 5132-5139.
333. J. S. Li and H. N. Xiao, *Tetrahedron Lett.*, 2005, **46**, 2227-2229.
334. C. J. Ferguson, R. J. Hughes, D. Nguyen, B. T. Pham, R. G. Gilbert, A. K. Serelis, C. H. Such and B. S. Hawkett, *Macromolecules*, 2005, **38**, 2191-2204.
335. B. Wenn and T. Junkers, *submitted*.
336. L. Lu, H. Zhang, N. Yang and Y. Cai, *Macromolecules*, 2006, **39**, 3770-3776.
337. A. S. Goldmann, M. Glassner, A. J. Inglis and C. Barner-Kowollik, *Macromol. Rapid Commun.*, 2013, **34**, 810-849.

> The whole secret of a successful life is to find out
> what is one's destiny to do,
> and then do it.
>
> Henry Ford